

**TSUNAMI VULNERABILITY ASSESSMENT OF
COX'S BAZAR DISTRICT**

TSUNAMI VULNERABILITY ASSESSMENT OF COX'S BAZAR DISTRICT

Prepared for

United Nations Office for Project Services (UNOPS) through Comprehensive Disaster Management Programme (CDMP) under the Ministry of Food and Disaster Management, Government of the People's Republic of Bangladesh

Under the project

"Development of a Disaster Preparedness Programme for Earthquake and Tsunami Hazards in Cox's Bazar area"

**Department of Civil Engineering
Bangladesh University of Engineering and Technology (BUET)
Dhaka-1000**

TSUNAMI VULNERABILITY ASSESSMENT OF COX'S BAZAR DISTRICT

A Report to

**Comprehensive Disaster Management Programme (CDMP)
Ministry of Food and Disaster Management
Government of the People's Republic of Bangladesh**

Project Director:

Dr. Ashutosh Sutra Dhar

Associate Professor, Department of Civil Engineering, BUET

Co-Researchers:

Dr. Mohammad Asad Hussain

Assistant Professor, Institute of Water & Flood Management, BUET

Dr. Mehedi Ahmed Ansary

Professor, Department of Civil Engineering, BUET

Research Assistants:

A.B. Afifa Imtiaz

Md. Zahid Hasan Siddiquee

Mahfuza Shamim

June 2008

Department of Civil Engineering

Bangladesh University of Engineering and Technology (BUET)

Dhaka-1000

Executive Summary

Bangladesh is one of the countries that are most prone to natural disasters. The threat of tsunamis has taken on added urgency in recent years after the devastating tsunami occurred in Indonesia's Sumatra Island in December 2004 and the further tsunami occurrences in the Indian Ocean. Though Bangladesh was relatively less affected by the Giant Tsunami, but it has raised the question whether and to what extent the country and its huge coastal population are vulnerable to tsunami hazard. This research thus highlights the potential for tsunamigenic earthquakes in the Bay of Bengal and the vulnerability posed on the region. A tsunami can pose a very significant threat to the large coastal population of the country. For the implementation of tsunami mitigation strategies it is therefore essential to investigate the scenario of this hazard in this region. The outputs provided in this report are expected to be useful for comprehensive coastal inundation modeling, evacuation planning and public education.

In this research work, Tsunami Vulnerability Assessment of Cox's Bazar District was performed with respect to the potential of occurring Tsunamigenic Earthquakes around Bangladesh and the vicinity. The affects on the Coast of Bangladesh has also been evaluated based on Tsunami Propagation in case of any Tsunami generation. The Potential of Occurrence of Tsunamigenic Earthquake in Bangladesh and the vicinity was investigated through historical records and the available research documents. The affect of tsunami on the coast of Bangladesh was assessed through numerical modeling of wave propagation from tsunami source based on the bathymetry, local geographical conditions and topographical features of the region. It has been revealed that the potential of tsunami hazard from Indian Ocean region in Bangladesh Coast is relatively low. However, more concern and concentration should be put forth for future studies in the Andaman–northern Sumatra region and Myanmar (Arakan) Subduction zone to assess the likelihood of a giant tsunamigenic earthquake in those regions. The study of tsunami propagation showed that if any tsunami originates in the Bay of Bengal and vicinity or even from any distant source, the continental shelf along the Coast of Bangladesh would significantly reduce the motion of the tsunami propagation. Potential inundation of the areas of Cox's Bazar district based on hypothetical tsunami surge was developed on the basis of computational modeling of the propagation of the surge over the continent.

Acknowledgement

The authors acknowledge the funding of this research project by United Nation Office for Project Service (UNOPS) through Comprehensive Disaster Management Program (CDMP) of the Ministry of Disaster Relief and Rehabilitation of Bangladesh Government.

The authors would also like to acknowledge the contribution of Mr. Thisara Welhena, Lecturer, Department of Civil Engineering, University of Moratuwa, Sri Lanka for his help regarding tsunami propagation modeling.

Table of Contents

Sl. No	Description	Page No.
	Executive Summary	4
	Acknowledgement	5
	Table of Contents	6
	List of Figures	7
	List of Tables	9
1	Introduction	10
2	Causes of Tsunami	11
3	Conditions for Generating Tsunami	14
3.1	Tsunamigenic Fault	14
3.2	Earthquake Magnitude on the Tsunamigenic Fault	15
3.3	Depth of earthquake epicenter	17
3.4	Ocean Topography	18
4	Aspects of Tsunami Hazard Assessment	18
5	Seismotectonics of the Indian Ocean Region	18
6	Earthquake of December 26, 2004	26
7	Historical Tsunamis in the Bay of Bengal	28
8	Evaluation of Tsunami Potential in Bangladesh	31
8.1	Risks from Indian Ocean	31
8.2	Factors Affecting Tsunami Potential in Bangladesh	34
8.3	Tsunami Hazard Assessment of ICZMP	39
9	Analysis of Tsunami Propagation	41
9.1	Modeling Tsunami Propagation	42
9.1.1	Formulation of a Numerical Model	42
9.1.2	Numerical Scheme	47
9.2	Model Input Data	50
9.3	Numerical Experiments and Results of Tsunami Propagation	51
9.3.1	Effects of the Location of Tsunami Generation	53
9.3.2	Effects of the Subduction Amplitude of Tsunami	54
9.3.3	Effects of the Subduction Orientation of Tsunami (case 2 and 4)	55
9.3.4	Effects of the Proximity of Tsunami Source (case 5 and 6)	57
9.3.5	Effects of Continental Shelf	58
10	Modeling Tsunami Inundation	60
10.	Overview of the 3D Model	60
10.1	Development of Digital Elevation Model for Cox's Bazar	61
10.2.1	Digitizing FINNMAPS	61
10.2.3	DEM Preparation	63
10.3	Development of Inundation Maps	67
10.3.1	Water Surface Elevation and Corresponding Velocity Vectors	68
11	Discussions and Conclusions	69
	REFERENCES	72
	Appendix A	77
	Appendix B	89

List of Figures

- Figure 1: The three principal types of plate margins and various associated features
- Figure 2: Earth's Plates and Boundary Activity
- Figure 3: A Typical Oceanic-Oceanic Convergent Plate Motion
- Figure 4: A Megathrust
- Figure 5: Trenches, the deepest parts of the oceans and the topographic expression of subduction zones
- Figure 6: Cross-sectional illustration of normal and reverse dip-slip faults
- Figure 7: Tectonic Plates of Indian Ocean
- Figure 8: Migration of Indian Tectonic Plate
- Figure 9: General Seismicity of Indian Ocean (416 AD-2005)
- Figure 10: Tsunami Sources in the Indian Ocean (416 AD-2005)
- Figure 11: List and Locations of Catastrophic Tsunamis in the Indian Ocean
- Figure 12: Subduction Zone in Indian Ocean
- Figure 13: Locations of Tsunamis in the Indian Ocean (After, rastogi et. al. 2006)
- Figure 14: Base Map of the Sumatra Subduction Zone showing Seismicity associated with 2004 Earthquake
- Figure 15: North-East Indian Ocean Seismicity
- Figure 16: Section of the Subduction Megathrust in Indian Ocean
- Figure 17: Tectonic classification of the Bengal basin
- Figure 18: Thick Sedimentation in Bengal fan
- Figure 19: Bathymetry of Bay of Bengal
- Figure 20: Tsunami Vulnerability Map of Bangladesh (Uddin, 2005)
- Fig 21: No radial line could be drawn to the Bangladesh Coast from Sumatra
- Fig 22: Space domain of the governing equations
- Fig 23: Applicability range of linear long wave theory
- Figure 24: Arrangement of points in staggered leapfrog scheme
- Figure 25: Grid Arrangement
- Figure 26: Koshimura subduction model (3D view on the left and 2D on the right)
- Figure 27: Seven cases of tsunami generated at different sources and with different subduction depths

List of Figures (contd.)

Figure 28: Comparison of tsunami wave heights of Case 0 and Case 2

Figure 29: Comparison of tsunami arrival times at continental shelf for Case 0 and Case 2

Figure 30: Comparison of tsunami wave heights of Case 2 and Case 3

Figure 31: Comparison of tsunami arrival times at continental shelf for Case 2 and Case 3

Figure 32: Comparison of tsunami wave heights of Case 2 and Case 4

Figure 33: Comparison of tsunami arrival times at continental shelf for Case 2 and Case 4

Figure 34: Comparison of tsunami arrival times at continental shelf for Case 5 and Case 6

Figure 35: Wave height distributions at every 10 minutes after tsunami generation

Figure 36: Sample FINN Map and Location Index

Figure 37: Digitizing in Arc-View

Figure 38: Study Area Cox's Bazar in FINN Map Grids

Figure 39: Referenced Images and Spot Heights

Figure 41: Digital Elevation Model of The study area Cox's Bazar

Figure 42: Scattered Points

Figure 43: Points in Regular grids

Figure 44: Typical distribution of water surface elevation (m) with 2 m wave height of tsunami at the Cox's Bazar coast, Bangladesh

Figure 45: Wave height distribution and velocity vectors at the Cox's Bazar coast, Bangladesh at three different time intervals after tsunami generation.

List of Tables

Table 1: Earthquake magnitude and possible tsunami destruction

Table 2: Historical Earthquake & Tsunami

Table 3: List of selected tsunami data of Indonesia Region

Table 4: List of Tsunamis that affected Indian Ocean and Vicinity

Table 5: Four Earthquakes located in the Western Coast of Bay of Bengal

Table 6: List of Numerical Experiments

1. Introduction

The great Sumatra–Andaman earthquake and Indian Ocean tsunami of 2004 has triggered renewed interest in the study of historic earthquakes and ocean disturbances in the Indian Ocean as well as Bay of Bengal region. Bangladesh, the South Asian country prone to various natural calamities, is situated in the active plate collision zone and consequently endangered due to large earthquakes. The northern part of Bangladesh, lying beside the Bay of Bengal has millions of people residing the near shore of coastal region. Therefore it is very urgent to assess whether this region as well as the huge population are at risk of tsunami. This report puts forward an effort to summarize the available knowledge and views on the existence of tsunamigenic faults, tsunami potential and associated risk of the region. The investigations through the currently available documented research works so far reflect that the idea that the tectonics in the northern Bay of Bengal suggests large tsunami-generating earthquakes are unlikely, is no more compelling. Many scientists (The Sunday Times Online, 2007) are on the opinion that northern tip of the Bay of Bengal should be put on the tsunami hazard radar since there have been found some evidences of the coast's changing in response to active subduction.

Tsunamis, one of the scariest natural hazards, along with their tremendous destructive nature, have been responsible for great loss of lives and properties throughout history. The majority of this disaster with high intensity and wide scale devastation has been generated in the Pacific Ocean. Indian Ocean and the Mediterranean Sea are the other regions where there are historical records of occurring dreadful tsunamis. The most prominent tsunami in the region of the Indian Ocean so far is the Sumatra-Andaman Island earthquake of a moment magnitude of 9.3 that took place on December 26, 2004. The great displacements of the sea floor associated with the earthquake produced exceptionally large tsunami waves that spread death and destruction throughout the Bay of Bengal, from Northern Sumatra to Thailand, Sri Lanka, and India. Since the 1980s, scientists (Geotimes, 2007) have thought that the subduction zone where the tectonic plates bearing India and Southeast Asia meet, which also caused the 2004 Sumatra-Andaman earthquake, continues north through the Bay of Bengal and along the Myanmar coast. As previous data from that region did not show any active subduction, the danger of large earthquakes in the more northern part of the bay was considered to be nominal that led to be relatively little concern about the subduction zone in the northern Bay of Bengal along the coast

of Myanmar. Very recently, Phil Cummins (Cummins, 2007), a senior seismologist at Geoscience Australia, made an intensive study on this issue and highlighted that the Myanmar coast has the potential for large, tsunami-generating earthquakes. According to him, the tectonic environment of this part has similarities to other subduction zones that experience giant megathrust earthquakes, stress and crustal strain observations, which indicate that the seismogenic zone is locked. Again historical records also indicate that giant tsunamigenic earthquakes have occurred there in the past. To him, these are all consistent with active subduction in the Myanmar subduction zone and he suggests that the seismogenic zone extends beneath the Bengal Fan. He concludes therefore that giant earthquakes probably occur off the coast of Myanmar. Though the threat does not appear to be immediate but if so happens a large and vulnerable population will thereby be exposed to a significant earthquake and tsunami hazard. Cummins (2007) indicated his work as a preliminary step and suggested that further geodetic measurements and geological studies in the area along the coast of Myanmar (Arakan portion) and Bangladesh are essential to determine whether the ground is really moving in a way consistent with a locked subduction zone which might be building up stress towards a tsunamigenic earthquake.

2. Causes of Tsunami

Tsunami is described as a series of very long wavelength ocean waves caused by the sudden displacement of water by dynamic processes of the Earth such as plate tectonics, earthquakes, landslides, or submarine slumps and can also be triggered by anthropogenic activities such as dam breaks, avalanches, glacier calving or explosions. The rigid lithospheric plates of the Earth form three different types of boundaries: convergent, divergent and strike-slip (Figure 1). Depending on the type of boundary, two lithospheric plates can override each other, slip along each other or separate from each other (Figure 2). Obviously, the convergent plate boundary has the largest potential of accumulating stress which is eventually released through visco-elastic deformation and earthquakes. These plate boundaries are also known as subduction zones.

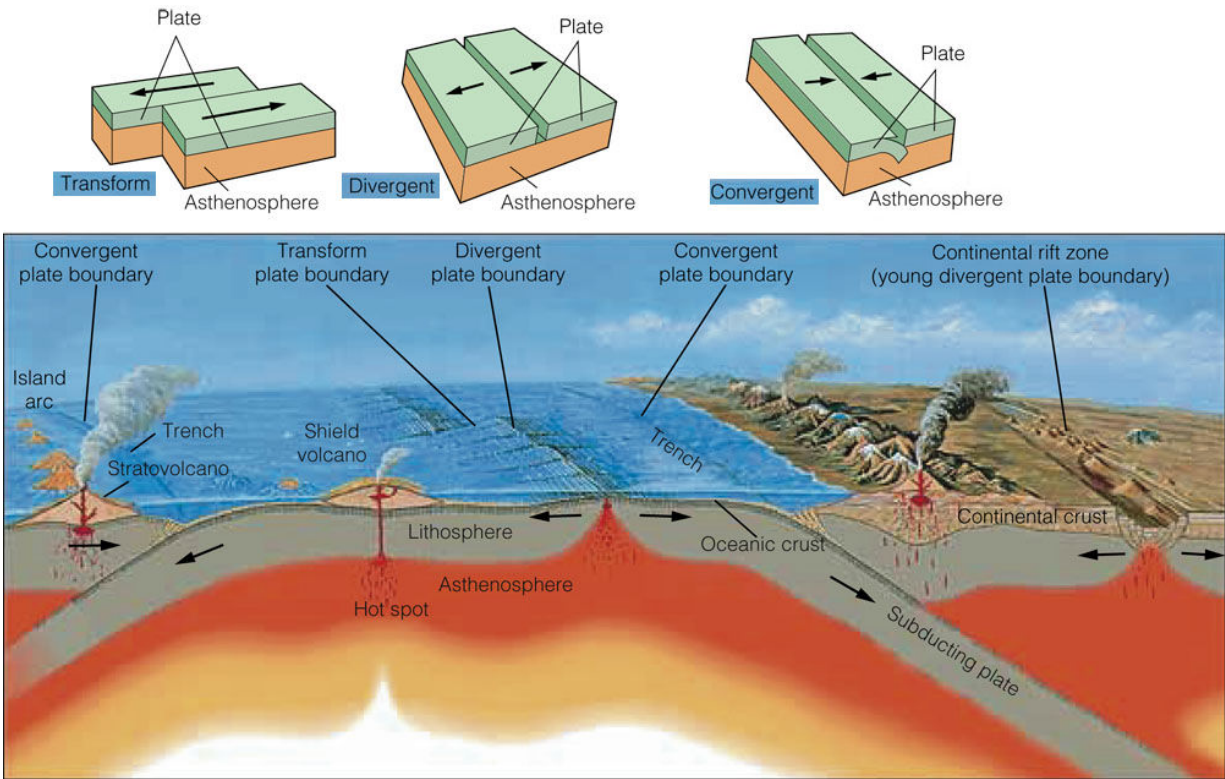


Figure 1: The three principal types of plate margins and various associated features

(<http://www.indiana.edu>)

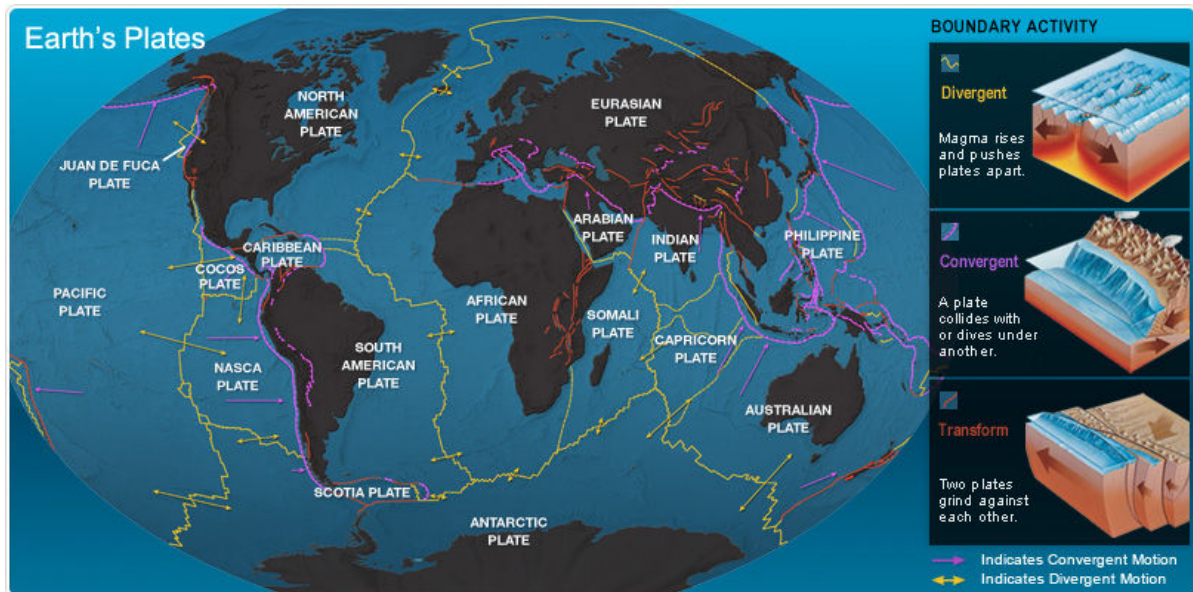


Figure 2: Earth's Plates and Boundary Activity (<http://science.nationalgeographic.com>)

Two plates which override each other with a convergence rate of a few cm/year do not show continuous movement but do exhibit periodic relative movement. A Typical Oceanic-Oceanic Convergence Plate Motion is shown in Figure 3. For long time periods, the motion is locked and the relative motion is transformed into stress and strain. Such contact between the two plates is an earthquake fault, sometimes called a megathrust and has been shown in Figure 4. After a certain yield stress has been exceeded, the plates overcome the friction and move again. This causes a sudden displacement of lithospheric material, which also displaces the water column above, since water is incompressible. In reality, tsunamis are the combination of multiple explosion sources and propagate with the highest energy in a direction perpendicular to the line of sources, e.g. a ruptured fault zone.

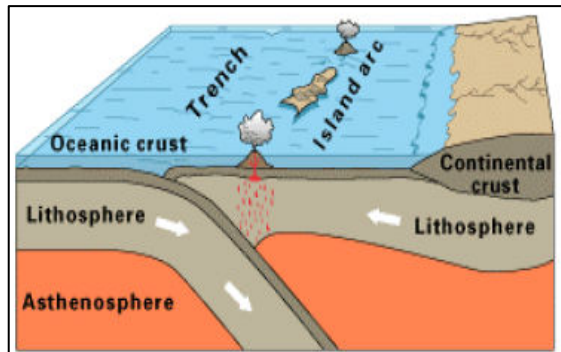


Figure 3: A Typical Oceanic-Oceanic Convergent Plate Motion (ICMAM, 2005)

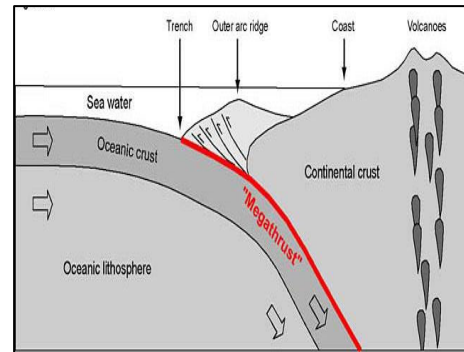


Figure 4: A Megathrust (Caltech, 2004)

When strong earthquakes occur underwater, the crustal movement disturbs a large volume of water like a giant paddle and ripples spread out in all directions at speeds of 600-800 kilometers per hour. In the open ocean, they go unnoticed but once they reach shallower waters they slow down and begin to crest. An earthquake that causes a tsunami is termed as tsunamigenic earthquake. A tsunamigenic earthquake is apprehended to be of 8 and greater magnitudes in Richter scale while local tsunami may occur by magnitudes between 7 and 8 provided other conditions are fulfilled. The nature of a tsunamigenic fault movement is essentially thrust. The focal depth has to be within 10-15 km. There are also limits to the obliquity of plate boundary convergence beyond which such rapid vertical slip is unlikely, or at least less, likely to occur. Only active plate subduction zones are susceptible to such kind of rupture due to thrust fault

movement. The earthquake's magnitude, depth, fault characteristics and coincident slumping of sediments or secondary faulting also determine the size of the tsunami. Subduction of older lithosphere, especially where strike-slip displacement transfer occurs (back-arc spreading), is less likely to produce tsunamis. Hasan et. al. (2007) report that most major earthquakes of magnitude greater than 7 (M_w) and shallow focus (≈ 15 km) under sea are tsunamigenic. The tsunamigenic earthquakes are distributed along the active subduction zones of the plate margin. Table 1 shows an empirical assessment of tsunami potential with regard to the magnitude of earthquakes.

Table 1: Earthquake magnitude and possible tsunami destruction (Hasan et al, 2007)

Sl. No.	Magnitude	Destruction
a	$M > 7.8$	Possibility of ocean-wide destructive tsunami
b	$7.8 > M > 7.5$	Possibility of a destructive regional tsunami with effects limited to within 1000 km of epicenter
c	$7.5 > M > 7$	Possibility of a destructive local tsunami with effects limited to within 100 km of epicenter
d	$7 > M > 6.5$	Very small possibility of a destructive local tsunami

3. Conditions for Generating Tsunami

The conditions for earthquake generated tsunami are mainly:

- i. Existence of tsunamigenic Fault
- ii. Earthquake magnitude on the tsunamigenic fault
- iii. Depth of earthquake epicenter
- iv. Ocean topography.

A brief description of each of the conditions is given below:

3.1 Tsunamigenic Fault

Generally earthquakes are induced at the fault of plate boundary. Larger earthquake occur where the oceanic plate subducts below the continental plate. But all the larger earthquakes do not generate tsunamis. Tsunami occurs due to the earthquakes in the Subduction Zone (Figure 5) and mainly due to the Thrust (Dip-Slip) faults (Figure 6) those cause uplifting of the water column above the plate.

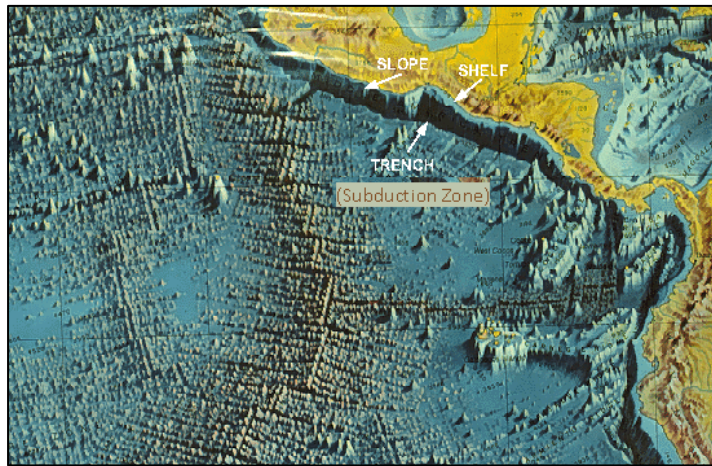


Figure 5: Trenches, the deepest parts of the oceans and the topographic expression of subduction zones (www.indiana.edu)

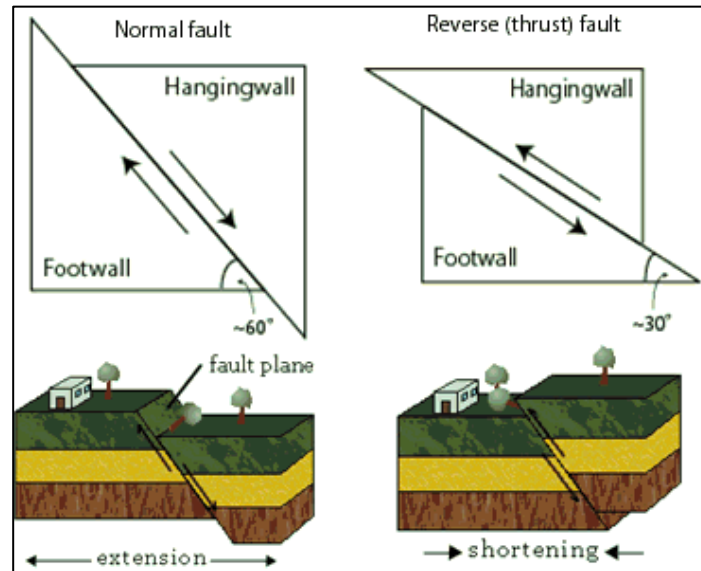


Figure 6: Cross-sectional illustration of normal and reverse dip-slip faults (www.nationmaster.com)

3.2 Earthquake Magnitude on the Tsunamigenic Fault

Energy dissipated from an earthquake is also a governing factor for tsunamis. The earthquake should have generate sufficient energy that can uplift the water and provide with a momentum to cause the water to flow. In general, an earthquake with higher magnitude has greater potential of generating tsunami than an earthquake with lower magnitude. Table 2 shows some historic earthquakes that generated tsunamis. It is revealed that an earthquake of magnitude greater than 7 in Richter scale generated tsunamis. Depth of the focus for those earthquakes ranged between 8 and 30 km. The effect of depth of epicenter is discussed further in the following section.

Table 2: Historical Earthquake & Tsunami

Date	Location	Earthquake magnitude	Time delayed (hr)	Ht. of wave (m)	Run-up (m)	Deep sea wave velocity (km/hr)	Depth of focus (000, m)	Damage in money (million)	Lost life	Ref
1/04/1946	Alaska Uimak island	7.8	5	35	-	-	-	\$ 26	165	a
4/11/1952	Kamchatka Peninsula	8.2	0.5	18.4	9	-	-	\$ 1	-	a
9/03/1957	Andreanof island, Alaska	8.3	-	16	3.9	-	-	\$5	-	a
22/05/1960	Chilean	9.5	-	-	-	-	-	\$500	2300	a
28/03/1964	Alaska	8.4	1	15	1600,000/1300,000/ w	-	-	\$106	120	a
29/11/1975	Hawaiian	7.2	-	7.9	-	-	-	\$4.1	-	a
26/05/1983	Japan sea	7.9	-	-	-	-	-	\$0.5	104	a
19/09/1985	Mexico	7.5	-	--	-	-	-	-	-	a
2/09/1992	Pacific coast	7.6	-	-	10	-	-	-	-	a
12/07/1993	Japan	7.8	-	-	-	-	-	\$600	239	a
07/04/1995	Pago, Samoa	7.4	-	5	-	-	-	-	-	a
17/07/1998	Papua New Guinea	7.1	1	-	-	-	33	-	1000	a
26/11/1999	Vanuatu	7.3	-	2-3	30,000	-	33	-	12000	a
23/06/2001	Peru	8.4	0.5	-	30,000	-	8	-	20	b
26/12/2004	Indonesia	9.3	0.5	25	580	1000 km/hr	30	-	300,000	c
17/07/2006	Java; Indonesia	7.7	-	2	-	-	-	-	100	a
12/09/2007	Java; Sumatra Indonesia	8.5	-	0.9	34,000	-	-	-	25	d

Here,

a: Carayannis (2004), b: USGS (2001), c: Tsunami (2004), d: USGS (2007)

3.3 Depth of earthquake epicenter

The tsunamis due to earthquake are greatly influenced by the depth of epicenter. A list related to tsunami and depth of earthquake epicenter is shown in Table 3 for the region of Indonesia (after Latief et al., 2000)

Table 3: List of selected tsunami data of Indonesia Region (after Latief et al., 2000)

Date (Y-M-D)	Lat.	Lon.	D (Km)	Ms	m	H _{max}	F	Affected region
1908/03/24	-8.7	124.7	33	6.6	2.0	25	-	Timur island
1913/03/14	4.8	126.6	25	7.9	-	-	-	North Sulawesi
1938/05/19	-1.0	120.0	60	7.6	1.5	3	-	Central Sulawesi
1961/03/16	-8.2	122.0	75	6.3	-	-	6	Flores
1975/01/15	-5.0	130.0	33	6.9	-	-	-	Bandanaira
1975/03/05	-2.4	126.1	33	6.5	1.0	2	-	Sanana,sula island
1975/07/30	-10.1	123.8	16	6.1	-	-	-	Timor island
1977/08/27	-8.0	125.3	25	6.8	-	-	2	Flores
1979/12/17	-8.4	115.9	33	6.6	-	-	27	Sumbvawa,Lombok
1982/03/12	-4.4	128.1	-	5.8	-	-	-	Molucca
1982/08/19	-0.1	121.6	44	5.2	-	-	-	North Sulawesi
1982/12/25	-8.4	123.0	33	5.9	1.0	-	13	Larantuka
1984/01/08	-2.9	118.7	95	5.9	-	-	-	South sulawesi
1987/11/26	-8.4	124.3	33	6.5	1.0	-	83	Flores, Pantar Is
1989/07/14	-8.1	125.1	52	6.2	0.0	-	7	Alor island
1989/07/31	-8.1	121.4	13	6.3	0.0	-	3	Flores
1991/07/04	-8.1	124.7	29	6.2	-	-	13	Alor island
1992/06/20	2.0	122.8	-	6.2	0.0	-	-	North sulawesi

Here, D is earthquake focal depth, Ms is earthquake magnitude of surface wave, m is tsunami magnitude (a number which characterizes the strength of a tsunami based on the tsunami wave amplitudes), H_{max} is maximum vertical run- up, F is number of fatalities, Lat. is latitude of earthquake epicenter and Lon. is longitude of earthquake epicenter

As expected, an earthquake with deeper focal depth appears to produce a less run-up and an earthquake with greater magnitude caused a greater devastation.

3.4 Ocean Topography

Topography of the ocean surface governs propagation of the tsunami after being generated from an earthquake. If the propagating water faces less hindrance on the way of propagation it can travel a greater distance. Also, a water mass can travel faster in a straight direction than if the direction of flow is not straight. The direction of water flow is governed by ocean topography and the presence of continents.

4. Aspects of Tsunami Hazard Assessment

Vulnerability of an area to Tsunami Hazard is assessed based on analysis of the potential of the hazard and propagation of the water into the area. Activities involved in a tsunami hazard assessment are as below:

a. Analysis of Tsunami Potential

Analysis of tsunami potential involves determination of tsunamigenic faults in the region and determination of the potential of tsunamigenic earthquakes in those faults. Earthquake of specific magnitude and epicenter depth would be required for the generation of tsunami.

b. Tsunami Propagation

Tsunami wave propagation depends on the topography of the ocean floor, presence and characteristics of continental shelf and slope and topography of the surrounding terrain. Digital Elevation Model of the study area would be required to determine the affect of tsunami in the area. Analyses of tsunami potential in Bangladesh and tsunami propagation with reference to Cox's Bazar area have been provided in the following sections.

5. Seismotectonics of the Indian Ocean Region

According to Gupta (2005), there are three major belts globally which account for almost 95% of earthquake activity. Among them the Alpide-Himalaya seismic belt which starts from southeast Asia near Java-Sumatra, continues through Andaman Nicobar Islands, India-Burma border region, swings through north of India in the foothills of Himalayas and then moves west through Iran into Greece and Italy. This is the second most active belt (after ICMAM, 2005). Scientists at Columbia University's Lamont-Doherty Earth Observatory

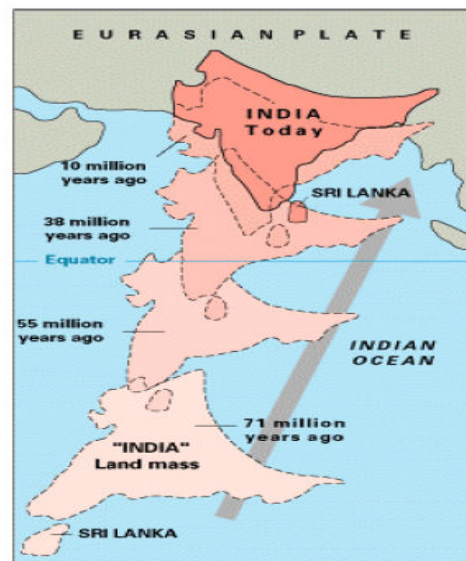
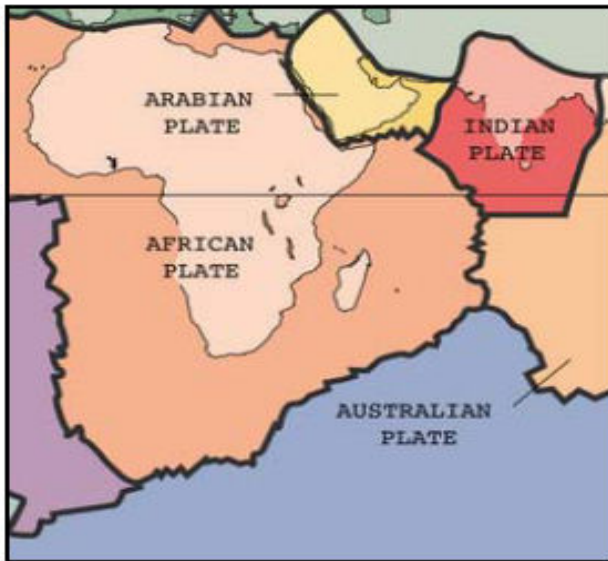


Figure 7: Tectonic Plates of Indian Ocean

Figure 8: Migration of Indian Tectonic Plate

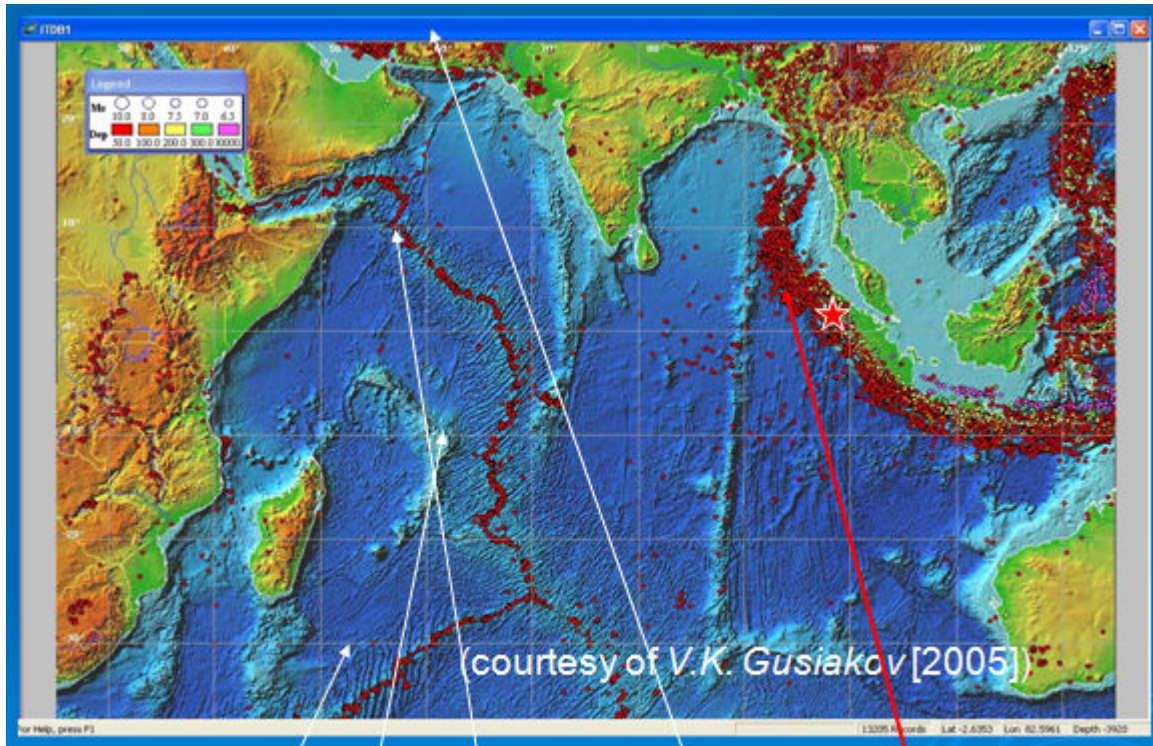
(LDEO) report (after ICMAM, 2005), direct evidence that one of the Earth's great crustal plates is cracking into two. Orman et al. (1995), have confirmed that the Indo-Australian Plate, long identified as a single plate on which both India and Australia lie, appears to have broken apart (Figure 7), just south of the Equator beneath the Indian Ocean. The break has been underway for the past several million years, and now the two continents are moving independently of one another in slightly different directions. According to USGS (ICMAM, 2005), the Indian tectonic plate has been drifting and moving in a north/northeast direction (Figure 8) for some 50 million years, colliding with Eurasian tectonic plate and forcefully raising the Tibetan Plateau and the Himalayan Mountains. As a result of such migration and collision with both the Australian and the Eurasian tectonic plates and sub-plates, the Indian plate's eastern boundary is a diffuse zone of seismicity and deformation, characterized by extensive faulting and earthquakes that can generate moderate to destructive tsunamis.

To the east, of Indian Ocean, subduction of the Indo-Australian Plates beneath the Burma and Sunda Plates has formed the extensive Sunda Trench - a very active seismic region where large earthquakes are frequent. The volcanoes of Krakatau, Tambora and Toba, well known for their violent eruptions, are byproducts of such tectonic interactions. A divergent boundary separates the Burma plate from the Sunda plate in the north. The Burma plate encompasses the northwest portion of the island of Sumatra as well as the Andaman and the Nicobar Islands, which separate the Andaman Sea from the Indian Ocean. Destructive tsunamis can originate from earthquakes

that occur along these principal tectonic sources. The major tectonic feature in the region is the subduction zone Sunda Arc or the Sunda Trench that extends approximately 5,600 km (after ICMAM, 2005) between the Andaman Islands in the northwest and the Banda Arc in the east. The Australian Plate subducts beneath the Sunda Plate (which forms part of the larger Eurasian Plate in the Pacific). The Sunda Arc consists of three primary segments; the Sumatra segment, the Sunda Strait Segment and the Java Segment. These locations represent the area of greatest seismic exposure, with earthquake magnitudes of 8 or even more on the Richter scale - as the 26 December 2004 proved. Active tectonic interaction of this great arc has produced destructive earthquakes and tsunamis in the distant past and as recently as 1977, 1992 and 1994 (ICMAM, 2005).

The eastern part of Sunda Arc is where relatively old (over 100 million years) oceanic lithosphere subducts offshore Java. Very few classical subduction zone earthquakes occur in this region. On the other hand, further to the north-west on the Sunda Arc, young (40 million years) oceanic lithosphere subducts offshore Sumatra. The subduction of such young oceanic lithosphere can cause the most massive thrust earthquakes that generate huge tsunamis. However, this subduction zone is not as active as the ones in the Pacific Rim, which cause frequent tsunamis. Also, the thrust earthquakes that do occur as a result of this subduction and the propagation characteristics of the tsunamis that they do generate have been such as to cause local effects but not affect to coasts thousands of kilometres away in the northern part of the Indian Ocean.

An earthquake releases the strain that accumulates over centuries between plates pushing into each other. For this reason, it may be a very long time before anything like a magnitude 9.3 earthquake of Sumatra 2004 erupts again in this part of the fault line. But there are other areas that still have built-up strain and the segments to the south can break anytime (after Schirber, 2005). Figure 9 shows the general seismicity of Indian Ocean where the main seismic area is the extensive subduction zone near the NE margin of the Indian Ocean (Fine et. al. 2005). There are also other zones: the SW, Central, Carlsberg and Murrey ridges. Most of tsunami source region in the Indian Ocean (Figure 10, Fine et. al. 2005) are along the Sunda Trench subduction zone (along Burma, Andaman and Nichobar Islands, Sumatra and Java). However there are sources in the NW part of the Ocean (Murrey Ridge).



SW Central Carlsberg Murrey Ridges NW margin of Indian Ocean

Figure 9: General Seismicity of Indian Ocean (416 AD-2005)

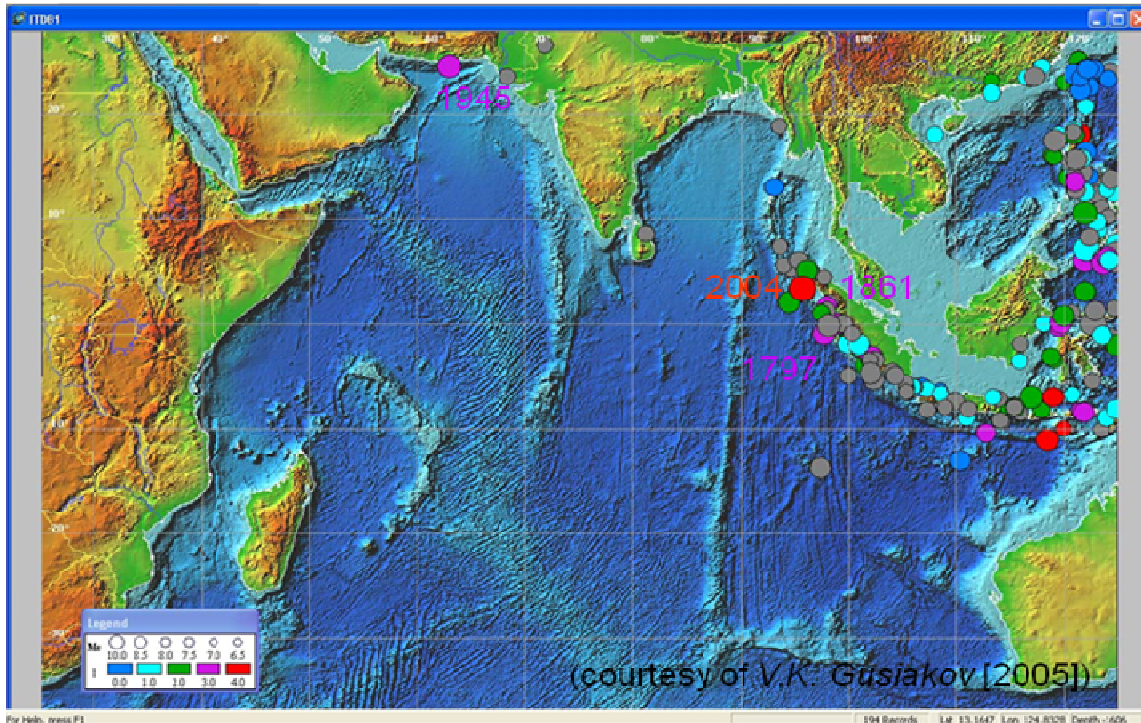


Figure 10: Tsunami Sources in the Indian Ocean (416 AD-2005)

Tsunamis are rarer in the Indian Ocean as the seismic activity is much less than in the Pacific. However, there have been 7 records of Tsunamis (www.iri.columbia.edu) set off by Earthquakes near Indonesia, Pakistan and one at Bay of Bengal. Figure 11 (Satake, 2004) shows few catastrophic tsunamis and their locations in the Indian Ocean. Figure 12 (USGS, seismo.html) shows the subduction zone in Indian Ocean producing catastrophic tsunami occurrences. Eighty percent of the tsunamis in the Indian Ocean are from Sunda arc region where on an average tsunamis are generated once in three years (Rastogi et. al., 2006). In rest of the Indian Ocean tsunamis can be generated once in ten years or so. Figure 13 shows the major Tsunami locations in Indian Ocean and the list of Tsunamis affecting the region is provided in Table 4 (Rastogi et. al., 2006).

Catastrophic Tsunamis in the Indian Ocean				
Year	Region	M	i	Deaths
1797	SW SUMATRA	8.0	3.0	300
1833	SW SUMATRA	8.2	2.5	-
1861	SW SUMATRA	8.5	3.0	11,700
1881	BAY OF BENGAL	7.9	?	-
1883	KRAKATAU, INDONESIA	Volcanic Explosion	4.0	36,500
1896	SW SUMATRA	7.6	2.0	400
1935	SW SUMATRA	7.9	?	-
1941	ANDAMAN SEA	8.6	?	>5,000
1945	ARABIAN SEA (KARACHI)	8.5	?	>4,000
1989	SW SUMATRA	8.1	?	-
2004	NW SUMATRA/ANDAMAN	9.3	4.0	300,000

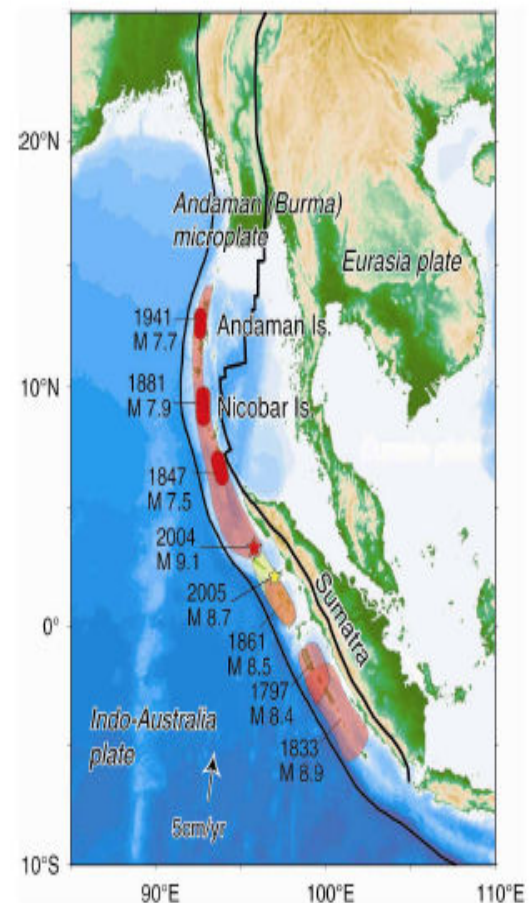


Figure 11: List and Locations of Catastrophic Tsunamis in the Indian Ocean

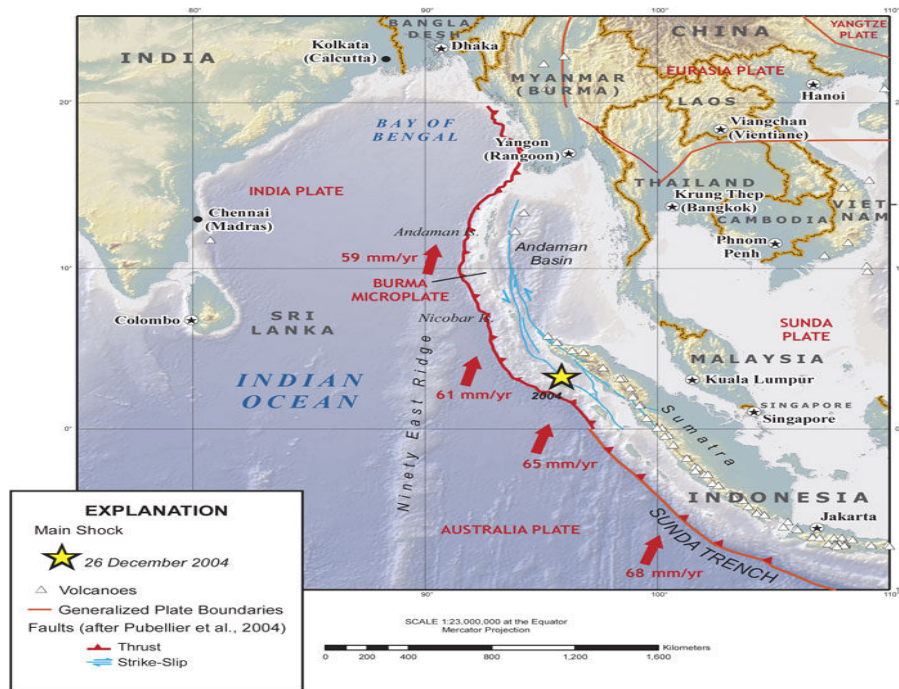


Figure 12: Subduction Zone in Indian Ocean

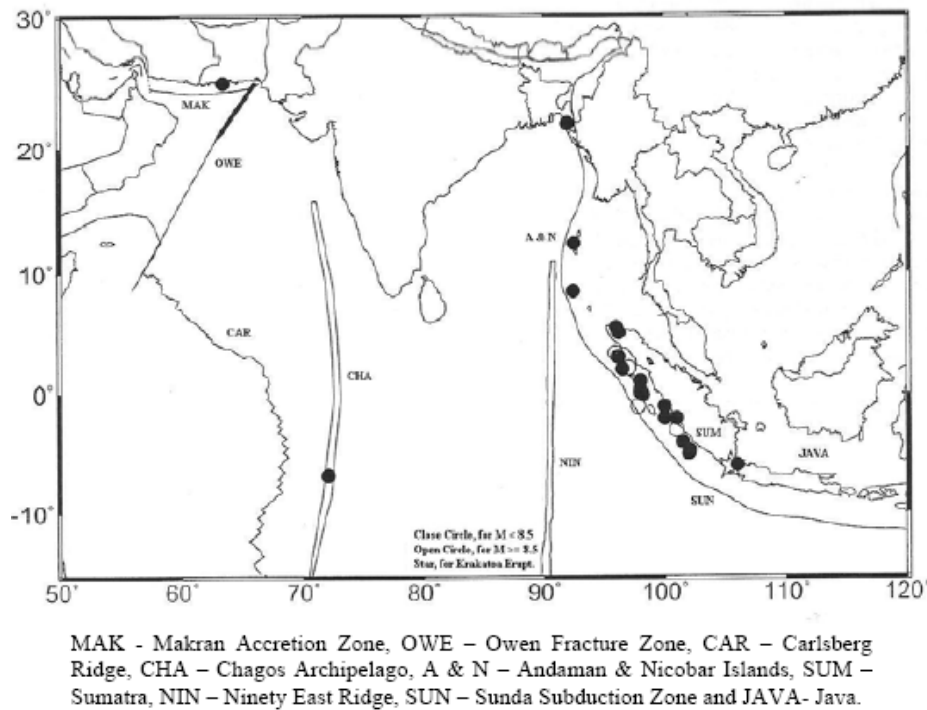


Figure 13: Locations of Tsunamis in the Indian Ocean (After, rastogi et. al. 2006)

Table 4: List of Tsunamis that affected Indian Ocean and Vicinity

List of Tsunamis that Affected Indian Region and Vicinity

S. N.	Date	Location	Long.	Lat.	Eq. Mag	Cau	Pr o	I	Max Run up (run ups)	Ref.
1	326 B.C.	Indus delta /Kutch region				1	4			Lisitzin (1974)
2	About 500 AD	Poompuhar, Tamilnadu (probably due to Krakatau eruption)	79.52	11.12			4			Wikipedia
3	900 AD	Nagapattinam, Tamilnadu (may be from Sunda-Andaman arc)	79.53	10.46			4			Kalaki Krishnamurthy
4	1008	Iranian Coast	60	25		1	4			Murty et al. (1999)
5	1762.04.12	Bay of Bengal (Bangladesh)	92	22		1	4		>2 (1)	Mathur (1988)
6	1819.06.16	Kutch	26.6	71.9	Mw 7.8	1	3			Macmurdo
7	1842.11.11	N.Bay of Bengal	90	21.5		1	4		(3)	Oldham (1883)
8	1845.06.19	Kutch	23.6	68.37		1	3			Nelson
9	1847.10.31	Little Nicobar Island	93.667	7.333	Mw 7.5-7.9	1	3			Berninghausen (1966), Heck,1947
10	1868.08.19	Andaman Islands	92.73	11.67		1	4		4	NGDC/NO AA
11	1874	Sunderbans (Bangladesh)	89	22		1	2			Mihir Guha, Free Journal
12	1881.12.31	W. of Car Nicobar	92.43	8.52	Mw 7.9	1	4		1.2	Berninghausen (1966), Ortiz and Bilham (2003)
13	Jan. 1882	Sri Lanka (may be from Indonesia)	81.14 E	8.34		1	3			Berninghausen (1966)
14	1883.08.27	Krakatau (Volcanic Eruption)	105.25	-6.06		6	4	4.5	2	Berninghausen (1966)
15	1884	W. of Bay Of Bengal								Murty et al. (1999)
16	1935.05.31	Andaman-Nicobar			Mw 7.5	1	4		(1)	NGDC/NO AA
17	1935.11.25	Andaman-Nicobar	94	5.5	Ms 6.5	1	2			NGDC/NO AA
18	1941.06.26	Andaman Islands	92.5	12.1	Mw 7.7	1	4		1.25	Bilham et al. 2005
19	1945.11.27	Makran Coast	63.5	25.2	Mw 8.0	1	4		17	Murty et al. (1999)
20	1983.11.30	Chagos ridge	72.11	-6.85	Mw 7.7	1	4		1.5 (2)	NGDC/NO AA
21	2004.12.26	Off west coast of Sumatra and Andaman-Nicobar	95.947	3.307	Mw 9.3	3	4	3.0	30	NGDC/NO AA

In the Table 4, I is tsunami intensity, max. run-up is in meters, reported number of run-ups are given within brackets. According to Rastogi et. al. (2006), the data are taken from National Geophysical Data Center (NGDC); National Oceanic and Atmospheric Administration (NOAA) and National Environmental Satellite, Data, and Information Service (NESDIS). A "-1" is used as a flag (missing) value in some fields. The cause and probability of the tsunamis are shown by "Cau." and "Pro." respectively. The cause and probability of the tsunamis are given by following codes.

Cause Code: Cause code indicates the cause or source of the tsunamis. Valid values: 1 to 12 .

Meanings of different cause code, probability etc. are given below:

- 1 = earthquake
- 2 = questionable earthquake
- 3 = earthquake and landslide
- 4 = earthquake and volcano
- 5 = earthquake, volcano and landslide
- 6 = volcano
- 7 = volcano and earthquake
- 8 = volcano and landslide
- 9 = volcano, earthquake, and landslide
- 10 = landslide
- 11 = meteorological
- 12 = explosion

Event Probability:

Probability of actual tsunami occurrence is indicated by a numerical rating of the validity of the reports of that event:

Valid values: 0 to 4

- 4 = definite tsunami
- 3 = probable tsunami
- 2 = questionable tsunami
- 1 = very doubtful tsunami
- 0 = erroneous entry

Tsunami Magnitude: Tsunami magnitude, M_t is defined in terms of tsunami-wave amplitude by Iida et al. (1967) as, $M_t = \log_2 H_{\max}$.

Tsunami Intensity: Tsunami intensity scales have been suggested based on its effect and damage caused by it. There are many formulae for intensity based on tsunami run-ups. Tsunami intensity is defined by Soloviev and Go (1974) as, $I = \log_2 (21/2 * h)$, where "h" is the maximum run up height of the wave.

6. Earthquake of December 26, 2004

On 26th December 2004, the most devastating tsunami in the Indian Ocean has been recorded in the history. The tsunami was triggered by an earthquake of magnitude M_w 9.3 at 3.316°N, 95.854°E off the coast of Sumatra in the Indonesian Archipelago at 06:29 hrs making it the most powerful in the world in the last 40 years (ICMAM, 2005).

The earth-quake that primarily measured 8.9 on the Richter Scale of the West Coast on Northern Sumatra set off a series of other earthquakes lasting 12 hours on the 26th of December, 2004 led to widespread catastrophe particularly in Sri Lanka, India, Maldives, Indonesia and Thailand with damage also in Malaysia, Bangladesh, Somalia and Seychelles. The 9.0 Earthquake at 6.58 hours at the epicenter (and in Sri Lanka) led to a sequence of 15 other quakes across the Andaman region.

The earthquake took place at the interface between the Indian and Burma plates, where Burma plate has been referred by Andaman/Nicobar ridge that acts as a small tectonic plate (Curry et al., 1982). In this region, the Burma plate is characterized by significant strain partitioning due to oblique convergence of the India and Australia plates to the west and the Sunda and Eurasian plates to the east. It is a typical oceanic-oceanic convergent plate boundary (Figure 3) where the Indian plate moving at a rate of 5 cm a year relative to the Burma plate came together collided and the Indian plate dived (subducted) under the Burma plate (Figure 14). Two major plate tectonic features on either side of a narrow strip show the high seismically activeness of the region.

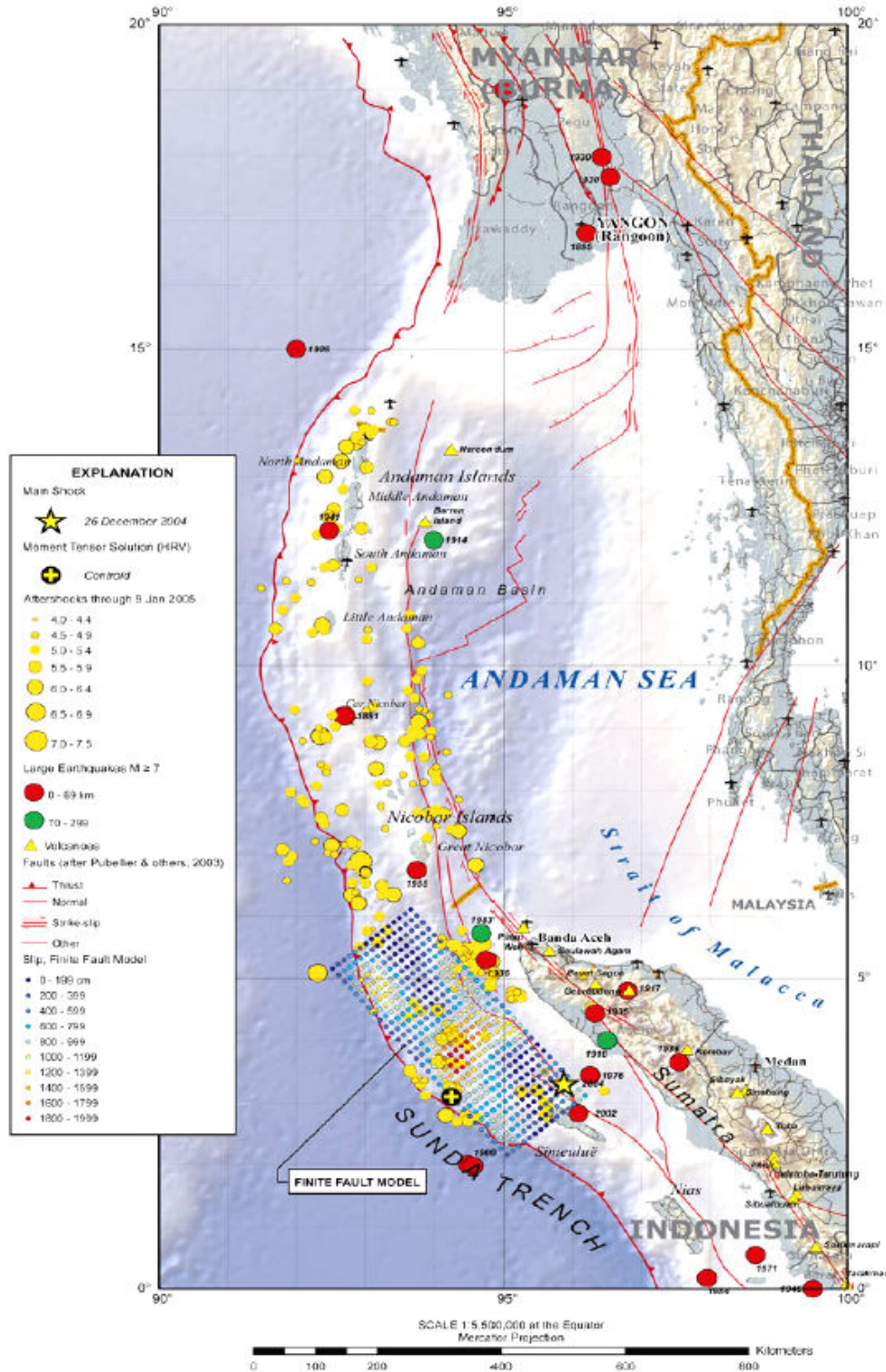


Figure 14: Base Map of the Sumatra Subduction Zone showing Seismicity associated with 2004 Earthquake (After ICMAM,2005)

The collision is due to compression between the Indian and Burmese plates. The initial 8.9 eruption happened near the location of the meeting point of the Australian, Indian and Burmese plates. Scientists (after ICMAM, 2005) have shown that this is a region of compression as the Australian plate is rotating counterclockwise into the Indian plate. This also means that a region of seismic activity has become active in the South Eastern Indian Ocean. A lethal combination of huge magnitude and shallow depth focus led to high vertical displacement of the Burma plate that acted like a great piston deforming the sea.

The earthquake originated along the boundary between the Indian/Australian and Eurasian tectonic plates, which arcs 5,500 kilometers (3,400 miles) from Myanmar past Sumatra and Java toward Australia. History reveals that the subduction megathrust does not rupture all at once along the entire 5,500-kilometer plate boundary. The U.S. Geological Survey (Caltech, 2004) reports that the rupture began just north of Simeulue Island. From the analysis of seismograms, Caltech seismologist Chen Ji (Caltech, 2004) has found that from this origin point, the major rupture propagated northward about 400 kilometers (249 miles) along the megathrust at about two kilometers per second. By contrast, the extent of major aftershocks suggests that the rupture extended about a thousand kilometers (620 miles) northward to the vicinity of the Andaman Islands. During the rupture, the plate on which Sumatra and the Andaman Islands sit lurched many meters westward over the Indian plate.

7. Historical Tsunamis in the Bay of Bengal

Though the Indian subcontinent is in a seismically active region, tsunamis along the coastline of India and Bangladesh have been rare, but not unprecedented.

The historical records suggest that on night of 11th and 12th October, 1737 a furious hurricane stroke at the mouth of the river Ganges. At the same time a violent earthquake triggered throwing down a great many houses along the river at Kolkata. The water rose to 40ft higher than the usual level in the river Ganges (Gentlemen's Magagine, 1738-1739) (after Khan, 2007).

In earliest known and well documented tsunami in the Bay of Bengal (Mathur, 1998) occurred in 02 April 1762, caused by an earthquake on Myanmar's, Arakan Coast. The epicenter is believed to be 40 km SE of Chittagong, or 61 km N of Cox's Bazaar, or 257 km SE of Dhaka,

Bangladesh. The earthquake triggered on April 2, 1762 was felt all over Bengal and more severely in the northern part of the east coast of the Bay of Bengal. This earthquake had thrown volumes of water and mud from the fissures. At a place called Bakerchanak near the coast, a tract of land sank, and 200 people with all their cattle, were lost. In the northwest coast of Chedua island, about 22 ft above sea level, there said to have caused a permanent submergence of 60 square miles near Chittagong (Bangladesh District Gazetteers Chittagong, 1975) (after Khan, 2007). The Arakan coast was elevated for more than 160 km. The water in the Hoogly River in Kolkata rose by two meters. The rise in the water level at Dhaka was so sudden that hundreds of boats capsized and many people were drowned. This is the earliest well-documented tsunami in the Bay of Bengal.

An earthquake on 11th November 1842 near the northern end of Bay of Bengal (Rastogi et. al., 2006) caused a tsunami by which waters of the distributaries of the Ganges Delta were agitated. Boats were tossed about as if by waves in a squall of wind.

Guha, former Director General of the India Meteorological Department, indicated that a tsunami struck Sunderbans (Bangladesh) in May 1874, killing several hundred thousand people (<http://www.freejournal.net>). It was the result of an earthquake in Bhola district. Earthquake and tsunami both played havoc in vast areas of Sunderbans, 24-Prganas, Midnapore, Barishal, Khulna and Bhola (Rastogi et. al., 2006). Even Kolkata felt its impact. It was the same year that the meteorological center in Alipore was set up. However, no written record of such an earthquake or tsunami is available.

The December 1881 tsunami in the Bay of Bengal has been studied in detail by Roger Bilham of the United States and Modesto Ortiz of Mexico (Berninghausen, 1966). The earthquake of magnitude Mw 7.9 occurred at Car Nicobar Island on 31 Dec. 1881. A tsunami was generated by this earthquake in the Bay of Bengal. Though the run-ups and waves heights were not large, its effects were observed in the Andaman & Nicobar Islands and were recorded on the east coast of India (Rastogi et. al., 2006). Waves attributed to this tsunami were also observed at Batticaloa and Trincomalee on the east coast of Sri Lanka (Berninghausen, 1966). No tsunami was reported from tidal gauges in Myanmar (Ortiz and Bilham, 2003). Analysing the data from eight tide gauges surrounding the Bay of Bengal at that time, they conclude that the tsunami generated had

a maximum wave height - what is known as the tsunami 'run-up' - of 0.8m - 1.0m. These analyses of the amplitude and waveform of the tsunami indicates that the 7.9 magnitude quake was due to a 2.7m slip of a 150 km long rupture in the subduction front on the Indian/Andaman plate boundary off Car Nicobar, which resulted in a 10-60 cm uplift of the island. The results of their simulation appears to match fairly well with the original tide gauge data of the wave heights at various points, which they have been able to retrieve from archival sources. The analysis shows that wave heights reached were of the order of 0.5 m and the tsunami waves arrived about 4 hours after the event. The source of the waves was about 2,440 km from the Indian coast. Unofficial accounts have placed the wave height at Chennai to be about 1.5 m.

A tsunami was noticed at Dublet (mouth of Hoogly River) near Kolkata (Rastogi et. al., 2006) due to earthquake in the western part of the Bay of Bengal in 1884 (Murty et al. 1999) that reached up to Port Blair.

The next major earthquake that resulted in a tsunami in the Bay of Bengal was of magnitude 8.1 earthquake in the Andaman Sea (12.9°N, 92.5°E) in June 1941(Rastogi et. al., 2006) and the tsunami did hit the east coast of India, damaging masonry structures and property in places like Chennai. It had a magnitude of 7.7 (Mw). It was centred in the Bay of Bengal, roughly, 20.5 kilometres W of Flat Island, India. The quake ruptured the region near the Andaman Island. The number of dead in this event is not. On the basis of non-scientific and journalistic sources, Murty and Bapat (1999) suggest that the height of the tsunami wave was of the order of 0.75-1.25 m. Tremors from the earthquake were felt in cities along the Coromandel (eastern) coast of India and even in Colombo, Sri Lanka. Tremors were also experienced at Calcutta (now Kolkata), Chandernagar, Cuttack and also at Sylhet, Bangladesh.

The impact of Sumatra-Andaman earthquake and consequent tsunami of December 2004 was also felt all over Bangladesh. It was reported that all the water bodies of the country including the Bay of Bengal were agitated for about 2 hours and riverbeds were found to be elevated at few places by few meters. Some buildings in Chittagong got cracked and two deaths were caused in the coast.

8. Evaluation of Tsunami Potential in Bangladesh

Infrequent occurrence of tsunamis in the Bay of Bengal region kept the geoscientists of this region almost unconcerned about the potentiality of tsunami hazard. According to the Geological Survey of Bangladesh (www.ioc3.unesco.org), there are some evidences of Paleo-Tsunamis and low height tsunamis, but evidences of devastating tsunamis are not available. From the historical records it has been found that Bangladesh has experienced few major tsunamigenic earthquakes of magnitude between 7 and 8. From the Seismotectonic point of view, Bangladesh is located in a quite vulnerable zone. Now, the question is, the seismicity and other preconditions related to the generation of tsunami how far contributes in the context of Bangladesh. However, the above records do not justify strongly whether the coastal belt of Bangladesh is tsunamigenic or not. Considering the orography of the continental shelf, water depth, and tectonic framework of the Bay of Bengal, tsunami vulnerability status needs to be recast.

8.1 Risks from Indian Ocean

Eighty percent (Rastogi et. al., 2006) of the tsunamis of the Indian Ocean originate in Sunda Arc covering Java and Sumatra. The Sunda belt extends northward to Andaman-Nicobar Islands where a few tsunamis have originated. Further north, Bangladesh-Myanmar coast has produced some well-documented tsunamis. Along the Sunda arc, great earthquakes of magnitude 8.5 or greater can repeat every two centuries at a site but smaller tsunamigenic earthquakes can repeat every few decades. Figure 15 (USGS, 2005) shows the Seismicity of North-East Indian Ocean region.

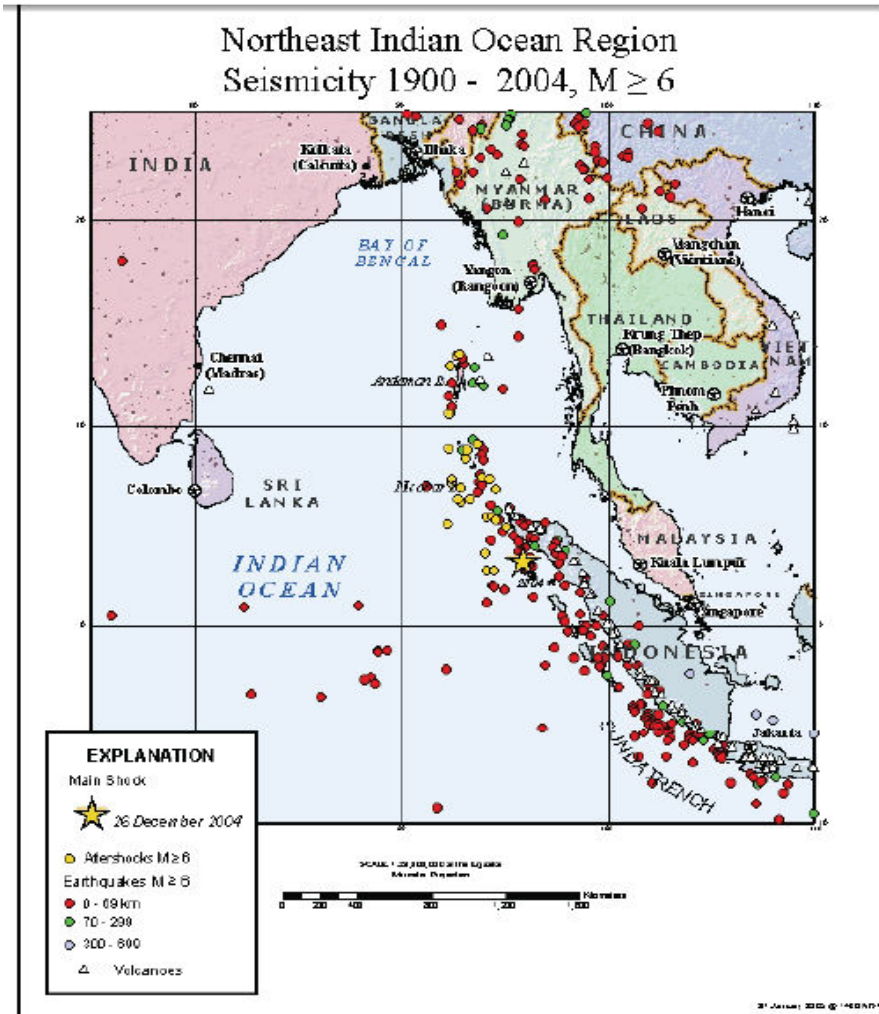


Figure 15: North-East Indian Ocean Seismicity

Along the Andaman–Sumatra trench the convergence rate is 15–20 mm/yr, giving return periods of 400 yr for $M 8.5$ earthquakes, with a slip of around 8 m (Caltech, 2004). However, some great earthquakes have occurred more frequently: $M 8.5$ earthquakes of 2005 occurred at the rupture zone of $M 8.7$ earthquake of 1861, and rupture zone of the 1833 $M 8.7$ earthquakes encompassed the 1797 $M 8.2$ earthquake rupture zone. Though smaller tsunamigenic earthquakes of magnitude 7.5 to 8.0 have occurred more frequently, but at intervals of over a few decades, like 1907 and 1935, major earthquakes occurred near the 1861 source zone. From these considerations the probability of a severe tsunami hitting through Bay of Bengal and the regions in vicinity, within a couple of decades, from Andaman–northern Sumatra region appears to be low, which has already produced 2004 and 2005 great earthquakes. Moreover, though the fault mechanism solutions of number of earthquakes along Andaman-Nicobar Island south of Port Blair show

dominancy in thrust fault rupture but that of the North of Port Blair is considered to be mostly strike-slip. It indicates that North of Port Blair zone is less potential of creating any tsunami. The southern Sumatra segment is rather a potential zone for a great earthquake. Figure 16 (USGS, Seismo.html) shows the section of the subduction megathrust that runs from Myanmar southward across the Andaman Sea, then southeastward off the west coast of Sumatra, that has produced many large and destructive earthquakes in the past two centuries

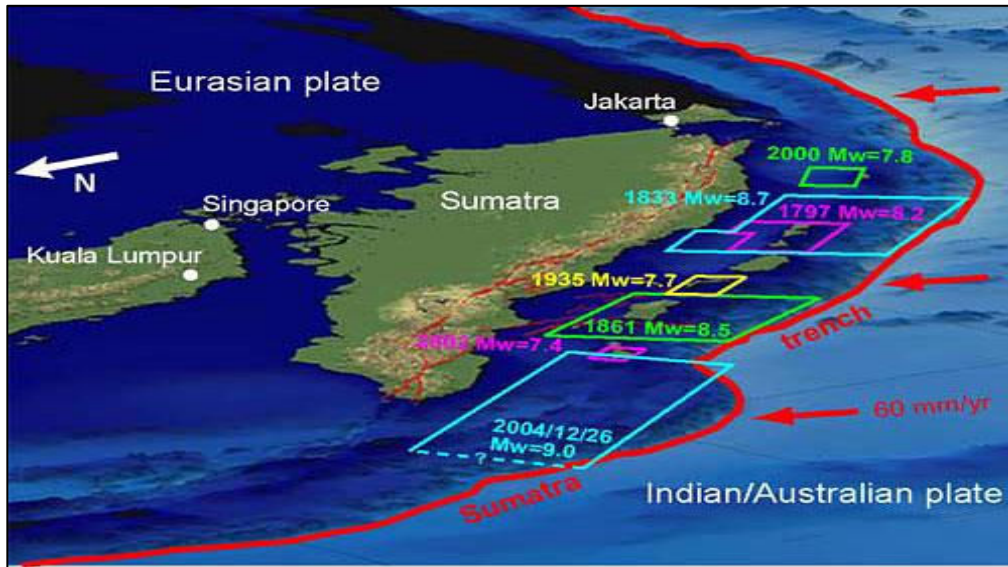


Figure 16: Section of the Subduction Megathrust in Indian Ocean

The 2004 earthquake was generated by the seismic rupture of only the northernmost portion of the Sumatran section of the megathrust. Therefore, the fact that most of the other part of the section has generated few great earthquakes in more than a hundred years is worrisome. Paleoseismic research (Caltech, 2004) has shown that seismic ruptures like the one in 1833 (rupture of a long segment offshore central Sumatra produced an earthquake of about magnitude 8.7 and attendant large tsunamis), for example, recur about every two centuries. Thus, other parts within the section of this fault should be considered dangerous over the next few decades. During rupture of a subduction megathrust, the portion of Southeast Asia that overlies the megathrust jumps westward (toward the trench) by several meters, and upward by 1-3 meters (3-10 feet). This raises the overlying ocean, so that there is briefly a "hill" of water about 1-3 meters high overlying the rupture. The flow of water downward from this hill triggers a series of broad ocean waves that are capable of traversing the entire Bay of Bengal. When the waves reach shallow

water they slow down and increase greatly in height--up to 10 meters (32 feet) or so in the case of the December 26 earthquake--and thus are capable of inundating low-lying coastal areas.

Again the plate tectonics theory predicts that great earthquakes recur at the plate boundaries more or less regularly. So, the probability of a 2004-sized tsunami on the Indian coast may continue to be negligible. But the current mega disaster has thrown new light on threat perceptions in the region from distant tsunamis in the Indian Ocean since tsunami run-up from 2004 earthquake also affected the distant shorelines of eight nations: Thailand, Sri Lanka, Myanmar, Malaysia, Bangladesh, the Maldives, Kenya, and Somalia.

8.2 Factors Affecting Tsunami Potential in Bangladesh

a. Geodynamics and Tectonics of Bangladesh

Geologically, the Bengal basin is the result of convergence of three lithospheric plates namely Indian Plate, Eurasian Plate and Burmese Plate-let/plate (Hasan et. al., 2007). Bangladesh within the Indian Plate which, at the eastern end, runs southward along a large dextral strike slip fault and continues through Burma to connect with the subduction of the Indian Plate under the Indonesian Plate.

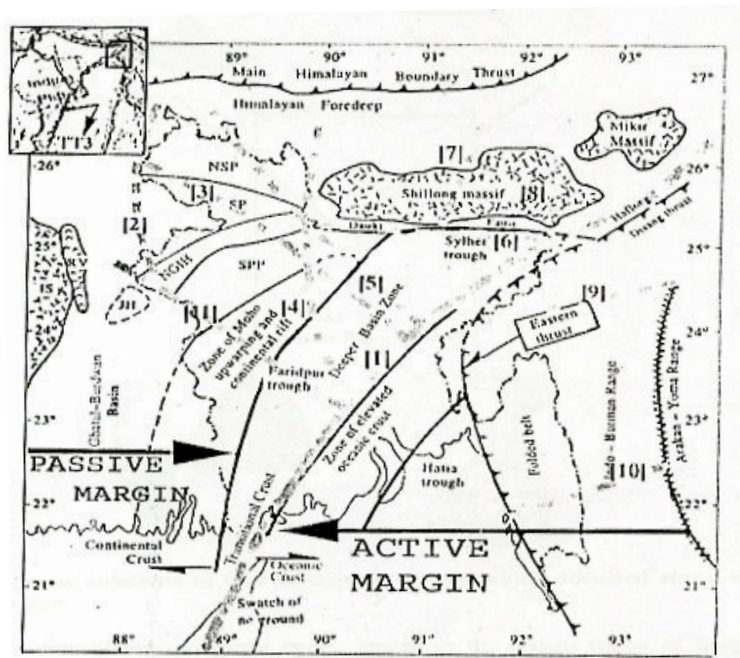


Figure 17: Tectonic classification of the Bengal basin

The different rates and direction of convergence of these plates (Figure 17, after Hasan et. al., 2007) as well as the rotational nature of Indian Plate greatly influenced the Bengal Basin in its geodynamic sense. The pull-apart segments of lithospheric plate beneath the Andaman-Nicobar and Arakan-Yoma tectono-stratigraphic province exhibit the oblique (both strike-slip and thrust) motion during the convergence. The fault plane solution of the earthquake events located in the eastern region of Bangladesh demonstrates dominantly strike-slip fault mechanism. The strike-slip fault solution for most of the earthquake events in the eastern region of Bangladesh is indicative of a changing pattern from convergence and subduction to strike-slip displacement in the Bengal basin. Again the earthquakes located in the Western Coast of Bay of Bengal (Table 5, after Hasan et. al., 2007) also show the strike-slip fault dominancy. Hence, characteristically the most Bay of Bengal region does not fulfill the major criteria for the generation of any potential tsunami.

Table 5: Four Earthquakes located in the Western Coast of Bay of Bengal

Event No	Date	Location	Focal Depth	Nature of Faulting
1	Nov 24, 1972	11.7 N 85.4 E	50	Strike-slip
2	Aug. 30, 1973	15 N 84.3 E	43	Strike-slip
3	Jun. 23. 1976	21.5 N 88.7 E	50	Strike-slip
4	Jul. 01, 1985	18.4 N 87.2 E	10	Strike-slip

Besides this, Hasan et. al. (2007) have identified that some favorable geological conditions such as thick sedimentation in the Bay of Bengal, thick sedimentation in Bengal fan (Figure 18), high density of seawater around/along the coast (suspended load) and anticlockwise oceanic current at Bay of Bengal (winter time) which reduced the effect of Sumatra 2004 tsunami and will also provide further protection against tsunami in future.

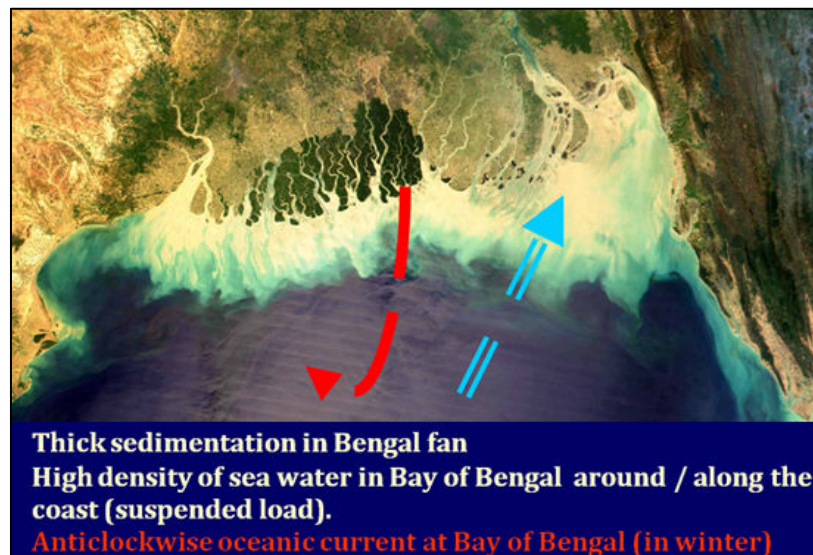


Figure 18: Thick Sedimentation in Bengal fan

In addition, once the large amount of pent-up energy in the compression zones of the plate boundaries have been released, it takes another buildup of energy for another event of similar magnitude. This is unlikely in the short-term. Since a large amount of pent-up energy in the compression zones along the plate boundaries has been released in the recent earthquake of 26th December 2004, it will take years for another incident of the same magnitude to recur.

b. Distance from Epicenter and Tsunami Energy Dissipation

It is presumed that if any tsunamigenic earthquake occurs in the Sunda Arc, the most seismically active zone near the Indian Ocean, it would have very less probability of affecting Bangladesh due to being at a long distance from the epicenter of the earthquake, the coast will be hit by greatly reduced energy of the tsunami wave (Figure 19, after Khan et.al., 2005). On the other hand, the plate boundary near Bangladesh, the principal source of tsunamigenic fault is north-south oriented which is along the direction of rupture zone on the northern, north-trending segment of December 2004 tsunamigenic earthquake hypocenter. Since tsunami amplitudes are largest perpendicular to the fault, tsunami may not be substantial in Bangladesh from this fault zone.



Figure 19: Bathymetry of Bay of Bengal

c. Influence of Location and Topography

The impact of Tsunami is influenced by the arrival time of the Tsunami waves from generation point and difference in the tidal heights of waves generated at the coastal sites. From the observation made by six tidal gauges established along the east coast of India by Survey of India (SOI observations), it was found that the extent of damages occurred at different ports from Sumatra Earthquake, have been clearly determined by unobstructed straight line location of the site from the epicenter of the earthquake and the continental slopes at the tide gauge sites. It was also found that the locations, in spite of being in the direct line from epicenter, where the underwater topography was gentle rather than being abrupt, there the tidal waves raised less. This finding leads to the assumption that the tsunamigenic earthquakes generated to the south eastern Indian Ocean will be obstructed before hitting Bangladesh which lies at the northern end of Bay of Bengal and the steep continental slope (avg. 17 km width) will reduce the propagating tsunami wave to the coast.

d. Influence of Continental Shelf in Bangladesh

Continental shelves are regarded as portions of continental masses which are locally submerged. They are very flat, with gradient less than 1:500 (Banglapedia, 2004). The width of the continental shelf off the coast of Bangladesh varies considerably. It is less than 100 km off the south coast of Bangladesh, between Hiron Point and the Swatch of No Ground and more than 250 km (Banglapedia) off the coast of Cox's Bazar. Seabed evidence suggests that the dominant transport of fine-grained sediment on the continental shelf of Bangladesh is from south and west. Sediments are fine seaward and westward with the thickest accumulation of mud near the submarine canyon, Swatch of No Ground. Most of the continental shelf of Bangladesh is covered by silt and clay. The shallow part (less than 20m) of the continental shelf off the coast of Chittagong and Teknaf is covered by sand and the intertidal areas show well-developed sandy beaches. Sand waves observed on the continental shelf in this area have considerable relief (3-5m) (Banglapedia), implying a high-energy environment. Even the shallower part of the southern continental shelf off the coast of the Sundarbans, Patuakhali, and Noakhali is covered by silt and clay; and extensive muddy tidal flats are developed along the shoreline. Some of the shoals and sand ridges present on this part of the continental shelf show an elongation pattern pointed towards the Swatch of No Ground. This indicates that even under present oceanographic conditions, sediments are being tunneled to the deeper part of the Bay of Bengal through the Swatch of No Ground.

It can be considered that the 200 km long continental shelf with a gradient 0.5 m/km in the upper 100 km zone and a gradient 2 m/km in the lower 100 km zone and then an abrupt shelf break with a gradient about 20 m/km acts as a potential barrier to the motion of the stressed water column.

e. Influence of other Tsunami Generating Sources

Swatch of No Ground and eastern canyon shoulder of Bengal Basin show layers of sediments with intercalated slump deposits and also growth faults. The growth faults indicate the instability of the canyon wall. Although there is no record of tsunami that originated from Swatch of no ground, there are records of slumps and growth faulting (Hasan et. al., 2007).

Thus detail investigation and study are needed to determine its potential for tsunami generation

The east side of Maheshkhali Island has a very narrow coastal area on the bank of the Maheshkhali Channel and fringed by the hill range. In Maheshkhali, in very recent years, two earthquakes of magnitude 5.2 and 4.3 (Hasan et. al., 2007) occurred. The eastern flank of Maheshkhali Anticline is faulted. There is a probability of earthquake triggered landslide in the eastern side of this Island, which may create local tsunami in the closed Maheshkhali Channel with some devastating effect on the Cox's Bazar coastal area. However, the depth of the channel is shallow in relation to generating devastating tsunami.

8.3 Tsunami Hazard Assessment of ICZMP

Considering the state of tsunami vulnerability and potential seismic sources, the coastal belt is classified into three tsunamigenic zones as shown in Figure 20 (ICZMP Report, Uddin, 2005)

The zones are:

- a) *Tsunami Vulnerability Zone - I: Chittagong-Teknaf coastline-Most vulnerable.* The intradeltaic coastline is very close to the tectonic interface of Indian and Burmese plates. The active Andaman-Nicobar fault system is often capable of generating tsunami waves
- b) *Tsunami Vulnerability Zone – II: Sundarban-Barisal coastline–Moderately vulnerable.* This old deltaic belt is vulnerable to local tsunamis due to presence of Swatch of No Ground.
- c) *Tsunami Vulnerability Zone – III: Barisal- Sandwip estuarine coastline – Low vulnerability.* The estuarine coastal belt considered to be less vulnerable due to presence of numerous islets and shoals in the upper regime of the continental shelf.

The classification reveals that Bangladesh coast has been identified as low to high vulnerable to tsunami hazards. The Cox's Bazar coast falls within Zone-I, which is reportedly most vulnerable. However, evaluation of the potential tsunami hazard requires analysis of tsunami wave propagation from the potential tsunami sources Analysis performed for tsunami propagation under this project is discussed in the following sections.

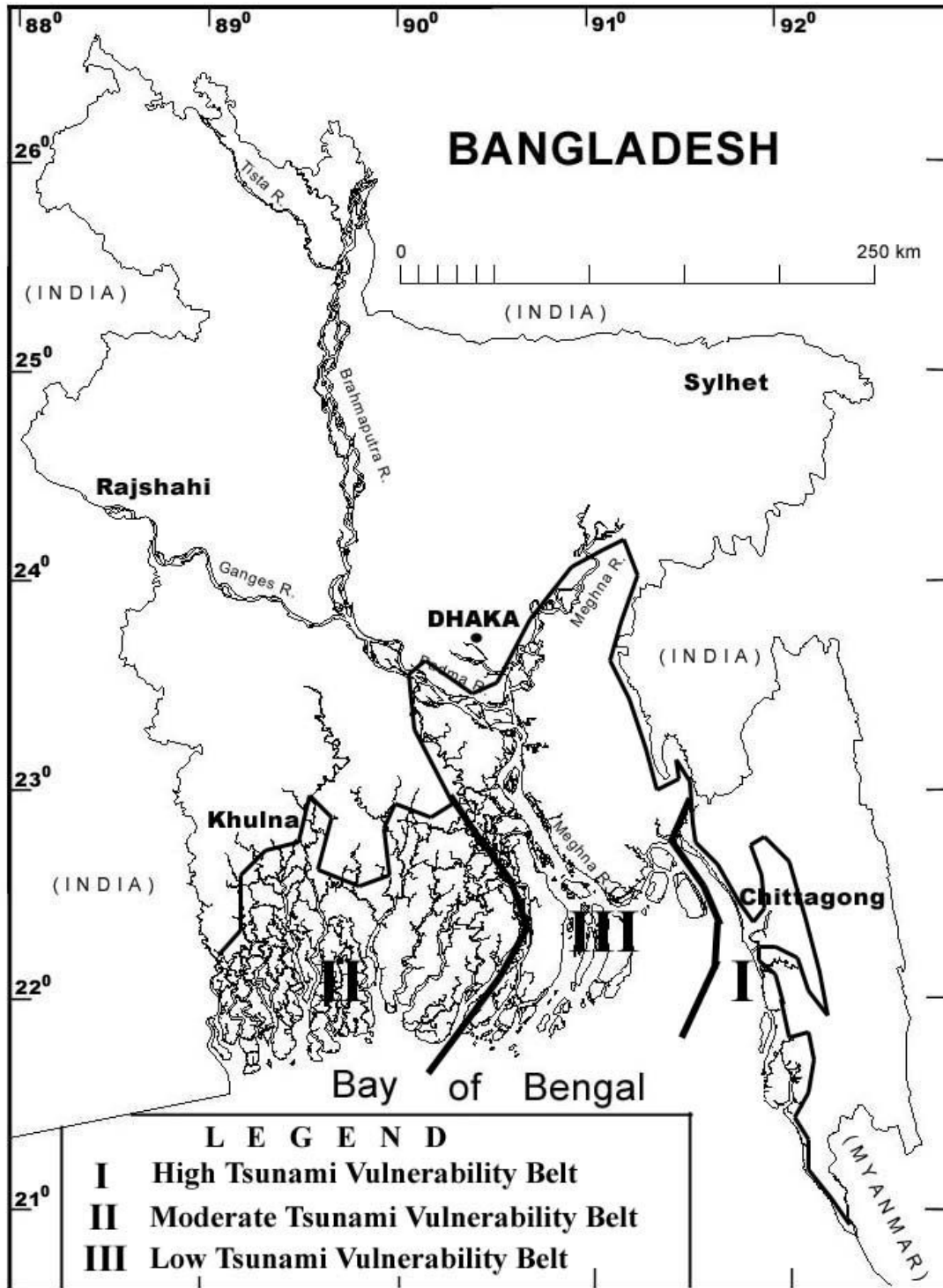


Figure 20: Tsunami Vulnerability Map of Bangladesh (Uddin, 2005)

9. Analysis of Tsunami Propagation

After generation of tsunami due to earthquake, water propagates around the source and if the propagation is not influenced by the topography it would propagate radially like a wave generated by a stone dropped in a pond. However, if the topography restricts the propagation of the water, the wave disperses in various directions. This may be one reason why the tsunami 2004 did not hit Bangladesh. From the source of tsunami (i.e. Sumatra), no radial line could be drawn to the Bangladesh Coast as shown in Figure 21.

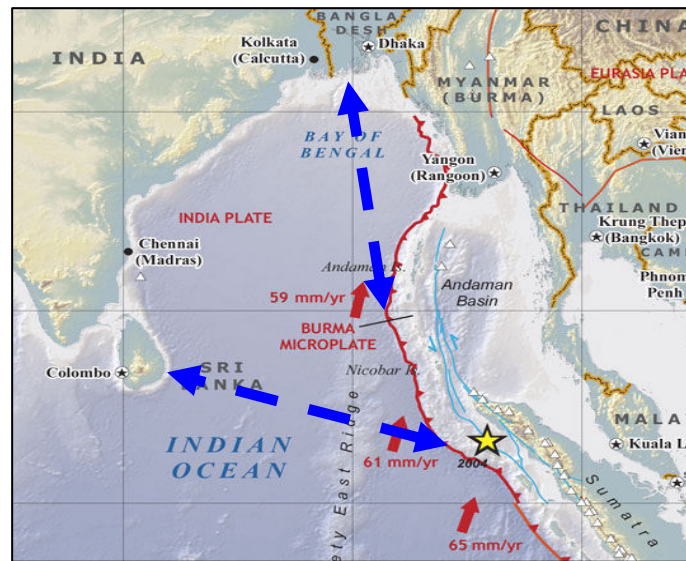


Fig 21: No radial line could be drawn to the Bangladesh Coast from Sumatra

However a radial line can easily be drawn up to Sri Lanka. Thus Sri Lanka was the most severely affected by the tsunami. A radial line to Bangladesh Coast can be drawn if an earthquake occurs in Andaman area, which may affect the Bangladesh Coast. However other factors like continental slope, continental shelf and ocean topography can influence the tsunami propagation to the coast of the Bay of Bengal.

In the present study, assessment of tsunami hazard at the Cox's Bazar coast has been performed through numerical modeling. The entire calculation was performed by a two step approach. The first step was to calculate the wave propagation from different potential sources of tsunami in the Indian Ocean, in order to obtain the wave height distribution along the Bangladesh coast. A computation domain consisting of coarser grid was used for this purpose. The second step was to

calculate tsunami run-up considering the local topographical features to determine the inundation map. For this part calculation with finer mesh was required.

For the first part of the computation a 2D numerical model based on Boussinesq wave model was used. The bathymetry, covering from 70⁰E to 84⁰E and 20⁰N to 120⁰N extracted from ETOPO2 dataset with a resolution of 2 minute was used. This would include the December 26, 2004 Sumatra tsunami source in the south and entire Bangladesh coast in the north. The breaking and run-up of tsunami was not considered at this stage. To exclude the possible effects of reflection from the southern boundary calculation was stopped before it affected the results.

From this computation, tsunami arrival time as well as wave height distribution along the coastline at the Cox's Bazar coast of Bangladesh was determined. Also, the approach velocity of tsunami propagation was obtained at this stage. The first part of the calculation was performed for several potential sources of tsunami which was determined from historic evidences. For those cases where the wave height distribution was significant near the coast the second stage of the calculation was performed.

In the next stage, tsunami run-up was calculated using a 3D model where the wave height distribution and tsunami approach velocity, obtained from the first stage of calculation, was utilized as the input flux at the open boundary. This computation was performed using finer grids and included the effects of local topographic features.

9.1 Modeling Tsunami Propagation

In this section some aspects of numerical model for tsunami propagation will be discussed.

9.1.1 Formulation of a Numerical Model

Research Review

Numerical simulation of tsunami has been running back decades since the importance of understanding the increasing threat of tsunamis were felt around the world. Following discussion will review of some tsunami numerical simulations, which introduced key turning points in numerical modeling.

Compared to the wave length and the wave height, tsunami can be considered as a long wave in the deep ocean since it has a wave length of several hundreds of kilometers, the depth to length ratio is in the order of 10⁻² and the wave steepness is in the order of 10⁻³

Hence according to Kajiura (1963), Aida (1978), Imamura (1995) showed that in the theory of long waves, the vertical acceleration of the water particles are negligible compared to the gravitational acceleration except for propagation over a continental shelf or propagation in a river. Consequently the vertical movement of water particles has no effect on the pressure distribution. Hence depth integrated equations are widely used as governing equations for tsunami propagation simulations. The following shallow water wave equation by Imamura (1995) was introduced for tsunami propagation calculations;

$$\frac{\partial \eta}{\partial t} + \frac{\partial P}{\partial x} + \frac{\partial Q}{\partial y} = 0 \quad \text{Eq (1)}$$

$$\frac{\partial P}{\partial t} + \frac{\partial}{\partial x} \left(\frac{P^2}{d} \right) + \frac{\partial}{\partial y} \left(\frac{PQ}{d} \right) + gd \frac{\partial \eta}{\partial x} + \frac{\tau_x}{\rho} = A \left(\frac{\partial^2 P}{\partial x^2} + \frac{\partial^2 P}{\partial y^2} \right) \quad \text{Eq (2)}$$

$$\frac{\partial Q}{\partial t} + \frac{\partial}{\partial y} \left(\frac{Q^2}{d} \right) + \frac{\partial}{\partial x} \left(\frac{PQ}{d} \right) + gd \frac{\partial \eta}{\partial y} + \frac{\tau_y}{\rho} = A \left(\frac{\partial^2 Q}{\partial x^2} + \frac{\partial^2 Q}{\partial y^2} \right) \quad \text{Eq (3)}$$

Where x and y are horizontal coordinates and z is the vertical coordinate. η is vertical displacement of water surface above the still water level (Fig 22) , g is the acceleration of gravity, d is the total water depth given by $d=h+\eta$, where h is the water depth. Where τ_x and τ_y are bottom frictions in the x and y directions. A is the horizontal eddy viscosity which is assumed to be constant in space and time.

M and N are considered as depth averaged water discharge across the unit width of model domain given as;

$$M = \int_{-h}^{\eta} u dz = \bar{u} d \quad N = \int_{-h}^{\eta} v dz = \bar{v} d$$

Where \bar{u} and \bar{v} are depth average water velocities in x and y directions respectively.

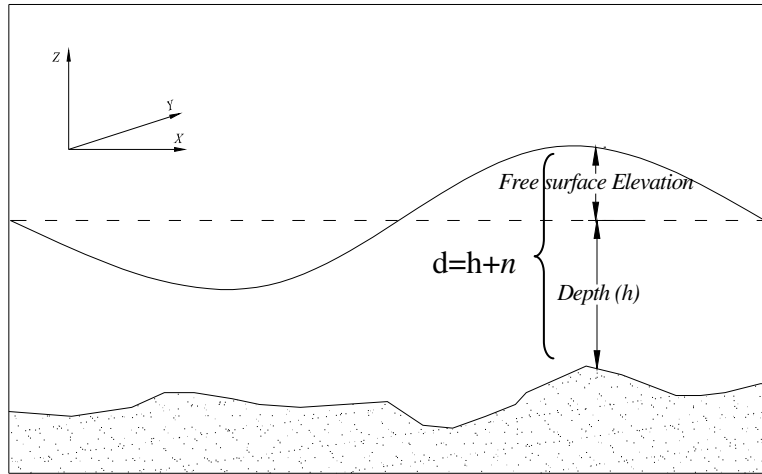


Fig 22: Space domain of the governing equations

However based on very small wave height to length ratio and wave steepness, tsunami can be considered as a linear long wave in the deep ocean.

Based on the Aida (1978) and Shuto (1991) it is shown that linear long wave theory gives the best representation of the tsunami waves in the deep ocean and even up to a considerable depth in the near shore. Therefore non-linear terms of the above equation 2 and 3 can be dropped in tsunami propagation calculations in Deep Ocean.

As the tsunami approaches shallow water it starts to feel the effect of sea bottom than that of Deep Ocean. Wave steepness becomes high. Hence it starts to deform by disappearing trough and increasing crest. Ultimately the shape of the wave becomes more similar to a solitary wave profile. Such waveforms are generally categorized as N waves. Hence nonlinear effects are important at this stage. According to tsunami wave theory reviewed by Satake (1995), which explains that linearity of waves, are valid even up to 50m depths. Figure 23 shows the applicability range of linear long wave theory according to Bryant (2001).

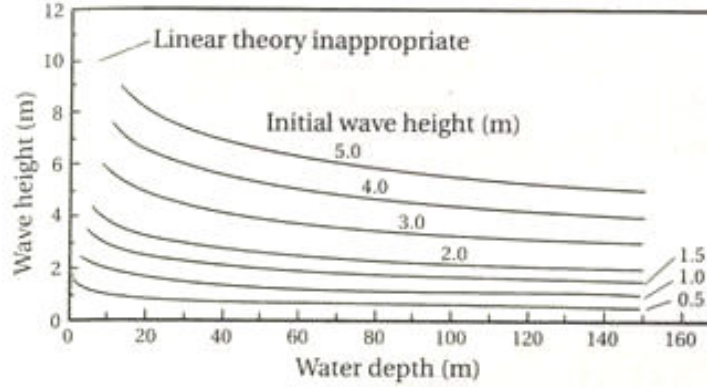


Fig 23: Applicability range of linear long wave theory

Other specialty is since depth of the oceans can never be greater than 5.0 km the majority of the tsunami is considered as shallow water waves. However, all the individual waves resulting in a tsunami generation do not travel by the same speed. Long period waves over run the short period waves, so that a tsunami wave train after traveling across an ocean tends to reach shore with regular long period waves followed by short period waves. This phenomenon is known as dispersion.

Hence in this research, the main calculations are divided into two parts where the linear long wave equation is considered in deep ocean propagation. Calculations in the shallow water are based on the original equation proposed by Imamura (1995).

Tsunami Propagation in Deep Ocean

Following equation has been considered as governing equations in deep ocean propagation

$$\frac{\partial \eta}{\partial t} + \frac{\partial P}{\partial x} + \frac{\partial Q}{\partial y} = 0 \quad \text{Eq (4)}$$

$$\frac{\partial P}{\partial t} + gd \frac{\partial \eta}{\partial x} + \frac{\tau_x}{\rho} = A \left(\frac{\partial^2 P}{\partial x^2} + \frac{\partial^2 P}{\partial y^2} \right) \quad \text{Eq (5)}$$

$$\frac{\partial Q}{\partial t} + gd \frac{\partial \eta}{\partial y} + \frac{\tau_y}{\rho} = A \left(\frac{\partial^2 Q}{\partial x^2} + \frac{\partial^2 Q}{\partial y^2} \right) \quad \text{Eq (6)}$$

Bottom Friction

Commonly used bottom friction formula given by Manning is considered, after Imamura (1995);

$$\frac{\tau_x}{\rho} = \frac{gn^2}{d^{7/3}} M \sqrt{M^2 + N^2} \quad \frac{\tau_y}{\rho} = \frac{gn^2}{d^{7/3}} N \sqrt{M^2 + N^2}$$

Where, n is the Manning's roughness coefficient, which is given by:

$$n = \sqrt{\frac{fD^{1/3}}{2g}}$$

For propagation of tsunami in the deep ocean n can be considered as 0.03. However the effect of bed friction is not much significant in deep ocean propagation.

Coriolis Force

Since the consideration domain is of several thousand of kilometers, it is important to consider the effect of the Earth rotation. Coriolis force is given by Maa (1990);

$$fq_y = 2\Omega \sin(\phi).Q$$

$$fq_x = 2\Omega \sin(\phi).P$$

Where Ω and ϕ are angular speed of earth rotation and altitude of the location being considered respectively. The effect of the rotation of earth is not so significant for tsunami propagation over a short distance close to the equator.

Horizontal Eddy Viscosity

The term A represents the Horizontal Eddy viscosity coefficient. Yan (1987) showed that horizontal eddy viscosity is around $0.001m^2s^{-1}$ for simulation of current field. Anyhow use of high eddy viscosity coefficient tends to result in stable calculation but other hand it tries to damp the wave heights unnecessarily.

9.1.2 Numerical Scheme

From the early stage of developing the numerical simulation, the finite difference based upon the Taylor expansion series has one of the most fundamental and standard numerical methods. In finite difference approach continuous domain is descriptive so that dependent variables exist only in discrete points.

However numerical schemes in marching problems can be divided as explicit and implicit. For explicit scheme only one unknown appears in the difference equation but in implicit scheme there are two or more unknowns appear, requiring simultaneous solution of several equations involving the unknowns.

There are several schemes available for simulation of long waves. Staggered Leapfrog, Crank-Nicholson and two-step Lax-Wendorff. Among them staggered leapfrog is the widely used since it is explicit, stable, efficient and produce enough accuracy in tsunami simulation. Crank-Nicholson is the basic implicit scheme and requires more CPU time compared to leapfrog scheme, Lax-Wendorff method is more popular in modelling shock waves and discontinuous flows, such as tsunami generation due to impact of meteorites.

In this study, staggered leapfrog scheme introduced by Imamura (1995) and Aida (1978) is used in securitizing the linear long wave equation. Following shows the one dimensional discretisation of the linear long wave equation neglecting friction, Coriolis and eddy viscosity terms, which is given for one dimensional case by;

$$\frac{\partial \eta}{\partial t} + \frac{\partial P}{\partial x} = 0 \quad \text{Eq (7)}$$

$$\frac{\partial P}{\partial t} + gd \frac{\partial \eta}{\partial x} = 0 \quad \text{Eq (8)}$$

Dicritization of Equation (7) and (8) are given by:

$$\frac{\lfloor \eta_{j+1/2}^{n+1/2} - \eta_{j+1/2}^{n-1/2} \rfloor}{dt} + \frac{\lfloor M_{j+1}^n - M_j^n \rfloor}{dx} + O(dx^2) = 0 \quad \text{Eq (9)}$$

$$\frac{\lfloor M_{j+1}^n - M_j^n \rfloor}{dt} + g \left(\frac{d_{j+1/2} + d_{j-1/2}}{2} \right) \frac{\lfloor \eta_{j+1/2}^{n+1/2} - \eta_{j-1/2}^{n-1/2} \rfloor}{dx} + O(dx^2) = 0 \quad \text{Eq (10)}$$

Where dx and dt are the model grid size and simulation time step respectively. Where the $O(dx^2)$ is the truncation error of the second order approximation, which is in fact the difference between the partial derivative and its finite differential representation. The point schematics for the numerical scheme and arrangement of the points in staggered leapfrog scheme are shown in the following Figures (24);

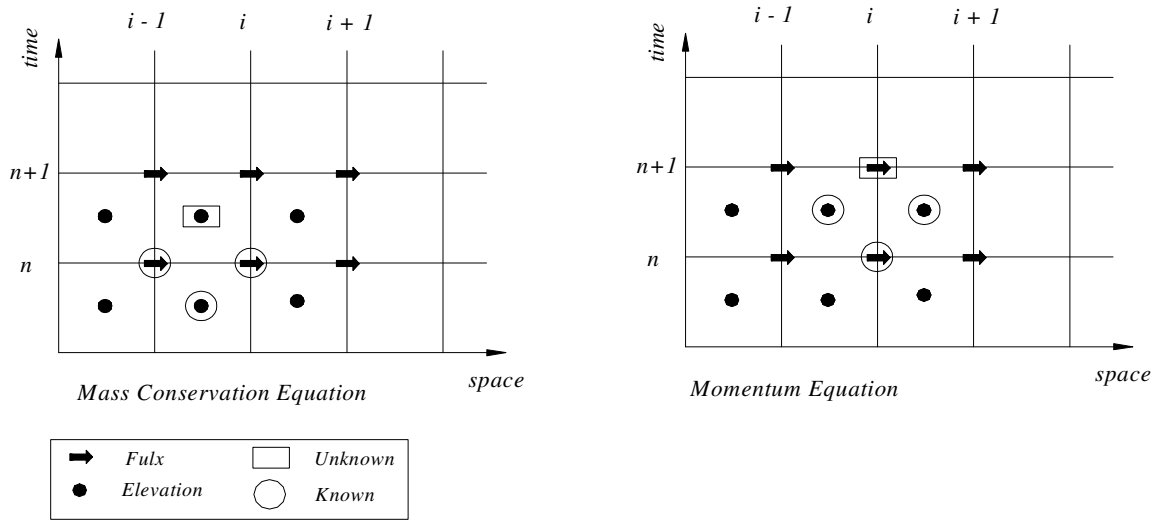


Figure 24: Arrangement of points in staggered leapfrog scheme

Simulation Grid

Selection of grid type, size and cell size is far most important in finite difference models since there is a high tolerance of results in depends upon the model domain, type of grid and cell size. Most commonly used grid is the rectangular grid. However Tsuji (2005) discussed that influence of the curvature of earth is important if the calculation domain has a length more than 1000 km. In that case he suggests using polar coordinate system to represent the governing equations. Grid

size was carefully chosen to make the effects of numerical and physical dispersion equal. Shuto (1991) has suggested that there are at least 20 grid cells to be used in representing one full wave length. Again Shuto (1991) suggest that considering finer mesh and coarser mesh, coarser mesh will give better approximation in representing the linear long wave.

Imamura et al. (1990) showed that the choice of the grid size can be evaluated using the Imamura number, I_m , defined as;

$$I_m = \frac{dx \sqrt{1 - \left(c_0 \frac{dt}{dx} \right)}}{2 \cdot h}$$

Where, $c_0 = \sqrt{gh}$

For simulating the linear long wave equation value of I_m should be less than 1.

In this simulation a rectangular grid of (1021 x 1024) has been selected. For deep (depths are greater than 2000m) ocean propagation calculations a cell size of dx of 2 min (3704 m) is used. Following figure (Figure 25) shows the arrangement of model grid used in this study.

On the other hand CFL condition should also be satisfied for stability in the numerical calculations. This is given by:

$$\frac{dx}{dt} = \sqrt{2 \cdot g \cdot h_{\max}}$$

Approaching to the shoreline h become smaller, hence in order to maintain the stability condition smaller dx is selected in near shore area keeping the dt constant. For these calculations, the dt was selected as 1.0 s, hence, which satisfies the CFL condition for the dx and h.

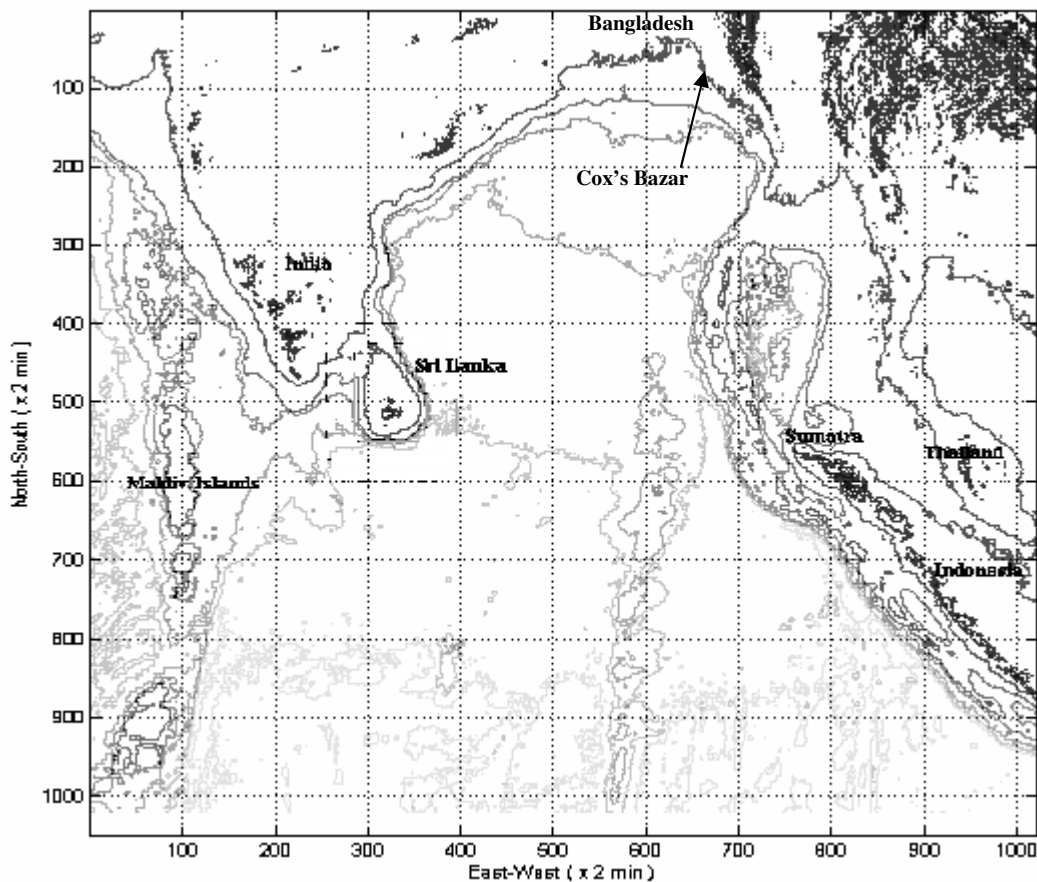


Figure 25: Grid Arrangement

9.2 Model Input Data

For any hydrodynamic modeling input data are very important. In case of tsunami simulation it is essential to have a reasonably accurate bathymetry and also correct tsunami initiation conditions. Accurate bathymetry would give a better result, even though the results of the numerical simulations are not up to the real life figures having appropriate boundary conditions. To initiate the tsunami, subduction of water surface was give as input. For 2004 Sumatra tsunami subduction model developed by Koshimura was used and for other hypothetical cases subduction amplitude and length were assumed. Figure 26 shows the Koshimura subduction model in a 3D view and along a section, where the trough is in the direction of Indian Ocean or Sri Lanka and the crest is on the Sumatra side.

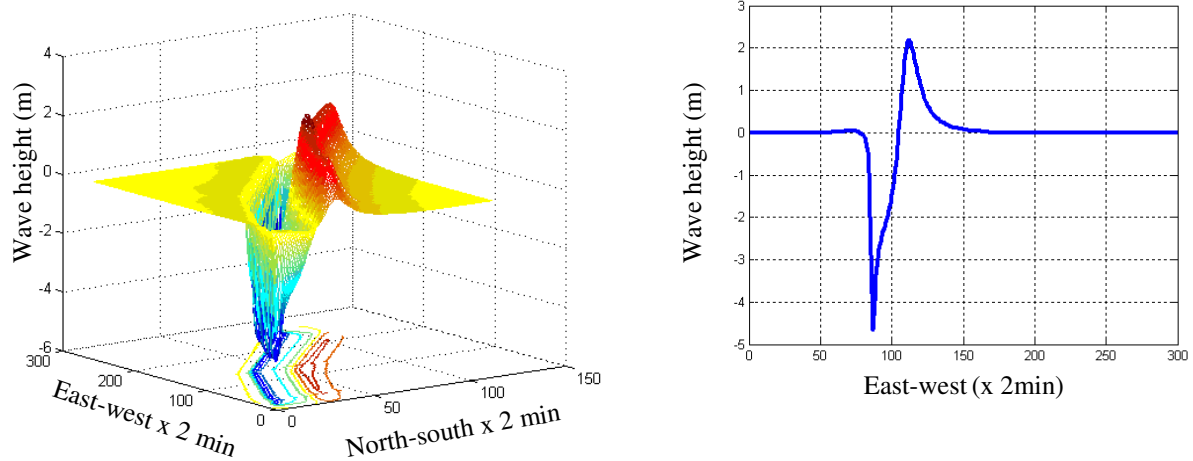


Figure 26: Koshimura subduction model (3D view on the left and 2D on the right)

Bathymetry Data

The widely used ETOPO 2 global data by NOAA (2005) are used to generate the model bathymetry.

Model validation with the Sumatra Tsunami at Sri Lanka coast (arrival time and wave height) is given in Appendix A.

9.3 Numerical Experiments and Results of Tsunami Propagation

To investigate the effects of different locations of tsunami generation, different amplitude and length of tsunami subduction, different orientation of the subduction as well as proximity of the tsunami generation to the coast, several numerical experiments were conducted in this study. Table 6 shows the list of numerical experiments. Figure 27 illustrates these cases.

Table 6: List of Numerical Experiments

Cases	Tsunami source	Amplitude (m)	Orientation	Remarks
Case 0	Sumatra coast	6	-	Original tsunami: Dec 26, 2004
Case 1	Myanmar coast	6	Angular	Shorter length of subduction
Case 2	Myanmar coast	6	Angular	Longer length of subduction
Case 3	Myanmar coast	9	Angular	
Case 4	Myanmar coast	6	Straight	
Case 5	Bay of Bengal	6	Straight	Far
Case 6	Bay of Bengal	6	Straight	Near

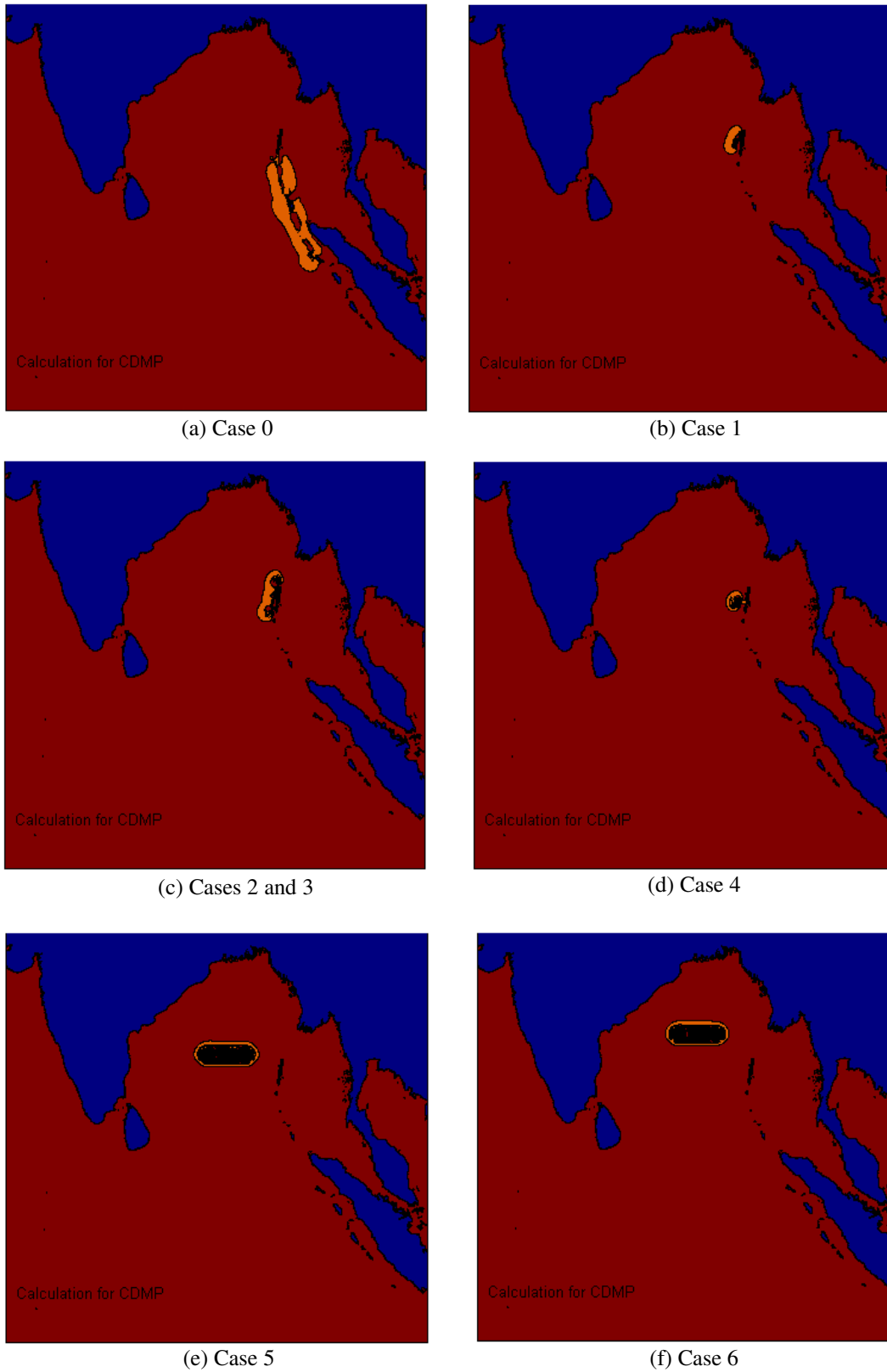


Figure 27: Seven cases of tsunami generated at different sources and with different subduction depths

9.3.1 Effects of the Location of Tsunami Generation

As discussed earlier, location of the source of tsunami might be decisive where it will affect a coast or not. Radial line that can be drawn straight from the tsunami source to the coast can give an idea regarding this. To investigate this issue Case 0 (the Sumatra tsunami of 2004 December) is tested along with Case 2, where the source of tsunami was in the Myanmar coast and from this point straight line can be drawn to the coast of Bangladesh.

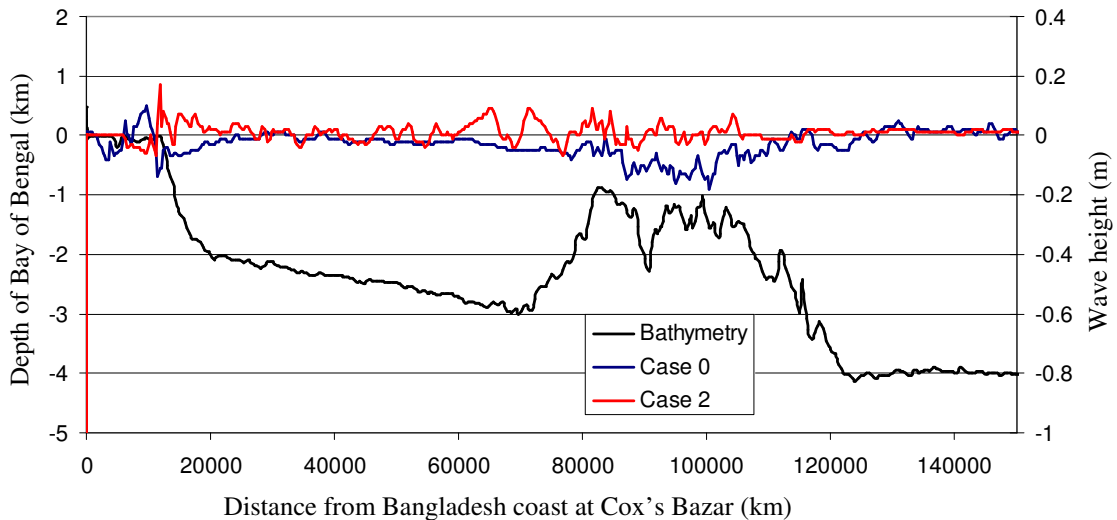


Figure 28: Comparison of tsunami wave heights of Case 0 and Case 2

Figure 28 shows the wave height distribution for Cases 0 and 2, when maximum wave height has been occurred at Cox's Bazar of Bangladesh. For both the cases maximum wave height do not go above 0.2m at Cox's Bazar indicating that the wave has already been dissipated when it crossed the continental shelf.

Figure 29 shows the tsunami wave height and arrival time for Cases 0 and 2 at the edge of continental shelf around 20km offshore from the Cox's Bazar coast. Even though both the cases show similar arrival time, the arrival wave height for the Case 2 is much larger compared to Case 0.

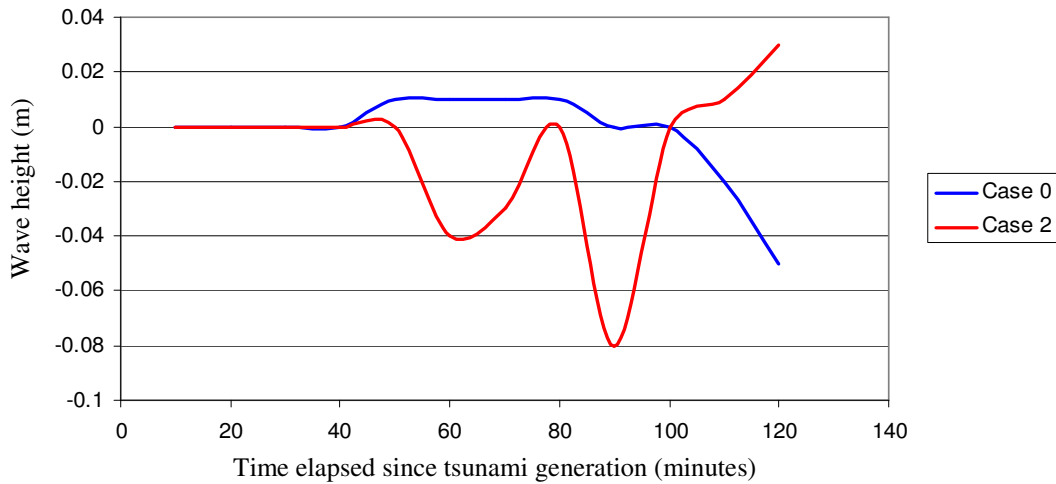


Figure 29: Comparison of tsunami arrival times at continental shelf for Case 0 and Case 2

9.3.2 Effects of the Subduction Amplitude of Tsunami

It may be rational to think that a tsunami with a larger subduction amplitude occurring at the Myanmar coast might have a greater impact at the coast of Bangladesh. For this reason Case 3 was compared with Case 2, where both the tsunamis have their origin at Myanmar coast but the first one have a subduction amplitude of 9m where as the later one have 6m.

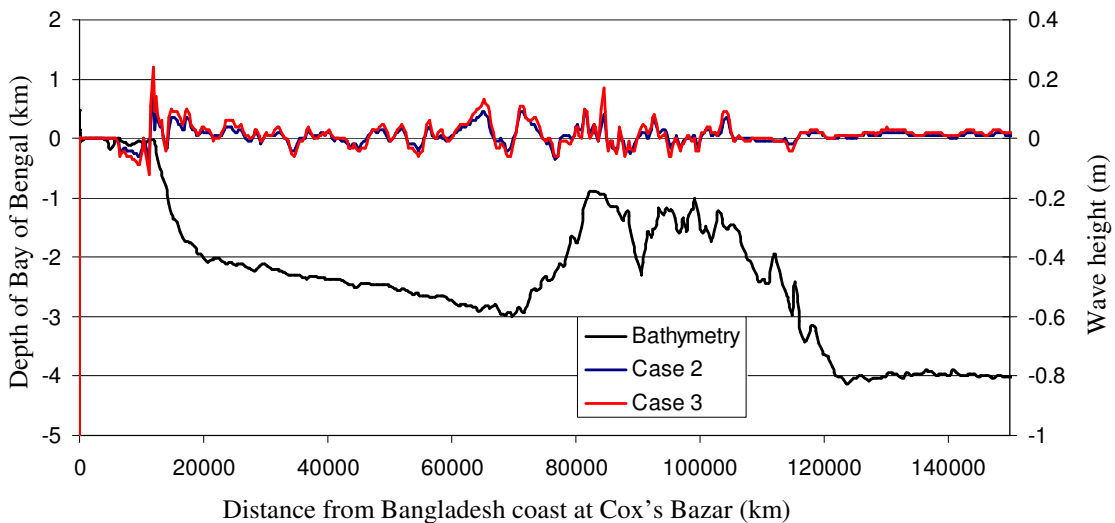


Figure 30: Comparison of tsunami wave heights of Case 2 and Case 3

Figure 30 shows the wave height distribution for Cases 2 and 3, which are very similar. Maximum wave height was 0.24m for Case 3 where as it was 0.17m for Case 2, indicating very small threat at Cox's Bazar coast.

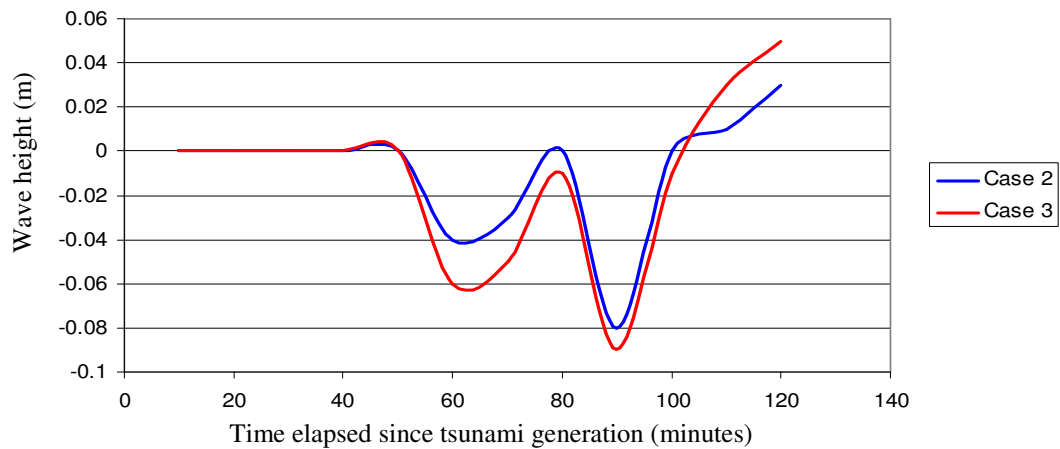


Figure 31: Comparison of tsunami arrival times at continental shelf for Case 2 and Case 3

Figure 31 shows the tsunami wave height and arrival time for Cases 2 and 3 at the edge of continental shelf and as expected they show exactly the same arrival time with a slightly larger wave height for Case 3.

9.3.3 Effects of the Subduction Orientation of Tsunami (case 2 and 4)

Other than the subduction amplitude, it is also believed that the direction of the fault line at the earthquake source may control the tsunami propagation. In other words, the orientation of the subduction may affect the tsunami wave height at the coast as the tsunami is assumed to propagate perpendicular to the fault line. To investigate this phenomena, Cases 2 and 4 were compared where both the tsunami sources are located at Myanmar coast but the afore mentioned one is in an angular position with respect to the Bangladesh coast and the later one is perpendicular.

Figure 32 shows the wave height distribution for Cases 2 and 4, indicating Case 4 has a smaller wave height at Cox's Bazar coast. It appears that much of the wave energy has been dissipated in the shallow areas of Andaman-Nicobar islands, and for Case 4 the wave height beyond the shallow zone is much smaller compared to those of Case 2. So it reveals that the topography of the ocean floor significantly control the tsunami propagation in the Bay of Bengal.

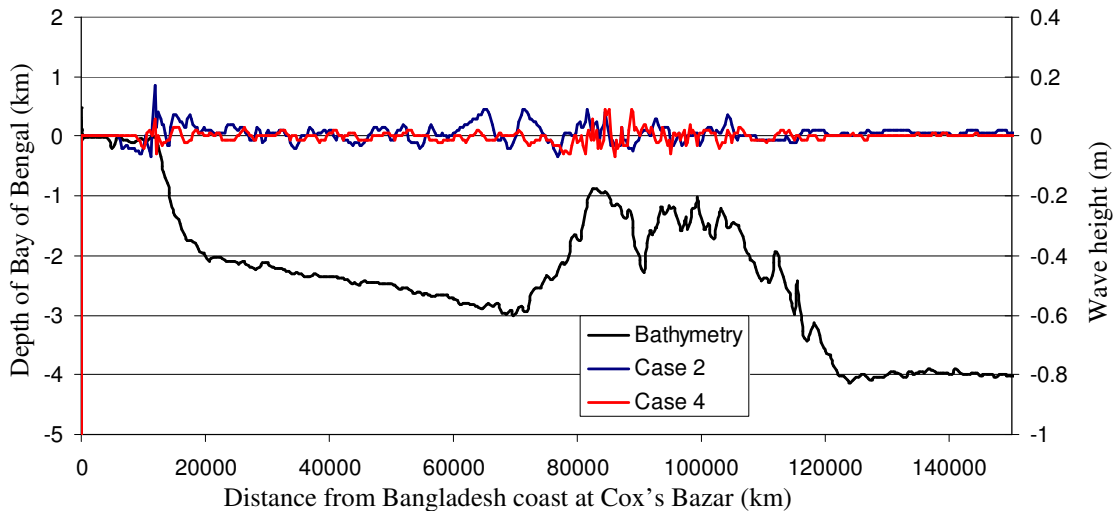


Figure 32: Comparison of tsunami wave heights of Case 2 and Case 4

Figure 33 shows the tsunami wave height and arrival time for Cases 2 and 4 at the edge of continental shelf. Case 4 has a smaller wave height at the edge of the shelf and interestingly it also has a longer arrival time in that area which may also be due to the shallow areas of Andaman-Nicobar island of the Bay of Bengal.

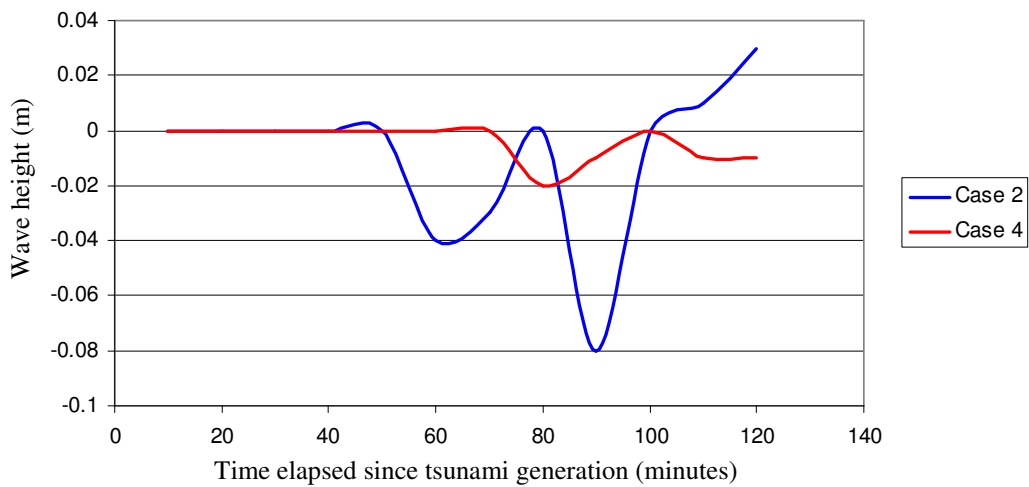


Figure 33: Comparison of tsunami arrival times at continental shelf for Case 2 and Case 4

9.3.4 Effects of the Proximity of Tsunami Source (case 5 and 6)

Two more cases were tested to investigate the effect of proximity of the tsunami source from the coast line. For both the cases tsunami source were at the Bay of Bengal at two hypothetical locations (as there is no fault line in those areas). For both the cases same amplitude and length of subduction were used, while Case 5 was located further from the coast line compared to Case 6. Wave height distribution did not show any significant difference at the Cox's Bazar coast. Figure 34 shows the tsunami wave height and arrival time at the edge of the continental shelf and as Case 6 was nearer to the coast it shows shorter arrival time as well as larger wave height at the vicinity of the continental shelf.

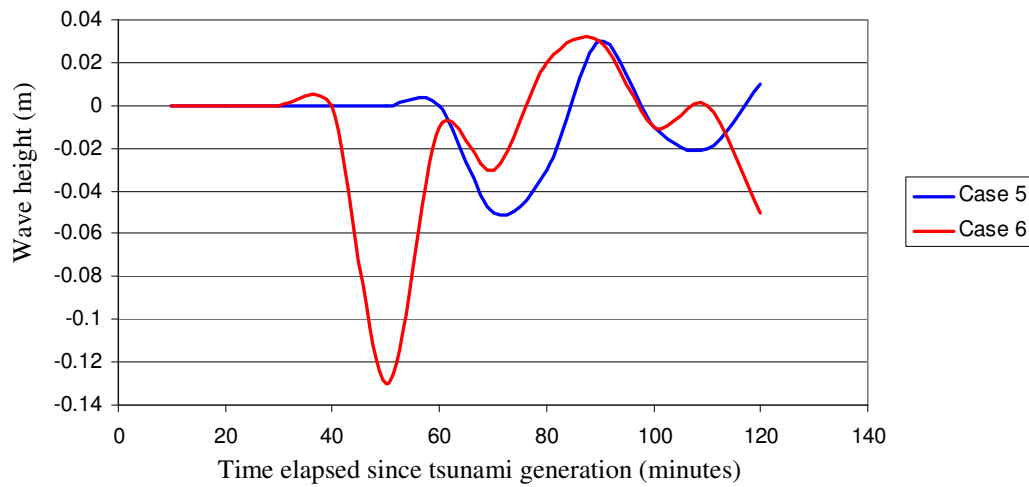


Figure 34: Comparison of tsunami arrival times at continental shelf for Case 5 and Case 6

From the discussion of the above four subsections it is clear that the continental slope and the location of continental shelf plays important role in retarding the tsunami propagation to the Bangladesh coast.

9.3.5 Effects of Continental Shelf

The effect of continental shelf on tsunami propagation is shown chronologically in Figure 35. It shows the height of tsunami wave in the ocean at every 10 minutes after the tsunami generation.

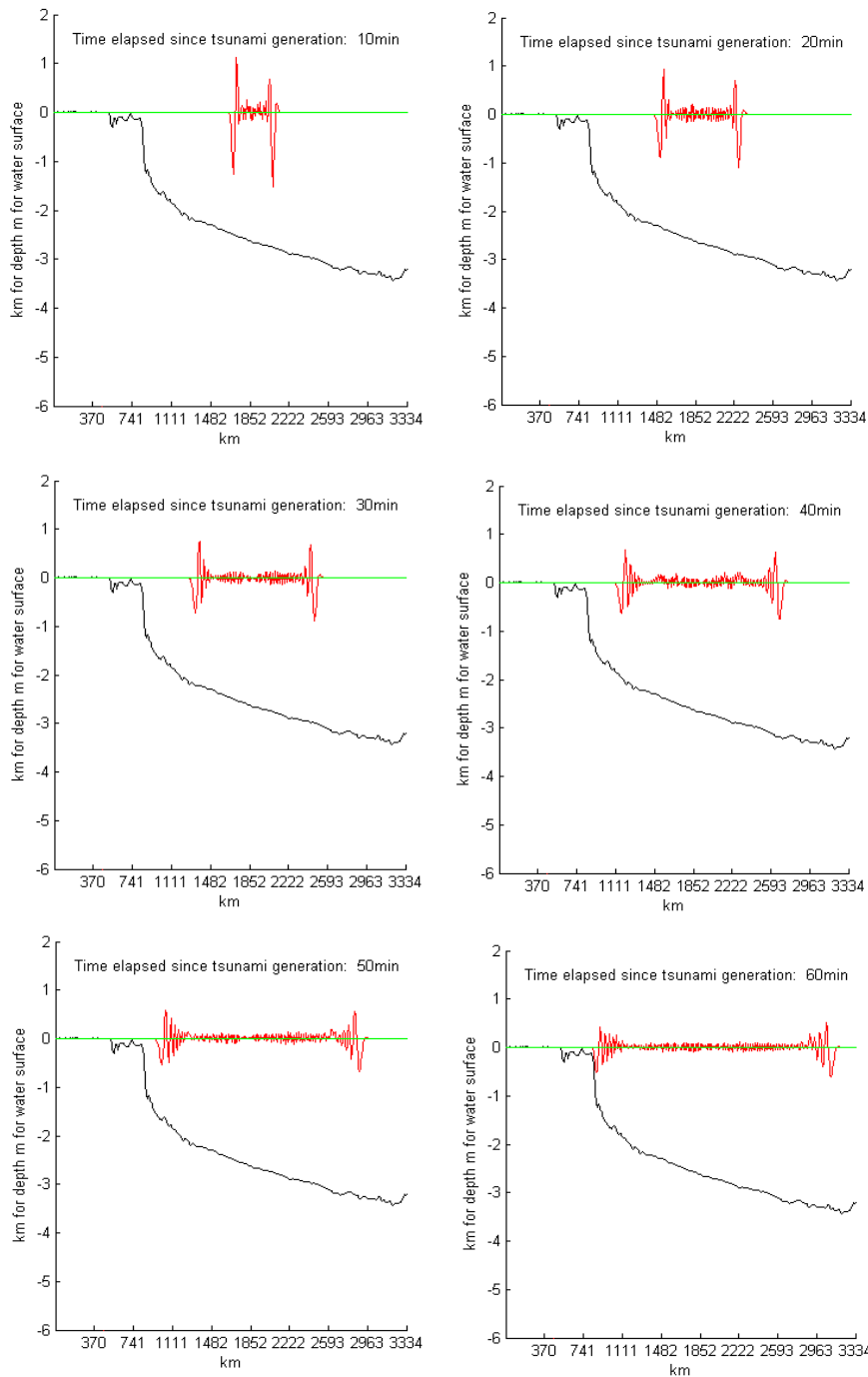


Figure 35: Wave height distributions at every 10 minutes after tsunami generation

(Continued to next page)

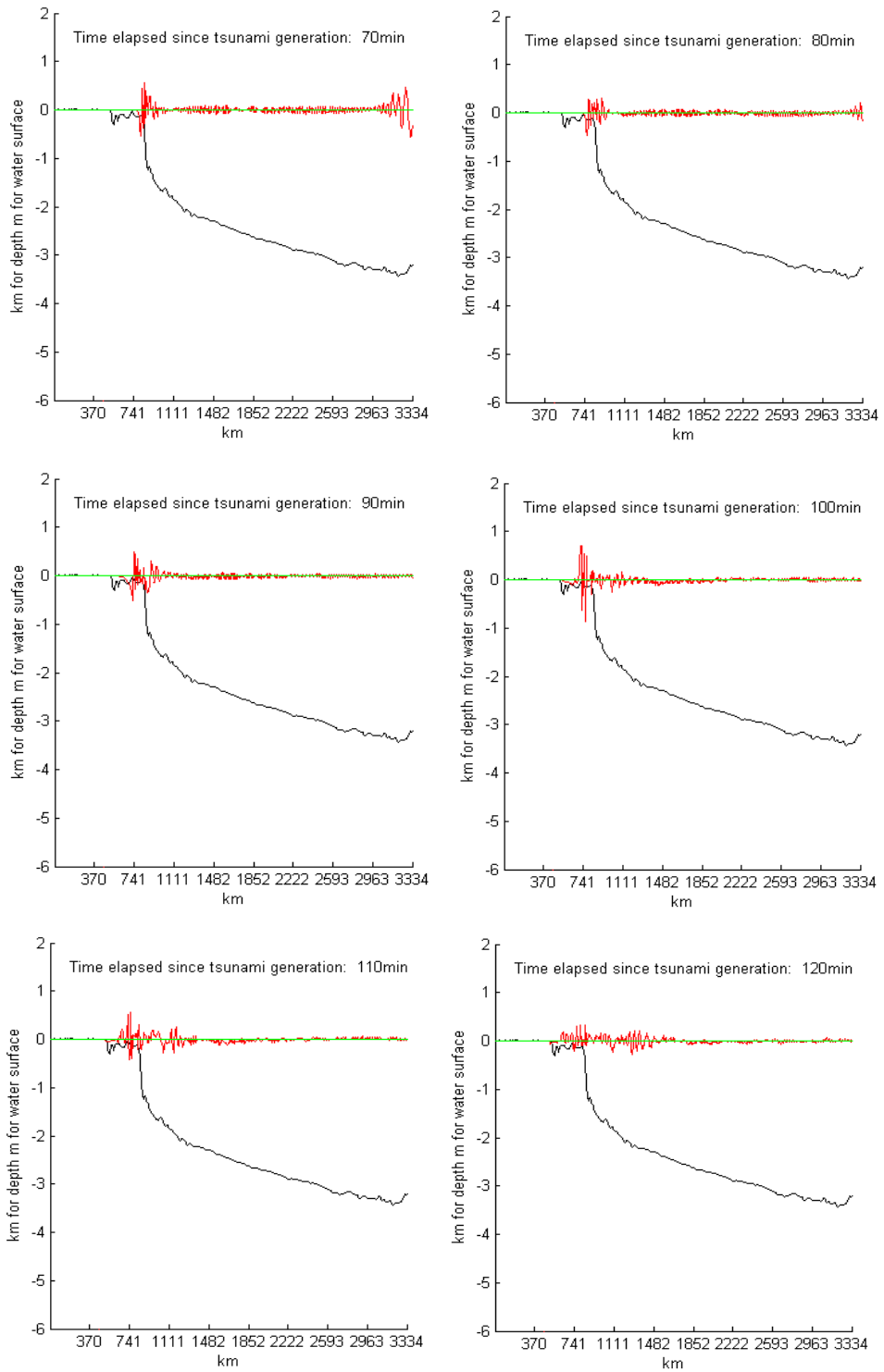


Figure 35: Wave height distributions at every 10 minutes after tsunami generation
(Continued from previous page)

From the Figure 35, it is evident that when the wave hits the edge of the continental shelf initially the wave height is further amplified (100 minute) and later some part of the wave is reflected back to the offshore direction and only a small portion travels towards the coast with a much smaller wave height (110 and 120 minutes). The amplitude is further dropped when it travels over the continental shelf and reaches to very small value when it reaches to the coast.

10. Modeling Tsunami Inundation

The previous section discussed the modeling of tsunami propagation from potential tsunami source up to the coastal zone using 2D Boussinesq Wave Model. The study provided the tsunami height expected along the Bangladesh Coast. The study has been extended in this section to investigate how the tsunami would inundate the land of Cox's Bazar district. Digital Elevation Model for the whole district was first developed for the ground surface topography. The propagation of tsunami water over the topography was thus investigated using numerical model based on Navier-Stokes Equations.

10.1 Overview of the 3D Model

The numerical model solves mass conservation and 3D Navier-Stokes equations for the conservation of momentum. It consists of two parts: hydrodynamic sub-model and water quality sub-model. The hydrodynamic sub-model is a f -plane quasi-3D σ -coordinate baroclinic circulation model including temperature and salinity (Sasaki and Isobe, 1996) and the water quality sub-model incorporates phytoplankton, zooplankton, nutrient cycling processes, detritus and dissolved oxygen (Koibuchi and Isobe, 2001). As part of a recent work by Hussain (2006), turbulence has been treated explicitly and equations for turbulent quantities such as turbulence velocity scale (or equivalently turbulence kinetic energy) and turbulence macroscale are also solved following Mellor-Yamada's (1982) turbulence closure scheme.

For solving the governing equations semi implicit (in vertical direction) finite difference scheme has been used with free surface dynamics. Two of the common approximations: hydrostatic approximation and Boussinesq approximation has been adopted in this model. Upwind scheme has been used for advection. Regular orthogonal Arakawa C grid has been used for horizontal discretization. Derivations of relevant governing equations are provided in Appendix A.

10.2 Development of Digital Elevation Model for Cox's Bazar

A digital elevation model (DEM) is a digital representation of ground surface topography or terrain. A DEM can be represented as a raster (a grid of squares) or as a triangular irregular network. Raster GIS represents the world as a regular arrangement of locations. In a DEM, each cell has a value corresponding to its elevation. The fact that locations are arranged regularly permits the raster GIS to infer many interesting associations among locations. DEMs are commonly built using remote sensing techniques; however, they may also be built from land surveying. DEMs are used often in geographic information systems, and are the most common basis for digitally-produced maps.

Digital elevation models may be prepared in a number of ways. Older methods of generating DEMs often involve interpolating digital contour maps that may have been produced by direct survey of the land surface; this method is still used in mountain areas, where interferometry is not always satisfactory. A DEM implies that elevation is available continuously at each location in the study area.

The contour map and spot height map of the area are usually merged together and a composite map having information about contours as well as spot height is formed. This combined map is further interpolated using map interpolation function available in GIS environment e.g. ArcView, Arc-Info and ArcGIS to generate a DEM of the area. This DEM are further checked for flats and pits present in it. These flats and pits are then removed using iterative map calculation functions and final DEM is generated.

10.2.1 Digitizing FINNMAPS

Base Maps covering the near-shore area of Cox's Bazar District were bought from Bangladesh Inland Water Transport Authority (BIWTA). The Maps are also known as FINN Maps., were developed by BIWTA in collaboration with FINNIDA (Finland) and Commission of the European Communities. Figure 36 shows a sample FINN Map where block of a region of Cox's Bazar district is presented. A total of seventy nine FINN Maps were digitized covering the whole of Cox's Bazar using UTM (WGS84) projection. Spot height data were extracted by onscreen

digitizing using ArcView (Figure 37). These data were further used for preparation of DEM and Inundation model.



Figure 36: Sample FINN Map and Location Index

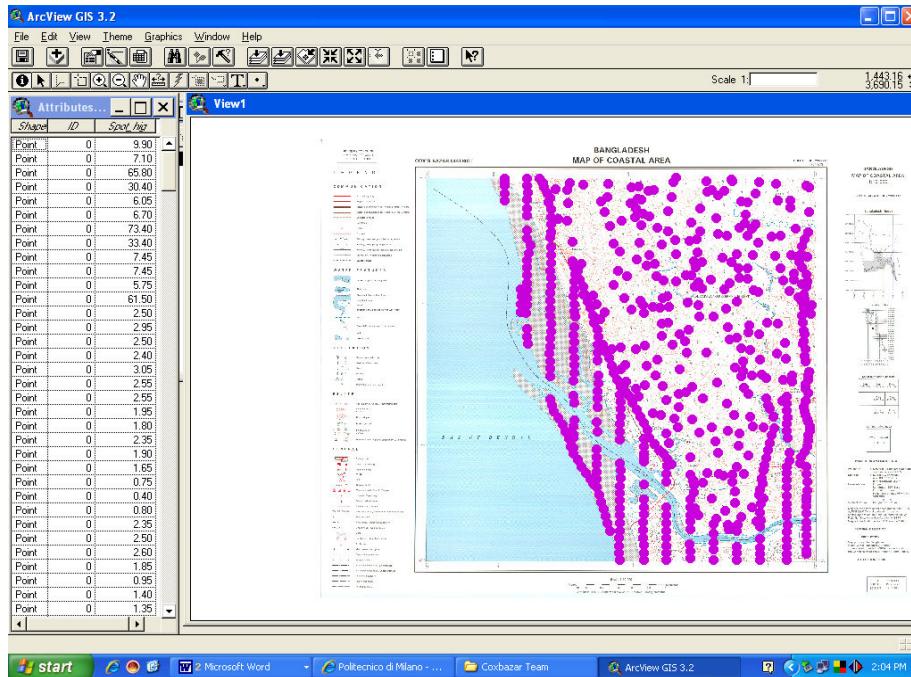


Figure 37: Digitizing in Arc-View

10.2.3 DEM Preparation

Digital Elevation Models (DEMs) are digital files consisting of points of elevations, sampled systematically at equally spaced intervals. This represents the undulation of the earth surface resulting from the height values. The elevation model can be both in Raster or Vector format. A vector format of DEM has been prepared here. The height values for DEM preparation can be obtained from different sources such as airborne laser Scanning, Aerial photography, GPS survey or paper based maps with spot heights.

The study area in Cox's Bazar (Figure 38) is around 2000 square kilometers. Digital Elevation Model is a key input here for modeling the Tsunami and preparation of inundation maps. The paper based spot height maps were found from the FINN Maps Discussed earlier.

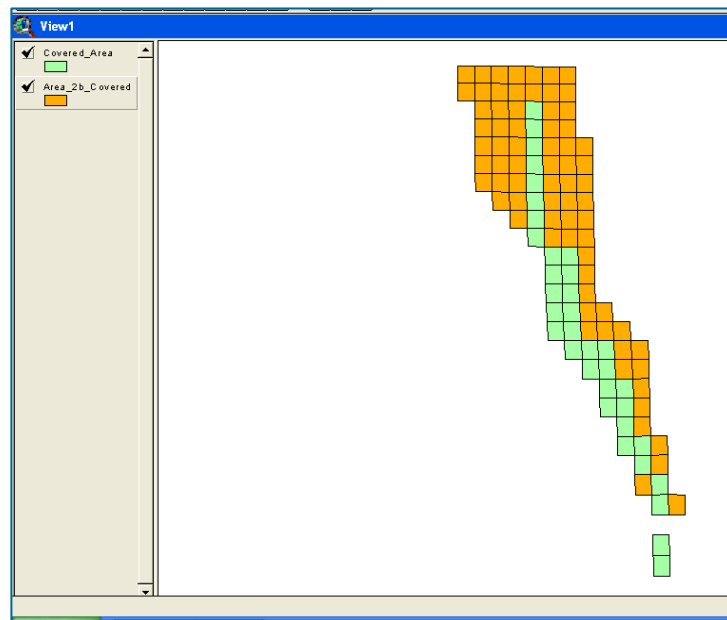


Figure 38: Study Area Cox's Bazar in FINN Map

The paper maps were geo-referenced (Figure 39) to fit them in the correct spatial position in the world space. Then the points on the maps are digitized along with their attributes. The paper maps were transformed into digital format in the aforesaid manner. This process was followed repeatedly to cover the study area. Arc GIS 9.0 is used to accomplish the task of referencing and digitizing (Figure 39).

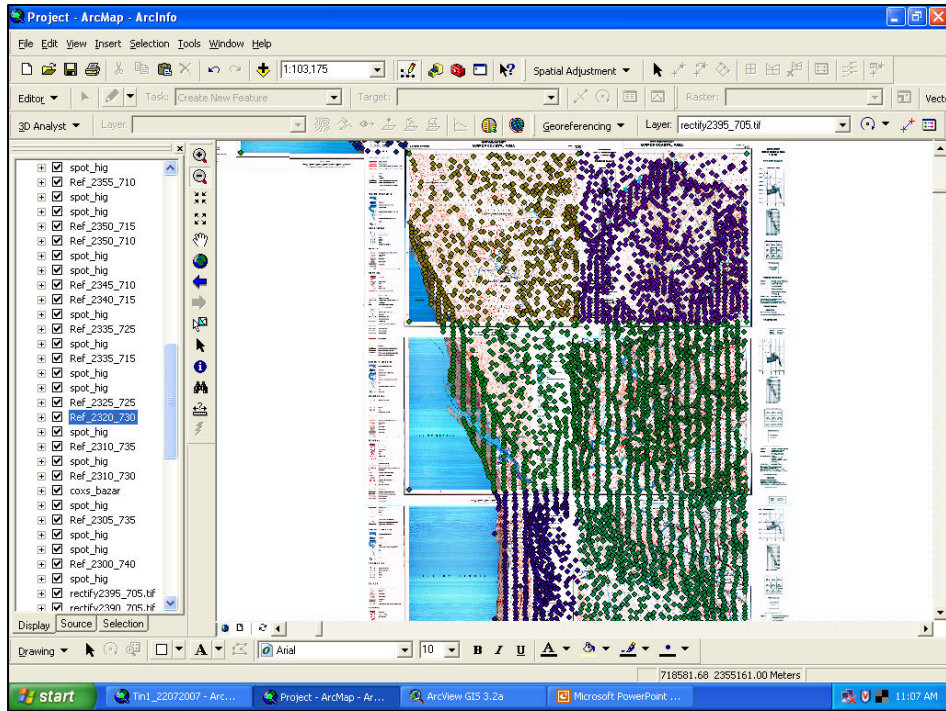


Figure 39: Referenced Images and Spot Heights

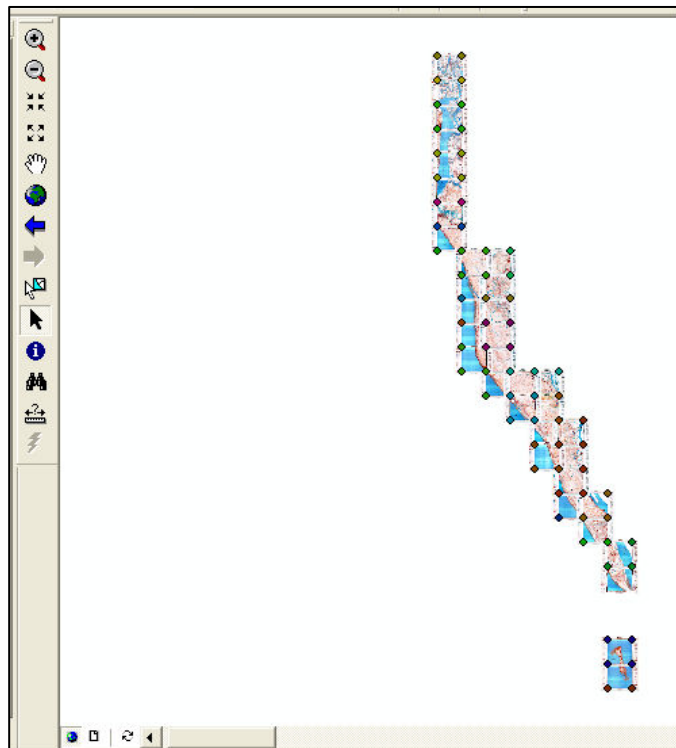


Figure 40: Geo-referenced Maps

Once the spot heights were ready in digital format the process of DEM preparation was started. Elevation of the individual spots was used to make the Digital Elevation Model. The basic principle of this model is a TIN surface. TIN stands for Triangular Irregular Network which actually makes surface connecting three adjacent points. This model (Figure 41) is further used to calculate the affected areas in case of any Tsunami.

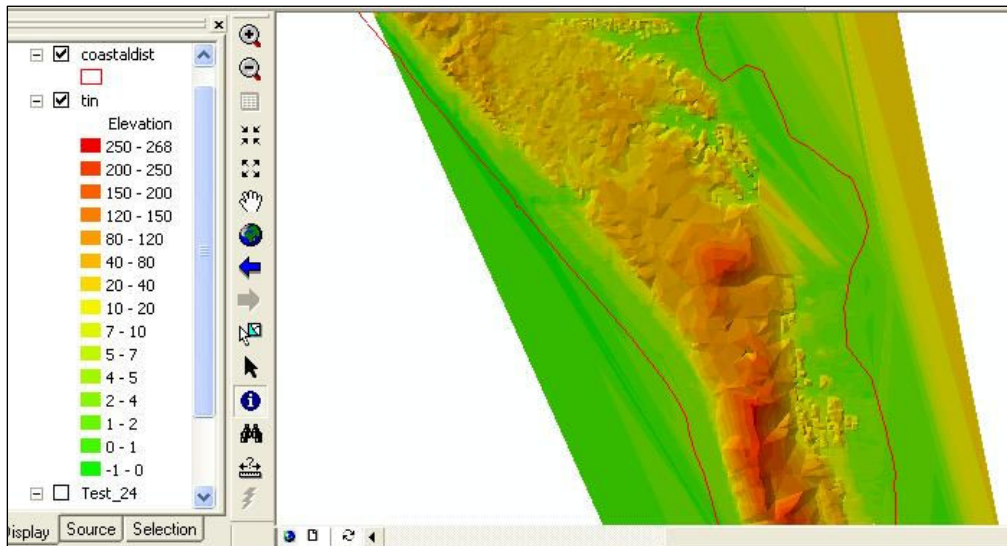


Figure 41: Digital Elevation Model of The study area Cox's Bazar

The spot height data were found ready from previously digitized map from paper format which were randomly spread (Figure 42) over the study area. But for using the elevation data in the Tsunami Model they had to be distributed over the space in a regular grid. So improvisation of a technique was needed to make the available data in regular grid.

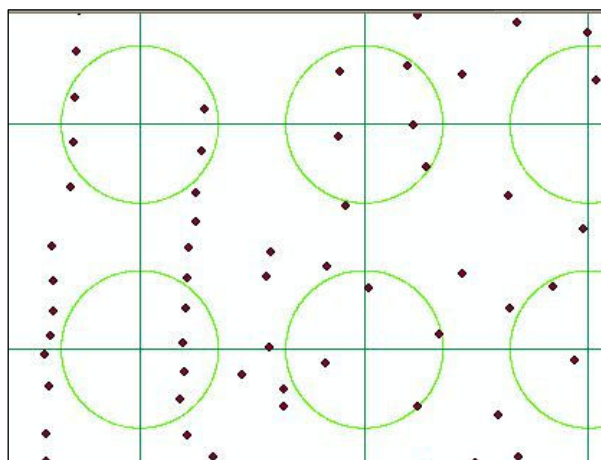


Figure 42: Scattered Points

For running the Tsunami model with an effective accuracy, points were located in the grids of 500 meter interval where required. For this reason grid lines were inserted with an interval of 500 meters and the circle of 150 m radius was put on the each intersection (Figure 43). The points only inside the circles are taken into consideration. At the end the point which has the closest proximity to the center of the circle is picked up for making the grids in desired intervals.

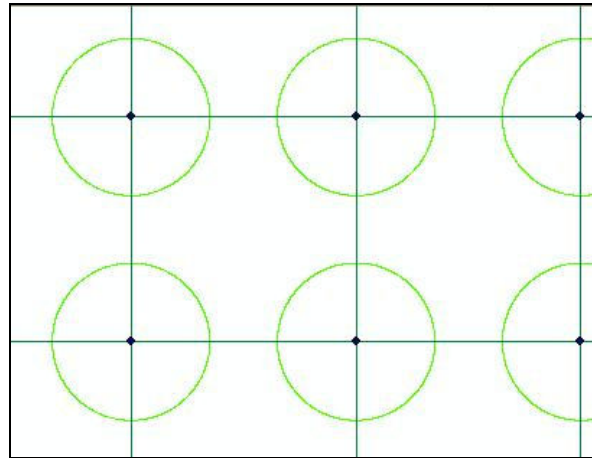


Figure 43: Points in Regular grids

10.3 Development of Inundation Maps

As the numerical experiments (section 9.4) did not show any significant wave heights approaching the Cox's Bazar coast of Bangladesh, one hypothetical wave with a height of 2m was induced at the southern coast to observe the inundation and wave height in the Cox's Bazar area. The arrival direction of this wave was straight from the south as shown in Figure 44. On the right panel of Figure 44 the wave height distribution along the Cox's Bazar coast is shown. Maximum wave height reached around 1.5m and from the figure it is evident that the wave moves along the coast resembling an edge wave (as seen from the ebb type wave in the blue zone of the waves).

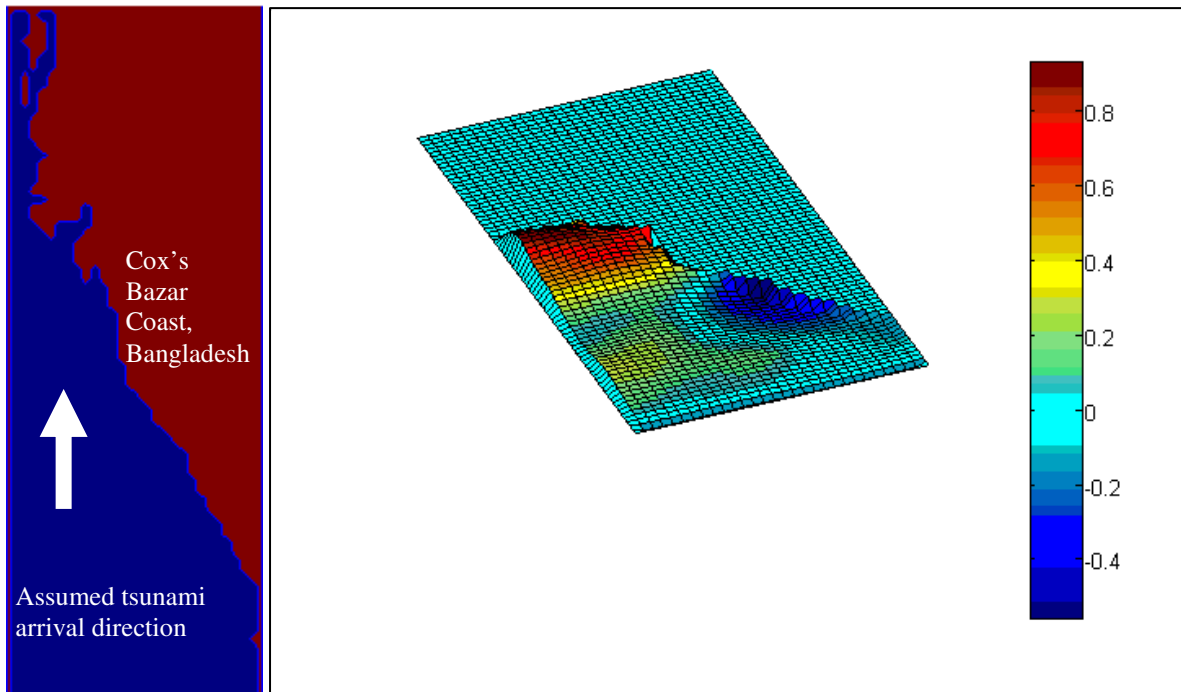


Figure 44: Typical distribution of water surface elevation (m) with 2 m wave height of tsunami at the Cox's Bazar coast, Bangladesh

10.3.1 Water Surface Elevation and Corresponding Velocity Vectors

Figure 45 shows the wave height distributions and velocity vectors at three different time intervals after the 2m wave was induced at the southern coast of Bay of Bengal.

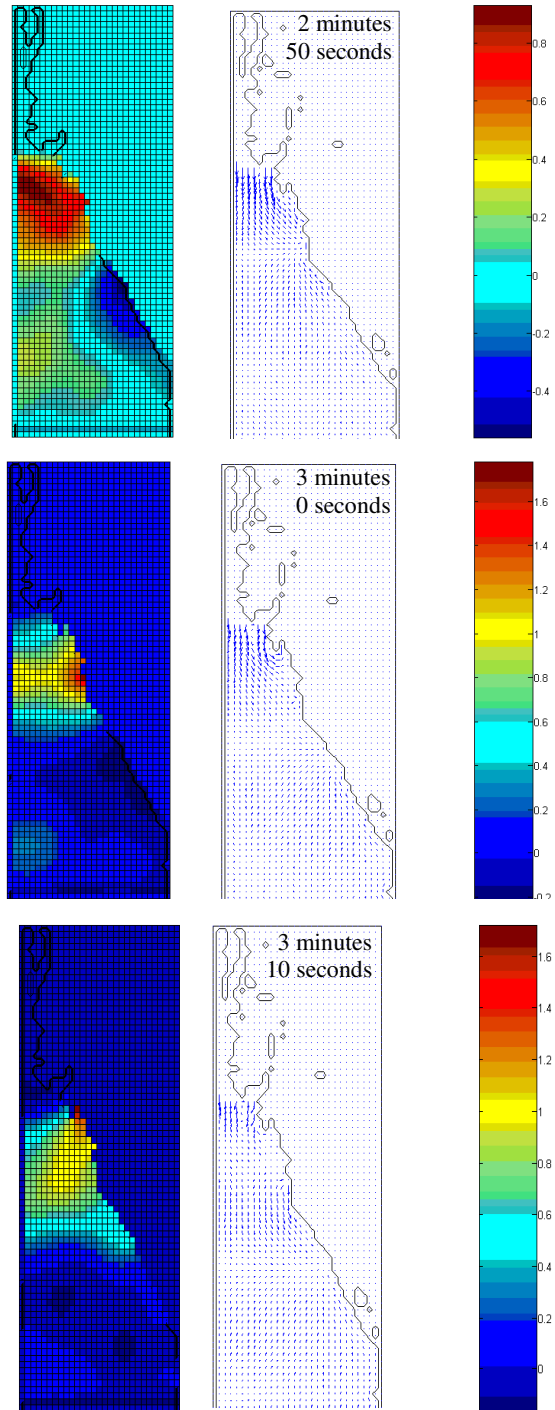


Figure 45: Wave height distribution and velocity vectors at the Cox's Bazar coast, Bangladesh at three different time intervals after tsunami generation.

From the figure it is evident that as the wave travels along the Cox's Bazar coast it takes the shape of edge wave and when it gets trapped in the northern part maximum wave height is incurred. This is why some of the velocity vectors show south-ward direction in the vicinity of the trapped zone.

11. Discussions and Conclusions

The research work presented in this report concludes into few findings regarding the potential of occurring Tsunamigenic Earthquakes around Bangladesh coast and the vicinity and the affect on the coast of Bangladesh from Tsunami Propagation in case of any Tsunami Generation.

Though Bangladesh is situated in a seismically active zone, the fault plane solution of the earthquake events in the region show strike-slip dominancy, which is less potential of generating tsunamigenic earthquake. But if tsunami occurs in The Bay of Bengal or Indian Ocean, then the coastal area of Cox's Bazar might be in a vulnerable condition. However risk from the most tsunami-generating region near Indian Ocean, Sunda Arc covering Java and Sumatra, is relatively low. According to the plate tectonics theory an earthquake releases the strain that accumulates over centuries. So it is predicted to take very long time before anything like Sumatra 2004 erupts again. Still there are segments to the south and some other areas that are gaining built-up strain. Again, Andaman-Nicobar Islands, situated to the North of Sunda belt, is considered as less seismically active zone which leads to the assumption that probability of a severe tsunami hitting through Bay of Bengal from Andaman–northern Sumatra region to be low. The probability of tsunami occurrence in Bangladesh due to the subduction of India-Burma plate of was of little concern in the available researches. But few recent studies have turned the focus on the region suggesting for rigorous investigations. More information and some quantitative measures are required to perform analysis on tsunami potential from this region. Study should be undertaken to thoroughly document the historical record of past earthquakes and tsunamis in the greater Bangladesh region. More geological studies are needed to find out whether large earthquakes and tsunamis occurred and how often they did. Since sufficient data is not available from the coasts of Andaman Islands, Bangladesh and Myanmar, it is the high time for scientists to get together to generate data on stress and strain measurements. The fault near Myanmar had not generated an earthquake for hundreds of years which is an important issue to

be considered this regard. Thus, evidence of palaeo-earthquakes and tsunamis along the Myanmar coast, Bangladesh and northern Andaman should be studied seriously.

From the Numerical Simulation performed in the present research, how Tsunami generated near Bangladesh Coast will propagate and affect the region, have been assessed. From the general review based the available research works, it has been observed that Bangladesh is at a long distance from the earthquake epicenter, and water wave from tsunamigenic earthquakes generated to the south eastern Indian Ocean is expected to be obstructed before hitting the country as per some favorable geologic conditions. Thus the coast will be hit by a greatly reduced energy of the tsunami wave produced in this region. On the other hand, the plate boundary near Bangladesh, is north-south oriented which is along the direction of rupture zone on the northern, north-trending segment of Sunda belt. Since tsunami amplitudes are largest perpendicular to the fault, tsunami affects may not be substantial in Bangladesh from this fault zone. Moreover the 200 km long and steep continental shelf acts as a potential barrier to the motion of the stressed water column and reduces the propagating tsunami wave to the coast.

From the numerical modeling, it has been observed that for the cases the Sumatra tsunami of 2004 December and a similar tsunami in the Myanmar coast (from which point straight line can be drawn to the Bangladesh coast), the maximum wave height do not rise above 0.2m at Cox's Bazar coast, indicating that the wave has already been dissipated when it crossed the continental shelf. Though arrival time was similar for the both cases but larger arrival wave height was found in case of tsunami in Myanmar region. When subduction amplitude was imparted on the tsunami originating at the Myanmar coast, the maximum wave increased slightly with varying amplitudes, indicating very small threat at Cox's Bazar coast. To investigate the effect of orientation of the subduction, a study with tsunami sources at Myanmar coast with orientation of the fault parallel and perpendicular to the Bangladesh coast was performed. It has been seen that the later one (fault perpendicular to coast) produced a smaller wave height at Cox's Bazar coast. The topography of the ocean floor also appeared to significantly control the tsunami propagation in the Bay of Bengal. The study showed that much of the wave energy has been dissipated in the shallow areas of Andaman-Nicobar islands, and the wave height beyond the shallow zone became much smaller compared to the former one. Smaller wave height was observed at the edge of the shelf and interestingly it also had a longer arrival time in that area which may also be

due to the shallow areas of Andaman-Nicobar Island of the Bay of Bengal. Two more cases were tested using numerical analysis to investigate the effect of proximity of the tsunami source from the coast line. For both the cases wave height distribution did not show any significant difference at the Cox's Bazar coast but Tsunami from the nearer to the coast showed shorter arrival time as well as larger wave height at the vicinity of the continental shelf. Through the Tsunami Model it was revealed that the continental slope and the location of continental shelf plays important roles in retarding the tsunami propagation to the Bangladesh coast. The phenomenon can be described like that when the wave will hit the edge of the continental shelf initially the wave height will be amplified, then some part will be reflected back to the offshore direction and finally a small portion will travel towards the coast with a much smaller wave height. The amplitude will further drop when it will travel over the continental shelf and will reach the coast with a very small value.

LIST OF REFERENCES

- ABC Science Online (2007). "Bay of Bengal risks tsunami too", by Dani Cooper, 6 September 2007, posted at <http://www.abc.net.au/science/articles/2007/09/06/2024000.htm>
- Aida I, 1978, Reliability of Tsunami Source Model derived from Fault Parameters, *Journal of Phys.Earth*, vol. 26, pp 57-73
- Banglapedia, 2004. http://banglapedia.org/ht/B_0361.HTM
- Bangladeshnews (2007). "Coastal areas under risk of local tsunami", Posted on September 14th, 2007, at <http://www.bangladeshnews.com.bd/2007/09/14/coastal-areas-under-risk-of-local-tsunami/>
- Bilham R. (1994). "The 1737 Calcutta Earthquake and Cyclone Evaluated", *Bull. Seism. Soc. Amer.* 84(5), 1650-1657, 1994.
- Bryant, E., 2001, *Tsunami; underrated hazard*, Cambridge University press, pp 1-pp 76.
- Berninghausen, W. H., (1966). Tsunamis and Seismic Seiches reported from regions adjacent to the Indian Ocean, *Bull. Seism. Soc. Am.*, 56 (1), 69-74.
- Caltech (2004). "The Science behind the Aceh Earthquake", Caltech Media Relations, NEWS RELEASE, For Immediate Release, December 30, 2004 posted at, http://mr.caltech.edu/media/Press_Releases/PR12628.html
- Carayannis, G. P. (2004). "Tsunami, Earthquakes, Hurricanes, Volcanic Eruptions and other Natural and Man-Made Hazards and Disasters" posted at <http://www.drgeorgepc.com/Tsunami2004Indonesia.html>
- Cummins P. R. (2007). The potential for giant tsunamigenic earthquakes in the northern Bay of Bengal, 449|6 September 2007| doi: 10.1038/nature06088.
- Curry, J. R., Emmel, F.J., Moore, D.G. and Raitt, R.W. (1982). Structure, tectonics and geological history of the NE Indian Ocean, in *The Ocean Basins and Margins*, vol. 6. The Indian Ocean, edited by A. E. M. Nairn and F. G. Sehli, Plenum, New York, 399-450.
- ETOPO-2, grided bathymetry data, 2008-06-09, <http://www.gebco.net/data and products/ grided bathymetry dart/>

- Fine I.V., Stephenson F. E., Rabinovich A. B., and Thomson R. E. (2005). "Tsunami Warning Systems, Efficient use of Tide Gauge Stations", posted at www.shoa.cl/servicios/tsunami/pdf_TSUNAMIS/STEPHENSON/Santiago2_2005.ppt
- Geotimes, (2007). "Tsunami risk high in Myanmar" posted at http://www.geotimes.org/nov07/article.html?id=nn_myanmar.html in November 2007
- Gupta H. K. (2005). Nature of Earthquakes, 58 p
- Hasan A. K. M. S. & Mondal A. M., Final report of the Project "Tsunami vulnerability Assessment of thr Growth Centres of the South-Eastern Bangladesh" implemented by the National Oceanographic and Maritime institute (NOAMI), 2007.
- Hussain, M. A. (2006): Numerical Simulation of Residual Currents and Water Quality in Semi-Enclosed Bays, Ph.D. Thesis, Department of Civil Engineering, The University of Tokyo.
- ICMAM (2005). "Preliminary Assessment of Impact of Tsunami in Selected Coastal Areas of India", Compiled by Department of Ocean Development, Integrated Coastal and Marine Area Management (ICMAM) Project Directorate, Chennai, March 2005, posted at <http://dod.nic.in/tsunami1.pdf>
- Imamura F., Review of tsunami Simulation with a finite difference method, long wave run up models, 1995, pp-25-42
- Imamura, F., N. Shuto and T. Goto, Study of numerical simulation of the transoceanic propagation; Part 2: characteristics of tsunami propagating over the Pacific Ocean. Jishin 2, 43, 389-402, 1990.
- Kajiura, K., 1963, "The Leading Wave of a Tsunami", Bulletin of the Earthquake Research Institute,. Vol. 41, pp. 535-571
- Khan A. A. (2007). "Assessing earthquake and tsunami risk in Bangladesh, Environment", The Daily Star Vol.5 Num 972, February 23, 2007
- Khan, Md. W. A. and Karim M. F. (2005), Government of the People's Republic of Bangladesh Ministry of Food and Disaster Management Country Paper high-level expert group meeting on technical options for disaster management systems: Tsunamis and Others, 22-24 June, 2005, Bangkok Thailand
- Koibuchi, Y. and Isobe, M. (2001): Temporal and spatial dynamics of water quality on Ariake Bay during the year of 2001, Proc. Coastal Engg. JSCE, 49, pp. 1056-1060.

- Koshimura, S., 2005, <http://www.dri.ne.jp/koshimuras/sumatra/>
- Latief H., Puspito N. T. and Imamura F., 2000. Tsunami Catalog and Zones in Indonesia. *J. N., Disaster Science*, 22 (1), 25-43
- Maa, J.P.Y., 1990, An Efficient Horizontal Two-Dimensional Hydrodynamic Model, *Coastal Engineering*, vol. 14, pp 1 – pp 18.
- Mathur, S.M., (1998). "Physical Geology of India", National Book Trust of India, New Delhi.
- Mellor, G.L. and Yamada, T. (1982): Development of a turbulence closure model for geophysical fluid problems, *Rev. of Geophysics and Space Physics*. 20(4), pp 851-875.
- Murty, T. S., A. Bapat & Vinayak Prasad (1999). Tsunamis on the coastlines of India, *Science of Tsunami Hazards*, 17 (3), 167-172.
- Ortiz, M., and Bilham, R. (2003). Source Area and Rupture Parametres of the 31 December 1881 Mw=7.9 Car Nicobar Earthquake estimated from tsunamis recorded in the Bay of Bengal, *J. Geophys. Res- Solid Earth*, 108(4), ESE 11, 1-16.
- Orman, J.V., Cochran, J.R., Weissel, J.K. and Jestin, F. (1995). Distribution of shortening between the Indian and Australian plates in the central Indian Ocean. *Earth and Planetary Science Letters*, 133: 35-46.
- Rastogi B. K. , Jaiswal R. K. (2006), "A Catalog Of Tsunamis In The Indian Ocean", *Science of Tsunami Hazards*, Vol. 25, No. 3, page 128 (2006), National Geophysical Research Institute, Hyderabad, India
- Sasaki, J. and Isobe, M. (1996): Development of a long-term predictive model of water quality in Tokyo Bay, *Proc. Estuarine and Coastal Modeling*, ASCE, pp. 564-580.
- Satake K. (2004). "Preparation for Future Earthquake and Tsunami Hazards: Lessons Learned from the 2004 Sumatra-Andaman Earthquake and the Asian Tsunami", First International Conference of Aceh and Indian Ocean Studies, Organized by Asia Research Institute, National University of Singapore & Rehabilitation and Construction Executing Agency for Aceh and Nias (BRR), Banda Aceh, Indonesia, 24 – 27 February 2007
- Satake K., Tanioka Y. (1995). Tsunami generation of the 1993 Hokkaido Nansei-Oki earthquake, *Tsunamis: 1992-1994. Their Generation, Dynamics and Hazard*. Edited by S.Satake and F.Imamura. *Pageoph Topical Volumes*, Birkhauser Verlag, 144, 3/4, 803-821.

Shuto N., Numerical simulation of tsunamis –its present and near future, Natural hazards, vol. 4, 1991, pp-171-191

Schirber, M. (2005). “Tsunami Earthquake Three Times Larger than First Thought”, 08 February 2005, posted at http://www.livescience.com/environment/050208_sumatra_quake.html

“Scientific Background on the Indian Ocean Earthquake and Tsunami” posted at <http://iri.columbia.edu/~lareef/tsunami/>

SOI (Survey of India) Observations. Tsunami hits East Coast-posted at <http://www.surveyofindia.gov.in/tsunami.htm>

The Sunday Times. “Massive Myanmar quake, tsunami could kill millions around Bay of Bengal” posted at <http://www.sundaytimes.lk/070909/International/i512.html>

Tsuji Y., Tsunami and Storm surges, Earthquake Research Institute, University of Tokyo, Japan. Lecture notes, pp 5-11. 2005.

Tsunami (2004). Posted at www.nipissingu.ca/faculty/ingridb/geology/Tsunami%202004.htm

Uddin, A.M. K. 2005. Tsunami: A Status Paper reflecting Bangladesh coast’s exposure and vulnerability, Program Development Office for Integrated Coastal Zone Management Plan (PDO-ICZMP)

USGS, Seismo.html. “Seismological Aspects of Tsunami Generation” posted at <http://walrus.wr.usgs.gov/tsunami/sumatraEQ/seismo.html>

USGS, Tectonics.html. “2004 M=9.0 Sumatra Earthquake, Tectonics of Sumatra-Andaman Islands (81 kb)” posted at <http://walrus.wr.usgs.gov/tsunami/sumatraEQ/tectonics.html>

USGS (2001) Tsunamis & Earthquakes- Western Coastal and Marine Geology, Tsunamis and Earthquakes Preliminary Analysis of the Tsunami Generated by the 23 June 2001 Peru Earthquake, posted at <http://walrus.wr.usgs.gov/tsunami/Peru01.html>

USGS (2004), posted at <http://earthquake.usgs.gov/eqcenter/eqarchives/poster/2004/20041226.php>

USGS (2005), posted at http://neis.usgs.gov/neis/eq_depot/2004/eq_041226/

USGS (2007), posted at

<http://earthquake.usgs.gov/eqcenter/eqinthenews/2007/us2007hear/#summary>

Yan, Y., 1987, Numerical modelling of current and wave interactions of an inlet-beach system, Ph.D. Dissertation, University of Florida, Fla.

http://science.nationalgeographic.com/staticfiles/NGS/Shared/StaticFiles/Science/Images/topic-images/tectonics13_infographic.jpg

http://www.nationmaster.com/wikimir/images/upload.wikimedia.org/wikipedia/en/2/2c/Nor_re v.png

<http://www.indiana.edu/~g105lab/1425chap13.htm>

http://ioc3.unesco.org/indotsunami/documents/nationalreports/IOC12_Assessment_Bangladesh.pdf

Appendix A

Derivation of Governing Equations

The equation expressing the conservation of momentum can be written in tensor notation as;

$$\rho \frac{\partial u_i}{\partial t} + \rho u_j \frac{\partial u_i}{\partial x_j} + 2\rho \varepsilon_{ijk} \Omega_j u_k = -\frac{\partial p}{\partial x_i} - g\rho \delta_{3i} + \frac{\partial \sigma_{ij}}{\partial x_j} \quad (\text{A1.1})$$

Here ρ is density of water, t is time, p pressure, Ω_j is the component of the Earth's angular velocity and σ_{ij} are the components of stress due to molecular viscosity. $\varepsilon_{ijk} = +1$, if i, j, k are in cyclic order and $\varepsilon_{ijk} = -1$, if i, j, k are in anti-cyclic order and $\varepsilon_{ijk} = 0$, if any pair or all three indices have the same value; $\delta_{3i} = 1$ when $i = 3$ and $\delta_{3i} = 0$ for otherwise.

Also, when μ is the molecular viscosity, the stress tensor σ_{ij} , can be expressed in terms of the rate of deformation of the fluid element by motion.

$$\sigma_{ij} = \mu \left(\frac{\partial u_i}{\partial x_j} + \frac{\partial u_j}{\partial x_i} \right) \quad (\text{A1.2})$$

An expansion into three equations can be made to obtain Navier-Stokes equation on f-plane, upon which the present model is based.

The present model is based on Navier-Stokes equations on f-plane, which are as follows;

$$\frac{\partial u}{\partial t} + u \frac{\partial u}{\partial x} + v \frac{\partial u}{\partial y} + w \frac{\partial u}{\partial z} = fv - \frac{1}{\rho} \frac{\partial P}{\partial x} + \frac{\partial}{\partial x} \left(A_x \frac{\partial u}{\partial x} \right) + \frac{\partial}{\partial y} \left(A_y \frac{\partial u}{\partial y} \right) + \frac{\partial}{\partial z} \left(A_z \frac{\partial u}{\partial z} \right) \quad (\text{A1.3})$$

$$\frac{\partial v}{\partial t} + u \frac{\partial v}{\partial x} + v \frac{\partial v}{\partial y} + w \frac{\partial v}{\partial z} = -fu - \frac{1}{\rho} \frac{\partial P}{\partial y} + \frac{\partial}{\partial x} \left(A_x \frac{\partial v}{\partial x} \right) + \frac{\partial}{\partial y} \left(A_y \frac{\partial v}{\partial y} \right) + \frac{\partial}{\partial z} \left(A_z \frac{\partial v}{\partial z} \right) \quad (\text{A1.4})$$

$$\frac{\partial w}{\partial t} + u \frac{\partial w}{\partial x} + v \frac{\partial w}{\partial y} + w \frac{\partial w}{\partial z} = -\frac{1}{\rho} \frac{\partial P}{\partial z} - g + \frac{\partial}{\partial x} \left(A_x \frac{\partial w}{\partial x} \right) + \frac{\partial}{\partial y} \left(A_y \frac{\partial w}{\partial y} \right) + \frac{\partial}{\partial z} \left(A_z \frac{\partial w}{\partial z} \right) \quad (\text{A1.5})$$

The conservation of mass can be expressed through the continuity equation

$$\frac{\partial \rho}{\partial t} + \frac{\partial \rho u_i}{\partial x_i} = 0 \quad (\text{A1.6})$$

which for an incompressible fluid becomes

$$\frac{\partial u_i}{\partial x_i} = 0 \quad (\text{A1.7})$$

In expanded form the equation of mass-conservation;

$$\frac{\partial u}{\partial x} + \frac{\partial v}{\partial y} + \frac{\partial w}{\partial z} = 0 \quad (\text{A1.8})$$

From hydrostatic pressure approximation,

$$\frac{\partial P}{\partial z} = -\rho g \quad (\text{A1.9})$$

Integrating between z to η

$$P(\eta) - P(z) = -\int_z^\eta \rho g \quad (\text{A1.10})$$

As, at surface $P(\eta) = 0$ and $\rho = \rho_0 + \rho'$, where ρ_0 is the constant reference density and ρ' is the deviation from it.

Equation (A1.10) becomes:

$$\begin{aligned} -P(z) &= -g \int_z^\eta (\rho_0 + \rho') dz \\ P(z) &= \rho_0 g (\eta - z) + g \int_z^\eta \rho' dz \\ \left. \begin{aligned} P_0 &\equiv \rho_0 g (\eta - z) \\ P' &\equiv g \int_z^\eta \rho' dz \end{aligned} \right\} \quad (\text{A1.11}) \end{aligned}$$

In equation (A1.3), Boussinesq approximation is used whereby density is held constant except in the hydrostatic equation.

$$\begin{aligned} \frac{1}{\rho} \frac{\partial P}{\partial x} &= \frac{1}{\rho_0} \frac{\partial}{\partial x} (P_0 + P') \\ \frac{1}{\rho} \frac{\partial P}{\partial x} &= \frac{1}{\rho_0} \frac{\partial}{\partial x} \left[\rho_0 g (\eta - z) + g \int_z^\eta \rho' dz \right] \\ \frac{1}{\rho} \frac{\partial P}{\partial x} &= g \frac{\partial}{\partial x} (\eta - z) + \frac{g}{\rho_0} \frac{\partial}{\partial x} \int_z^\eta \rho' dz \\ \frac{1}{\rho} \frac{\partial P}{\partial x} &= g \frac{\partial \eta}{\partial x} + \frac{g}{\rho_0} \frac{\partial}{\partial x} \int_z^\eta \rho' dz \end{aligned}$$

similarly from equation (A.1.4);

$$\frac{1}{\rho} \frac{\partial P}{\partial y} = g \frac{\partial \eta}{\partial y} + \frac{g}{\rho_0} \frac{\partial}{\partial y} \int_z^\eta \rho' dz$$

So the following two Boussinesq equations can be obtained from (A1.3) and (A1.4),

$$\begin{aligned} & \frac{\partial u}{\partial t} + u \frac{\partial u}{\partial x} + v \frac{\partial u}{\partial y} + w \frac{\partial u}{\partial z} \\ &= fv - g \frac{\partial \zeta}{\partial x} - \frac{g}{\rho_0} \frac{\partial}{\partial x} \int_z^\zeta \rho' dz + \frac{\partial}{\partial x} \left(A_x \frac{\partial u}{\partial x} \right) + \frac{\partial}{\partial y} \left(A_y \frac{\partial u}{\partial y} \right) + \frac{\partial}{\partial z} \left(A_z \frac{\partial u}{\partial z} \right) \end{aligned} \quad (\text{A1.12})$$

$$\begin{aligned} & \frac{\partial v}{\partial t} + u \frac{\partial v}{\partial x} + v \frac{\partial v}{\partial y} + w \frac{\partial v}{\partial z} \\ &= -fu - g \frac{\partial \zeta}{\partial y} - \frac{g}{\rho_0} \frac{\partial}{\partial y} \int_z^\zeta \rho' dz + \frac{\partial}{\partial x} \left(A_x \frac{\partial v}{\partial x} \right) + \frac{\partial}{\partial y} \left(A_y \frac{\partial v}{\partial y} \right) + \frac{\partial}{\partial z} \left(A_z \frac{\partial v}{\partial z} \right) \end{aligned} \quad (\text{A1.13})$$

Conversion into sigma coordinate system:

$$\begin{aligned} \sigma &= \frac{z+h}{\zeta+h} \\ \frac{\partial \sigma}{\partial z} &= \frac{1}{\zeta+h} \end{aligned}$$

For any function φ

$$\frac{\partial \varphi}{\partial z} = \frac{\partial \varphi}{\partial \sigma} \frac{\partial \sigma}{\partial z} = \frac{1}{\zeta+h} \frac{\partial \varphi}{\partial \sigma}$$

Now

$$\left. \frac{\partial \varphi}{\partial x} \right|_z = \left. \frac{\partial \varphi}{\partial x} \right|_\sigma + \left. \frac{\partial \varphi}{\partial \sigma} \frac{\partial \sigma}{\partial x} \right|_z$$

Here,

$$\left. \frac{\partial \sigma}{\partial x} \right|_z = \lim_{\Delta x \rightarrow 0} \frac{\sigma_0 - \sigma_1}{\Delta x}$$

$$\left. \frac{\partial \sigma}{\partial x} \right|_z = - \lim_{\Delta x \rightarrow 0} \frac{\sigma_1 - \sigma_0}{\Delta x}$$

$$\left. \frac{\partial \sigma}{\partial x} \right|_z = - \lim_{\Delta x \rightarrow 0} \frac{1}{\Delta x} \left\{ \frac{z_1 + h}{\zeta + h} - \frac{z_0 + h}{\zeta + h} \right\}$$

$$\left. \frac{\partial \sigma}{\partial x} \right|_z = - \lim_{\Delta x \rightarrow 0} \frac{z_1 - z_0}{\Delta x} \left\{ \frac{1}{\zeta + h} \right\}$$

$$\text{as } \lim_{\Delta x \rightarrow 0} \frac{z_1 - z_0}{\Delta x} = \lim_{\Delta x \rightarrow 0} \frac{\Delta z}{\Delta x} = \left. \frac{\partial z}{\partial x} \right|_\sigma$$

$$\therefore \left. \frac{\partial \sigma}{\partial x} \right|_z = - \frac{1}{\zeta + h} \left. \frac{\partial z}{\partial x} \right|_z$$

$$\left. \frac{\partial \sigma}{\partial x} \right|_z = - \frac{1}{\zeta + h} \frac{\partial}{\partial x} [\sigma(\zeta + h) - h]$$

$$\left. \frac{\partial \sigma}{\partial x} \right|_z = - \frac{1}{\zeta + h} \left[\sigma \frac{\partial}{\partial x} (\zeta + h) - \frac{\partial h}{\partial x} \right]$$

$$\left. \frac{\partial \sigma}{\partial x} \right|_z = - \frac{1}{(\zeta + h)^2} \left[(z + h) \frac{\partial}{\partial x} (\zeta + h) - \frac{1}{(\zeta + h)} \frac{\partial h}{\partial x} \right]$$

Mass conservation equation:

$$\left. \frac{\partial u}{\partial x} \right|_z + \left. \frac{\partial v}{\partial y} \right|_z + \left. \frac{\partial w}{\partial z} \right|_z = 0$$

$$\left. \frac{\partial u}{\partial x} \right|_z = \left. \frac{\partial u}{\partial x} \right|_\sigma + \left. \frac{\partial u}{\partial \sigma} \frac{\partial \sigma}{\partial x} \right|_z$$

$$\left. \frac{\partial v}{\partial y} \right|_z = \left. \frac{\partial v}{\partial y} \right|_\sigma + \left. \frac{\partial v}{\partial \sigma} \frac{\partial \sigma}{\partial y} \right|_z$$

$$\left. \frac{\partial w}{\partial z} \right|_z = \left. \frac{\partial w}{\partial \sigma} \frac{\partial \sigma}{\partial z} \right|_z = \frac{1}{\zeta + h} \left. \frac{\partial w}{\partial \sigma} \right|_z$$

$$\begin{aligned}
& \left. \frac{\partial u}{\partial x} \right|_{\sigma} + \left. \frac{\partial u}{\partial \sigma} \frac{\partial \sigma}{\partial x} \right|_z + \left. \frac{\partial v}{\partial y} \right|_{\sigma} + \left. \frac{\partial v}{\partial \sigma} \frac{\partial \sigma}{\partial y} \right|_z + \frac{1}{\zeta+h} \frac{\partial w}{\partial \sigma} = 0 \\
& \left. \frac{\partial u}{\partial x} \right|_{\sigma} + \frac{\partial u}{\partial \sigma} \left[\frac{1}{h+\zeta} \frac{\partial h}{\partial x} - \frac{\sigma}{h+\zeta} \frac{\partial(\zeta+h)}{\partial x} \right] + \left. \frac{\partial v}{\partial y} \right|_{\sigma} + \frac{\partial v}{\partial \sigma} \left[\frac{1}{h+\zeta} \frac{\partial h}{\partial y} - \frac{\sigma}{h+\zeta} \frac{\partial(\zeta+h)}{\partial y} \right] \\
& + \frac{1}{\zeta+h} \frac{\partial w}{\partial \sigma} = 0
\end{aligned} \tag{A1.14}$$

Also, vertical velocity in sigma coordinate system:

$$\begin{aligned}
\sigma' &= \frac{D\sigma}{Dt} = \frac{\partial \sigma}{\partial t} + u \frac{\partial \sigma}{\partial x} + v \frac{\partial \sigma}{\partial y} + w \frac{\partial \sigma}{\partial z} \\
\text{As; } \sigma &= \frac{z+h}{\zeta+h} \therefore \frac{\partial \sigma}{\partial t} = - \frac{z+h}{(\zeta+h)^2} \frac{\partial \zeta}{\partial t} = - \frac{\sigma}{(\zeta+h)} \frac{\partial \zeta}{\partial t} \\
\sigma' &= - \frac{\sigma}{h+\zeta} \frac{\partial \zeta}{\partial t} + u \left[\frac{1}{h+\zeta} \frac{\partial h}{\partial x} - \frac{\sigma}{h+\zeta} \frac{\partial(\zeta+h)}{\partial x} \right] + v \left[\frac{1}{h+\zeta} \frac{\partial h}{\partial y} - \frac{\sigma}{h+\zeta} \frac{\partial(\zeta+h)}{\partial y} \right] + w \frac{1}{h+\zeta} \\
\frac{\partial \sigma'}{\partial \sigma} &= - \frac{1}{h+\zeta} \frac{\partial \zeta}{\partial t} + u \left[- \frac{1}{h+\zeta} \frac{\partial(\zeta+h)}{\partial x} \right] + \frac{\partial u}{\partial \sigma} \left[\frac{1}{h+\zeta} \frac{\partial h}{\partial x} - \frac{\sigma}{h+\zeta} \frac{\partial(\zeta+h)}{\partial x} \right] \\
& + v \left[- \frac{1}{h+\zeta} \frac{\partial(\zeta+h)}{\partial y} \right] + \frac{\partial v}{\partial \sigma} \left[\frac{1}{h+\zeta} \frac{\partial h}{\partial y} - \frac{\sigma}{h+\zeta} \frac{\partial(\zeta+h)}{\partial y} \right] + \frac{\partial w}{\partial \sigma} \frac{1}{h+\zeta}
\end{aligned} \tag{A1.15}$$

Subtracting equation (A.1.15) from equation (A.1.14) and multiplying by $(h+\zeta)$

$$\begin{aligned}
- \frac{\partial \sigma'}{\partial \sigma} (\zeta+h) &= \frac{\partial \zeta}{\partial t} + u \frac{\partial(h+\zeta)}{\partial x} + v \frac{\partial(h+\zeta)}{\partial y} + \frac{\partial u}{\partial x} (h+\zeta) + \frac{\partial v}{\partial y} (h+\zeta) \\
\frac{\partial \zeta}{\partial t} + u \frac{\partial H}{\partial x} + H \frac{\partial u}{\partial x} + v \frac{\partial H}{\partial y} + H \frac{\partial v}{\partial y} + H \frac{\partial \sigma'}{\partial \sigma} &= 0 \\
\frac{\partial \zeta}{\partial t} + \frac{\partial(uH)}{\partial x} + \frac{\partial(vH)}{\partial y} + \frac{\partial(\sigma'H)}{\partial \sigma} &= 0
\end{aligned} \tag{A1.16}$$

Equation A.1.16 is the Mass conservation or Continuity equation in sigma coordinate system.

Also from (A.1.15) w can be obtained:

$$w = \frac{\partial \zeta}{\partial t} \sigma + \frac{u}{H} \left[\sigma \frac{\partial H}{\partial x} - \frac{\partial h}{\partial x} \right] + \frac{v}{H} \left[\sigma \frac{\partial H}{\partial y} - \frac{\partial h}{\partial y} \right] + H \sigma'$$

Momentum equations:

Momentum equation in x-direction:

$$\frac{\partial u}{\partial t} + u \frac{\partial u}{\partial x} + v \frac{\partial v}{\partial y} + w \frac{\partial w}{\partial z} = fv - \frac{1}{\rho} \frac{\partial P}{\partial x} + \frac{\partial}{\partial x} \left(A_x \frac{\partial u}{\partial x} \right) + \frac{\partial}{\partial y} \left(A_y \frac{\partial u}{\partial y} \right) + \frac{\partial}{\partial z} \left(A_v \frac{\partial u}{\partial z} \right)$$

In Boussinesq form:

$$\begin{aligned} & \frac{\partial u}{\partial t} + u \frac{\partial u}{\partial x} + v \frac{\partial v}{\partial y} + w \frac{\partial w}{\partial z} \\ &= fv - g \frac{\partial \zeta}{\partial x} - \frac{g}{\rho_0} \frac{\partial}{\partial x} \int_z^\zeta \rho' dz + \frac{\partial}{\partial x} \left(A_x \frac{\partial u}{\partial x} \right) + \frac{\partial}{\partial y} \left(A_y \frac{\partial u}{\partial y} \right) + \frac{\partial}{\partial z} \left(A_v \frac{\partial u}{\partial z} \right) \end{aligned} \quad (\text{A1.17})$$

Transforming the LHS of equation (A1.5) into sigma coordinate system:

$$\begin{aligned} & \left. \frac{\partial u}{\partial t} \right|_z + u \left. \frac{\partial u}{\partial x} \right|_z + v \left. \frac{\partial u}{\partial y} \right|_z + w \left. \frac{\partial u}{\partial z} \right|_z \\ &= \left. \frac{\partial u}{\partial t} \right|_\sigma + \left. \frac{\partial u}{\partial \sigma} \frac{\partial \sigma}{\partial t} \right|_z + u \left(\left. \frac{\partial u}{\partial x} \right|_\sigma + \left. \frac{\partial u}{\partial \sigma} \frac{\partial \sigma}{\partial x} \right|_z \right) + v \left(\left. \frac{\partial u}{\partial y} \right|_\sigma + \left. \frac{\partial u}{\partial \sigma} \frac{\partial \sigma}{\partial y} \right|_z \right) + w \left(\left. \frac{\partial u}{\partial \sigma} \frac{\partial \sigma}{\partial z} \right|_z \right) \\ &= \left[\left. \frac{\partial u}{\partial t} \right|_\sigma + u \left. \frac{\partial u}{\partial x} \right|_\sigma + v \left. \frac{\partial u}{\partial y} \right|_\sigma \right] + \left[\left. \frac{\partial u}{\partial \sigma} \frac{\partial \sigma}{\partial t} \right|_z + u \left. \frac{\partial u}{\partial \sigma} \frac{\partial \sigma}{\partial x} \right|_z + v \left. \frac{\partial u}{\partial \sigma} \frac{\partial \sigma}{\partial y} \right|_z + w \frac{1}{h+\zeta} \left. \frac{\partial u}{\partial \sigma} \right|_z \right] \end{aligned} \quad (\text{A1.18})$$

From (A1.12) and (A1.13)

$$\left. \frac{\partial u}{\partial t} \right|_z + u \left. \frac{\partial u}{\partial x} \right|_z + v \left. \frac{\partial u}{\partial y} \right|_z + w \left. \frac{\partial u}{\partial z} \right|_z = \left. \frac{\partial u}{\partial t} \right|_\sigma + u \left. \frac{\partial u}{\partial x} \right|_\sigma + v \left. \frac{\partial u}{\partial y} \right|_\sigma + \sigma' \frac{\partial u}{\partial \sigma} \quad (\text{A1.19})$$

Now RHS of momentum equation:

$$\left. \frac{\partial}{\partial x} \left(A_x \frac{\partial u}{\partial x} \right) \right|_z = A_H \frac{\partial^2 u}{\partial x^2}$$

$$\left. \frac{\partial}{\partial y} \left(A_y \frac{\partial u}{\partial y} \right) \right|_z = A_H \frac{\partial^2 u}{\partial y^2}$$

as $A_x = A_y = A_H$

$$\left. \frac{\partial}{\partial z} \left(A_v \frac{\partial u}{\partial z} \right) \right|_z = \frac{\partial}{H \partial \sigma} \left(A_\sigma \frac{\partial u}{H \partial \sigma} \right) = \frac{1}{H^2} \left(A_\sigma \frac{\partial^2 u}{\partial \sigma^2} \right) \quad (\text{A1.20})$$

Pressure terms on the RHS of momentum equation:

$$\begin{aligned}
\nabla_z P &= \frac{\partial P}{\partial x} \Big|_z + \frac{\partial P}{\partial y} \Big|_z \\
\nabla_z P &= \frac{\partial P}{\partial x} \Big|_\sigma + \frac{\partial P}{\partial \sigma} \frac{\partial \sigma}{\partial x} + \frac{\partial P}{\partial y} \Big|_\sigma + \frac{\partial P}{\partial \sigma} \frac{\partial \sigma}{\partial y} \\
\nabla_z P &= \nabla_\sigma P + \frac{\partial P}{\partial \sigma} \left(\frac{\partial \sigma}{\partial x} + \frac{\partial \sigma}{\partial y} \right) \\
\nabla_z P &= \nabla_\sigma P + \frac{\partial P}{\partial \sigma} \left(-\frac{1}{h+\zeta} \frac{\partial z}{\partial x} \Big|_\sigma - \frac{1}{h+\zeta} \frac{\partial z}{\partial y} \Big|_\sigma \right) \\
\nabla_z P &= \nabla_\sigma P + \frac{\partial P}{\partial \sigma} \left(-\frac{\partial \sigma}{\partial z} \frac{\partial z}{\partial x} \Big|_\sigma - \frac{\partial \sigma}{\partial z} \frac{\partial z}{\partial y} \Big|_\sigma \right) \\
\nabla_z P &= \nabla_\sigma P - \frac{\partial \sigma}{\partial z} \left(\frac{\partial z}{\partial x} \Big|_\sigma + \frac{\partial z}{\partial y} \Big|_\sigma \right) \frac{\partial P}{\partial \sigma} \\
\nabla_z P &= \nabla_\sigma P - \frac{\partial \sigma}{\partial z} (\nabla_\sigma z) \frac{\partial P}{\partial \sigma}
\end{aligned}$$

(A1.21)

Now

$$\begin{aligned}
\frac{\partial P}{\partial z} &= -\rho g \\
\frac{\partial P}{\partial \sigma} \frac{\partial \sigma}{\partial z} &= -\rho g \\
\frac{\partial P}{\partial \sigma} \frac{1}{h+\zeta} &= -\rho g \\
\frac{\partial P}{\partial \sigma} &= -\rho g (h+\zeta)
\end{aligned}$$

Equation (A.1.21) becomes

$$\begin{aligned}
\nabla_z P &= \nabla_\sigma P - \frac{1}{h+\zeta} (\nabla_\sigma z) (-\rho g (h+\zeta)) \\
\nabla_z P &= \nabla_\sigma P + \rho g (\nabla_\sigma z) \\
-\frac{1}{\rho} \nabla_z P &= -\frac{1}{\rho} \nabla_\sigma P - g \nabla_\sigma z
\end{aligned}$$

(A1.22)

As

$$\begin{aligned}
P &= P_0 + P' \\
\nabla_\sigma P &= \nabla_\sigma P_0 + \nabla_\sigma P'
\end{aligned}$$

$$\nabla_{\sigma} P = \nabla_{\sigma} \{ \rho_0 g (\zeta - z) \} + \nabla_{\sigma} P' \quad (\text{A1.23})$$

$$\rho = \rho_0 + \rho'$$

$$\rho \nabla_{\sigma} z = \rho_0 \nabla_{\sigma} z + \rho' \nabla_{\sigma} z$$

$$\nabla_{\sigma} z = \frac{\rho_0}{\rho} \nabla_{\sigma} z + \frac{\rho'}{\rho} \nabla_{\sigma} z$$

So, equation (A.1.22) becomes

$$-\frac{1}{\rho} \nabla_z P = -\frac{1}{\rho} \left[\nabla_{\sigma} \{ \rho_0 g (\zeta - z) \} + \nabla_{\sigma} P' \right] - g \left[\frac{\rho_0}{\rho} \nabla_{\sigma} z + \frac{\rho'}{\rho} \nabla_{\sigma} z \right]$$

$$-\frac{1}{\rho} \nabla_z P = -\frac{\rho_0}{\rho} g \nabla_{\sigma} \zeta + \frac{\rho_0}{\rho} g \nabla_{\sigma} z - \frac{1}{\rho} \nabla_{\sigma} P' - \frac{\rho_0}{\rho} g \nabla_{\sigma} z - \frac{\rho'}{\rho} g \nabla_{\sigma} z$$

$$-\frac{1}{\rho} \nabla_z P = -\frac{\rho_0}{\rho} g \nabla_{\sigma} \zeta - \frac{1}{\rho} \nabla_{\sigma} P' - \frac{\rho'}{\rho} g \nabla_{\sigma} z$$

$$-\frac{1}{\rho} \nabla_z P = -\frac{\rho_0}{\rho} g \nabla_{\sigma} \zeta - \frac{1}{\rho} \nabla_{\sigma} P' - \frac{\rho'}{\rho} g \nabla_{\sigma} \{ (h + \zeta) \sigma - h \}$$

$$(\text{A1.24})$$

$$\text{As } \sigma = \frac{z+h}{h+\zeta}; z = \sigma(h+\zeta) - h$$

Now

$$P' = \int_z^{\zeta} \rho' g dz$$

$$\therefore P' = \int_{\sigma}^1 \rho' g d\sigma$$

$$\text{As } \sigma = \frac{z+h}{h+\zeta}; d\sigma = \frac{1}{(h+\zeta)} dz; dz = H d\sigma$$

Equation (A.1.24) becomes

$$-\frac{1}{\rho} \nabla_z P = -\frac{\rho_0}{\rho} g \nabla_{\sigma} \zeta - \frac{1}{\rho} \nabla_{\sigma} \left(H \int_{\sigma}^1 \rho' g d\sigma \right) - \frac{\rho'}{\rho} g \sigma \nabla_{\sigma} h - \frac{\rho'}{\rho} g \sigma \nabla_{\sigma} \zeta + \frac{\rho'}{\rho} g \nabla_{\sigma} h$$

$$-\frac{1}{\rho} \nabla_z P = -\frac{g}{\rho} (\rho_0 + \sigma \rho') \nabla_{\sigma} \zeta - \frac{\rho' g}{\rho} (\sigma - 1) \nabla_{\sigma} h - \frac{1}{\rho} \nabla_{\sigma} \left(H \int_{\sigma}^1 \rho' g d\sigma \right) \quad (\text{A1.25})$$

Multiplying LHS of momentum equation with H and LHS of continuity equation with u and adding;

$$\begin{aligned}
& H * \left[\frac{\partial u}{\partial t} + u \frac{\partial u}{\partial x} + v \frac{\partial u}{\partial x} + \sigma' \frac{\partial u}{\partial \sigma} \right] + u * \left[\frac{\partial \zeta}{\partial t} + \frac{\partial(Hu)}{\partial x} + \frac{\partial(Hv)}{\partial y} + H \frac{\partial \sigma'}{\partial \sigma} \right] \\
&= \left[H \frac{\partial u}{\partial t} + u \frac{\partial \zeta}{\partial t} \right] + \left[Hu \frac{\partial u}{\partial x} + u \frac{\partial(Hu)}{\partial x} \right] + \left[Hv \frac{\partial u}{\partial y} + u \frac{\partial(Hv)}{\partial y} \right] + \left[H\sigma' \frac{\partial u}{\partial \sigma} + u \frac{\partial(H\sigma')}{\partial \sigma} \right] \\
&= \frac{\partial(Hu)}{\partial t} + \frac{\partial(Huu)}{\partial x} + \frac{\partial(Huv)}{\partial y} + \frac{\partial(Hu\sigma')}{\partial \sigma}
\end{aligned}$$

Similar operations in RHS will give;

$$\begin{aligned}
& H * \left[fv - \frac{1}{\rho} \frac{\partial P}{\partial x} + A_H \frac{\partial^2 u}{\partial x^2} + A_H \frac{\partial^2 u}{\partial y^2} + \frac{1}{H^2} A_\sigma \frac{\partial^2 u}{\partial \sigma^2} \right] \\
&= Hfv - \frac{H}{\rho} \frac{\partial P}{\partial x} + HA_H \left(\frac{\partial^2 u}{\partial x^2} + \frac{\partial^2 u}{\partial y^2} \right) + \frac{1}{H} A_\sigma \frac{\partial^2 u}{\partial \sigma^2}
\end{aligned}$$

Combining LHS and RHS; x direction momentum equation:

$$\frac{\partial(Hu)}{\partial t} + \frac{\partial(Huu)}{\partial x} + \frac{\partial(Huv)}{\partial y} + \frac{\partial(Hu\sigma')}{\partial \sigma} = Hfv - \frac{H}{\rho} \frac{\partial P}{\partial x} + HA_H \left(\frac{\partial^2 u}{\partial x^2} + \frac{\partial^2 u}{\partial y^2} \right) + \frac{1}{H} A_\sigma \frac{\partial^2 u}{\partial \sigma^2} \quad (A1.26)$$

y direction momentum equation:

$$\frac{\partial(Hv)}{\partial t} + \frac{\partial(Hvu)}{\partial x} + \frac{\partial(Hvv)}{\partial y} + \frac{\partial(Hv\sigma')}{\partial \sigma} = -Hfu - \frac{H}{\rho} \frac{\partial P}{\partial x} + HA_H \left(\frac{\partial^2 v}{\partial x^2} + \frac{\partial^2 v}{\partial y^2} \right) + \frac{1}{H} A_\sigma \frac{\partial^2 v}{\partial \sigma^2} \quad (A1.27)$$

In vector form:

$$\begin{aligned}
& \frac{\partial(H\tilde{u})}{\partial t} + \frac{\partial(H\tilde{u}u)}{\partial x} + \frac{\partial(H\tilde{u}v)}{\partial y} + \frac{\partial(H\tilde{u}\sigma')}{\partial \sigma} \\
&= Hf \begin{pmatrix} v \\ -u \end{pmatrix} - \frac{H}{\rho} \nabla P + HA_H \left(\frac{\partial^2 \tilde{u}}{\partial x^2} + \frac{\partial^2 \tilde{u}}{\partial y^2} \right) + \frac{1}{H} A_\sigma \frac{\partial^2 \tilde{u}}{\partial \sigma^2}
\end{aligned}$$

where;

$$-\frac{\nabla P}{\rho} = -\frac{g}{\rho} (\rho_0 + \sigma\rho') \nabla \zeta - \frac{\rho'}{\rho} g (\sigma - 1) \nabla h - \frac{1}{\rho} \nabla \left(H \int_\sigma^1 \rho' g d\sigma \right) \quad (A1.28)$$

Boundary conditions:

Boundary condition at bottom:

$$A_\sigma \frac{\partial u}{\partial \sigma} = H \frac{\tau_x^b}{\rho}$$

$$A_\sigma \frac{\partial v}{\partial \sigma} = H \frac{\tau_y^b}{\rho}$$

Boundary condition at surface:

$$A_\sigma \frac{\partial u}{\partial \sigma} = H \frac{\tau_x^s}{\rho}$$

$$A_\sigma \frac{\partial v}{\partial \sigma} = H \frac{\tau_y^s}{\rho}$$

$$\tau_x^b = \rho \gamma_b^2 u \sqrt{u^2 + v^2}$$

$$\tau_y^b = \rho \gamma_b^2 v \sqrt{u^2 + v^2}$$

$$\tau_x^s = \tau_s \cos \theta$$

$$\tau_y^s = \tau_s \sin \theta$$

$$\tau_s = \rho_a c_f U_{10}^2$$

Governing equations for Temperature and Salinity:

The governing equations for temperature and salinity can be converted into sigma coordinate system in a similar mannar.

$$\begin{aligned} \frac{\partial(HT)}{\partial t} + \frac{\partial(uHT)}{\partial x} + \frac{\partial(vHT)}{\partial y} + \frac{\partial(\sigma'HT)}{\partial \sigma} \\ = HK_H \left(\frac{\partial^2 T}{\partial x^2} + \frac{\partial^2 T}{\partial y^2} \right) + \frac{1}{H^2} \frac{\partial}{\partial \sigma} \left(K_V \frac{\partial HT}{\partial \sigma} \right) + \frac{1}{\rho C_p} \frac{dq(\sigma)}{d\sigma} \end{aligned} \quad (A1.29)$$

$$\frac{\partial(HS)}{\partial t} + \frac{\partial(uHS)}{\partial x} + \frac{\partial(vHS)}{\partial y} + \frac{\partial(\sigma'HS)}{\partial \sigma} = HK_H \left(\frac{\partial^2 S}{\partial x^2} + \frac{\partial^2 S}{\partial y^2} \right) + \frac{1}{H^2} \frac{\partial}{\partial \sigma} \left(K_V \frac{\partial HS}{\partial \sigma} \right) \quad (A1.30)$$

Equations related heat balance and salinity

Transport equation for Salinity

Transport equation for salinity is given as follows:

$$\frac{\partial(HS)}{\partial t} + \frac{\partial(uHS)}{\partial x} + \frac{\partial(vHS)}{\partial y} + \frac{\partial(\sigma' HS)}{\partial \sigma} = HK_h \left(\frac{\partial^2 S}{\partial x^2} + \frac{\partial^2 S}{\partial y^2} \right) + \frac{1}{H^2} \frac{\partial}{\partial \sigma} \left(K_v \frac{\partial(HS)}{\partial \sigma} \right) - RS \quad (A1.31)$$

Boundary condition at sea surface:

$$-\frac{1}{H^2} K_v \frac{\partial(HS)}{\partial \sigma} = S(P - E_{rate}) \quad (A1.32)$$

where E_{rate} is the rate of evaporation given as:

$$E_{rate} = 1.2 * 1.2 * 10^{-3} * W * \left(0.98 * \frac{0.622 E_w}{1 - 0.378 E_w} - E_a \right) \quad (A1.33)$$

$$E_w = \frac{1}{P_{air}} \left[6.1078 * 10^{\left(\frac{7.5 * T_w}{237.3 + T_w} \right)} \right] \quad (A1.34)$$

E_a : vapor pressure, given by

$$E_a = \frac{0.622 * E_p}{1 - 0.378 * E_p} \quad (A1.35)$$

$$E_p = \frac{vapor}{P_{air}} \quad (A1.36)$$

Transport equation for Temperature

Transport equation for temperature is given as follows:

$$\frac{\partial(HT)}{\partial t} + \frac{\partial(uHT)}{\partial x} + \frac{\partial(vHT)}{\partial y} + \frac{\partial(\sigma' HT)}{\partial \sigma} = HK_h \left(\frac{\partial^2 T}{\partial x^2} + \frac{\partial^2 T}{\partial y^2} \right) + \frac{1}{H^2} \frac{\partial}{\partial \sigma} \left(K_v \frac{\partial(HT)}{\partial \sigma} \right) + \frac{1}{\rho C_p} \frac{dq(\sigma)}{d\sigma} \quad (A1.37)$$

Boundary condition at the surface:

$$-\frac{1}{H^2} K_v \frac{\partial(HT)}{\partial \sigma} = \frac{Q_s}{\rho C_p} \quad (A1.38)$$

where Q_s is the net surface heat flux penetrating into the water column, given as

$$Q_s = (1 - A)Q_A - Q_B - Q_e - Q_h \quad (A1.39)$$

Q_A : Net short wave radiation

A : Albedo, the ratio of reflected to incident light ($A=.02$)

Q_B : Net long wave radiation

$$Q_B = s\sigma_h T_{wa}^3 \left\{ T_{wa} (0.49 - 0.066\sqrt{vapor})(1 - 0.65c) + 4(T_{wa} - T_a) \right\} \quad (A1.40)$$

s: coefficient of emissivity, relating the properties of radiating surfaces to those of a black body (0.97)

σ_h : Stefan-Boltzmann's constant: 5.67×10^{-8}

T_{wa} : Surface water temperature ($^{\circ}K$)

T_a : Air temperature ($^{\circ}K$)

c: cloud amount, in fractions of unity

Q_e : Latent heat, given as:

$$Q_e = (2.5 \times 10^6 - 2400 * T_w) * E_{rate} \quad (A1.41)$$

Q_h : sensible heat, given as

$$Q_h = 1006 * 1.2 * 1.2 * 10^{-3} (T_{wa} - T_a) * W \quad (A1.42)$$

Appendix B

Model Validation with the Sumatra Tsunami at the Sri Lankan Coasts

